THE MAGNETIC CIRCULAR DICHROISM OF

BIOLOGICALLY INTERESTING MOLECULES

by

Michael Edward McCarville

A Dissertation Submitted to the

Graduate Faculty in Partial Fulfillment of

The Requirements for the Degree of

DOCTOR OF PHILOSOPHY

Major Subject: Biophysics

Approved:

In Charge of Major Work

Head of Major Department

Dean of Graduate College

Iowa State University
Of Science and Technology
Ames, Iowa

1967

TABLE OF CONTENTS

# I. INTRODUCTION

## History

In the course of searching for a relationship between light and magnetism during the nineteenth century, a number of magneto-optical effects were discovered. In 1845 Faraday found that plane polarized light is rotated as it passes through a piece of lead glass in parallel with a magnetic field (1). Experimentation later indicated that any substance observed in this manner, whether diamagnetic or paramagnetic, exhibits the rotation of light to some degree. The discovery by Zeeman in 1896 that certain emission (or absorption) lines are split by a magnetic field provided an explanation for much of the Faraday effect observed in atoms (2).

During the early 1930's a practical quantum mechanical theory was developed for the magnetic optical activity of molecules (3). Also at about this time one of the first measurements of magnetic circular dichroism (MCD) was made through the absorption band of a molecular substance in solution (4). However, most of the applications of the Faraday effect were made on atomic or very simple linear molecular systems. An extensive bibliography of magneto-optics has recently been published which makes reference to much of this early work (5). The experimental apparatus necessary for sensitive and accurate measurements of circular dichroism was not available commercially until about 1960 (6). Modification of these machines for magnetic work has enabled a number of workers to explore the usefulness of the technique. An extension of the theory to cover the broad band systems of molecules was made by Stephens (7).

## Contemporary Work

Several workers are active in the MCD field today. The laboratory of Dr. Paul Schatz at the University of Virginia is studying various problems, but the emphasis of their work is on inorganic molecules. The techniques of MCD are often quite quantitative for these molecular systems and the results are very helpful for the assignment of energy levels to electronic transitions (8).

Dr. Carl Djerassi at Stanford has had workers making measurements of MCD, however in the results published so far little or no attempt has been made to interpret the spectra (9).

Dr. A. Dratz recently published his Ph.D. thesis from the University of California at Berkeley where his research included the study of the electronic structure of the metal porphyrins by the method of MCD (10).

In this laboratory the initial attempts to measure MCD were made for two reasons: first, because the necessary apparatus was available and second, because it seemed MCD might provide an optical method of obtaining the type of information usually requiring measurements of magnetic susceptibility or electron spin resonance. In particular it was hoped that the magnetic state of the respiratory protein, hemocyanin, might be determined by this new technique. However, we soon found both experimentally and from a study of the theory of the Faraday effect that MCD would not in general be sensitive to effects due to electron spin. In the process of making these first measurements a number of interesting but sometimes puzzling spectra turned up. The MCD spectra of hemoglobin and cytochrome c were particularly interesting, the porphyrin ring

prosthetic group being the cause of the absorption spectra. Investigation

of this ring system by MCD and correlation of the results with molecular

orbital theory has been advanced by the graduate work of Dratz mentioned

above (10). It was decided here to design experiments which would help

to interpret the MCD spectra of biologically important compounds. As a

result of both experimental and theoretical limitations, the information

which can be drawn from the MCD of these organic molecules is qualitative

or semi-quantitative. Despite these short-comings our research has yielded

a number of interesting developments. A portion of these results have

been published in a series of papers (11,12,13,14). The underlying motive

in this investigation is to determine the usefulness of the MCD technique

for problems in molecular biology.

## II. EXPERIMENTAL

### Instrumentation

The MCD spectra were obtained using a Roussel–Jouan dichrograph which had undergone the following modifications:

1. Replacement of the original monochromator with a Cary Model 15 double prism monochromator.

2. Replacement of the original light sources with a 450 watt xenon arc.

3. Replacement of the original modulating crystal with a Baird-Atomic crystal of potassium dideuterium phosphate, Model No. JV-1D(UV).

4. Installation of an Alpha Scientific Lab. electromagnet.

5. Replacement of the original signal detector and AC amplifier with a Princeton Applied Research Model JB-4 Lock-in Amplifier and change of the modulating frequency from 60 cps to 82 cps.

6. Arrangement of the optical components on a five foot lathe bed manufactured by Logan Eng. Co.. The experimental arrangement is outlined in Fig. 1.

The light from the xenon lamp is focused on the monochromator entrance slit by means of a mirror. Light emerging from the monochromator is focused on the photomultiplier tube. The ammonium dihydrogen phosphate crystal was replaced with a thicker crystal of potassium dideuterium phosphate with gold electrodes, solving problems of high voltage break-down experienced with the original crystal. The new modulating crystal requires only half the voltage required of the original to produce the
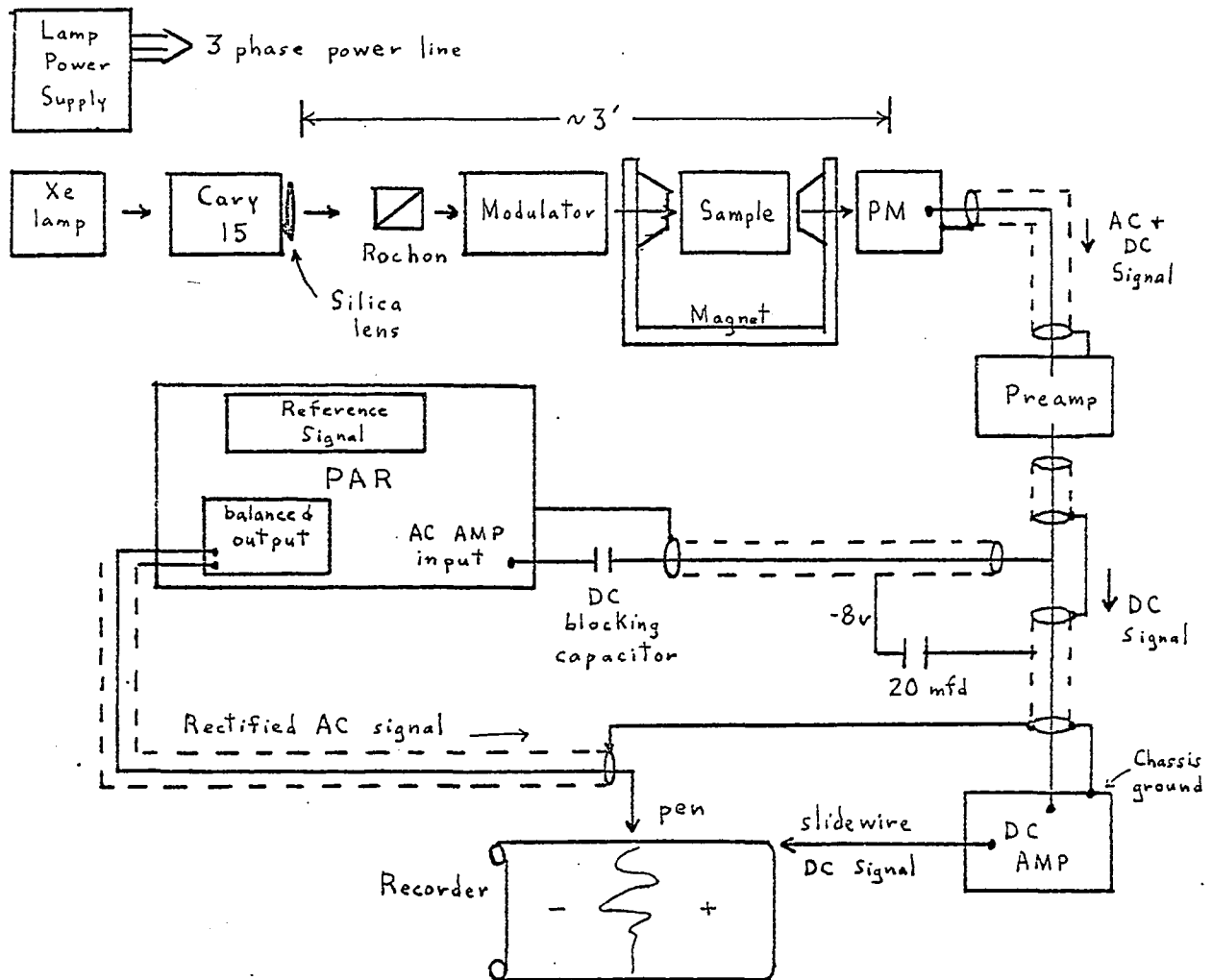
Fig. 1. Experimental arrangement for the dichrograph

same retardation. The modulating frequency was altered to avoid the 60 cps line voltage and was set at 82 cps when this proved to be the frequency with the lowest noticeable noise.

The power supply for the xenon lamp (see Fig. 2) is similar to one built earlier in this laboratory (15). This supply source has proven to be very satisfactory. The 360 cps ripple is less than 0.1% of the total voltage as measured by an oscilloscope across the lamp terminals with the lamp operating.

The power supply for the modulator is shown in Fig. 3. The source is taken from the reference output of the Princeton amplifier, a signal which is synchronized with the phase sensitive detector of the amplifier.

The magnet is an Alpha Scientific Laboratories Model AL7500M equipped with the AL7500 power supply and 7500R regulator. The light beam passes through a 1 cm bore. The magnet is operated at a regulated 9.5 amperes. For measurements of 1 cm path length a 22 mm gap is used yielding a 10.4 kilogauss field. With a 1 mm path length a 3 mm gap is used giving 13.1 kilogauss. The magnetic field measurements were obtained with a Bell gaussmeter using an axial probe.

The dichrograph was calibrated with a 1 mg/ml solution of 5-α-cholestan-3-one in methanol. For a 1 cm path length $\Delta A = 0.00369$ at 290 mμ, a value determined and supplied by Dr. Paul Schatz.

A diagram of the circuit used to operate the dichrograph automatically for multiple scans is shown in Fig. 4. The "gear microswitch" is coupled directly to the dichrograph wavelength drive where contacts are set to provide the desired frequency range. The interface needed
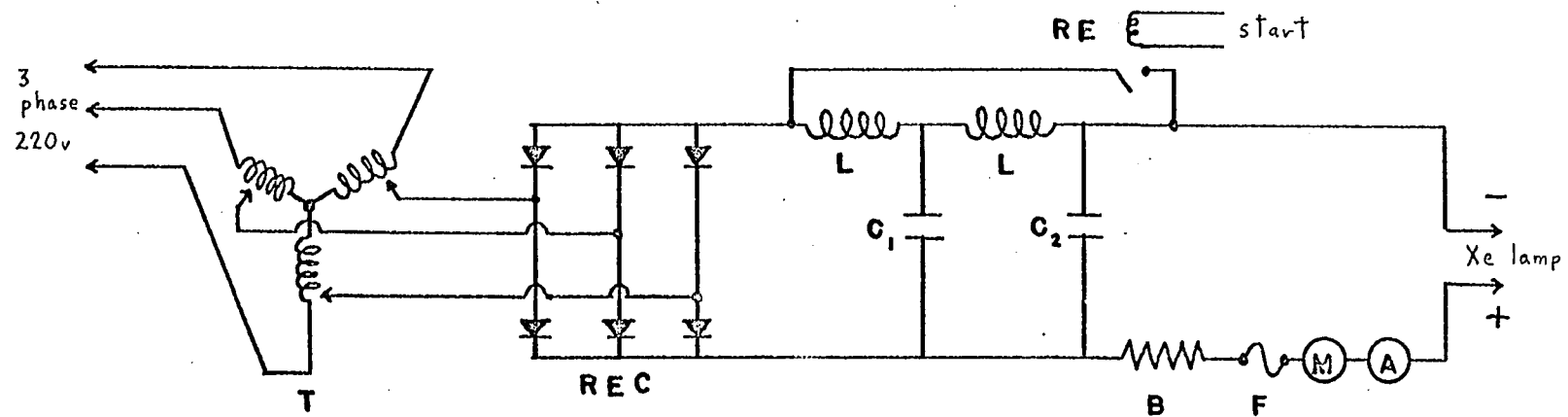
T    — Superior Electric Eo. 3 phase autotransformer Type #136-3
Rec  — Westinghouse 6-3-1B size K set of selenium rectifiers
L    — Chicago Standard Trans. Corp. .005 Hys. C-2689 Filter Choke
$C_1$   — Mallory 1000 mfd 150 vdc HC 15010 A V.V.  6 in parallel
$C_2$   — Mallory 1000 mfd 150 vdc HC 15010 A V.V.  2 in parallel
B    — Ballast 8 5 Ω 200-225 w resistors IRC 6448 Type 10 1/2 H in series
F    — Fuse 30 amp.
M    — Haydon hour meter
A    — Electro-Mechanical Inst. Co.  30 amp DC ammeter
RE   — Potter-Brumfield PR3AY relay 230v, 60 cycle coil rated at 25 amp. at 110 v

Fig. 2.   Lamp Power Supply

Fig. 3. Modulator power supply

Scan Segments

F o ●—————▷●

B o ●◁—————●

0 ●◁—●        ●

R ●—▷●        ●

pulse to CAT

110 v

110 v

6 v

24 v

NC

0.1 mfd

RF

Re 3

BO

Re 4

BR

Re 3
Motor
Reverse

FO

Re 1

FB

OR

gear
micro switch
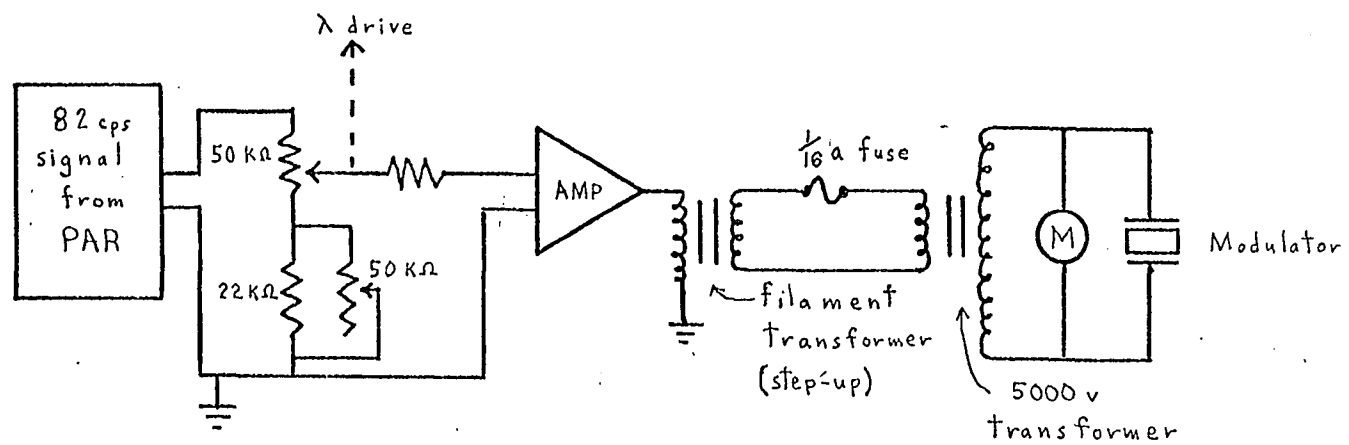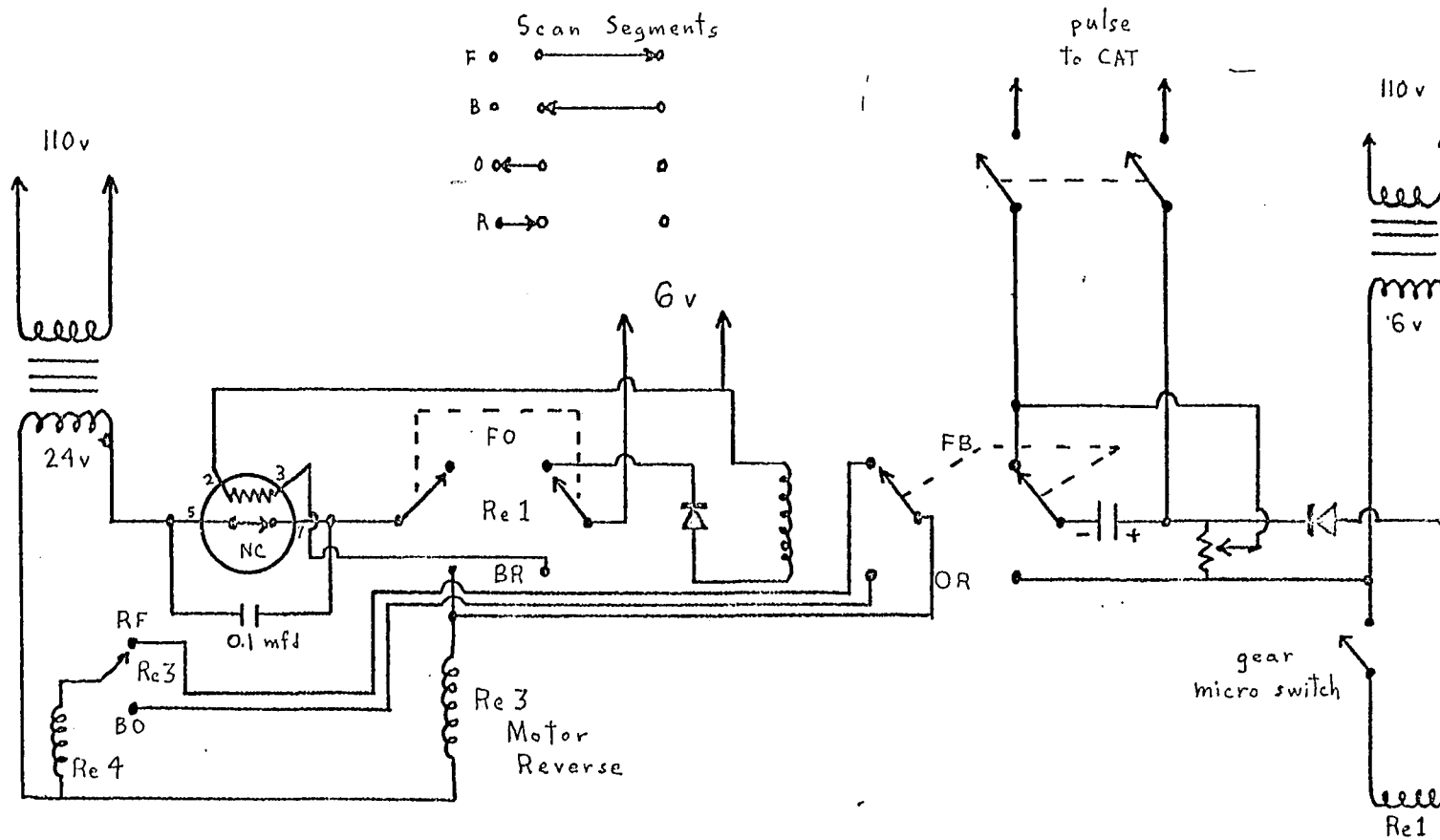
6 v

Re 1

Fgi. 4.   Automatic Scanner

6

between the final output of the dichrograph and the computer of average transients (CAT) input is shown in Fig. 5. The CAT used was a Japan Electron Optics Lab Co. Model JNM-RA-1.

The absorption spectra were determined on a Cary Model 15 spectrophotometer.

Measurements at other than room temperature were made with the sample held in a brass holder. Temperature of the brass holder was controlled by conduction from an attached reservoir. Depending on the temperatures desired, the reservoir was filled with liquid nitrogen, acetone-dry ice mixture, salt-ice mixture or heated oil. Temperature measurements were taken with a chromel-alumel thermocouple using a Keithley Instruments Model 149 milli-microvoltmeter.

## Materials

Most of the chemicals were used directly from the bottle unless their absorption spectra indicated impurities when compared to literature values. Special precautions had to be taken in this regard for samples of naphthalene, anthracene and benzimidazole. No further purification was deemed to be necessary for this work if the compound proved to be spectroscopically pure.

## Other Experimental Arrangements

The dichrograph in its present form is truly a versatile instrument. With the addition of only a few optical components it is capable of measuring linear dichroism and birefringence. It is also theoretically capable of measuring magnetic linear dichroism and birefringence (the
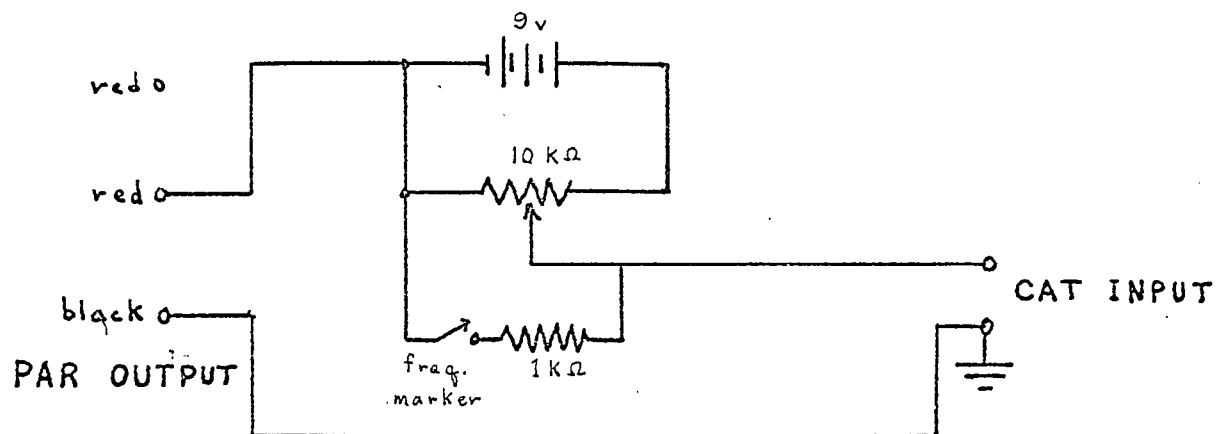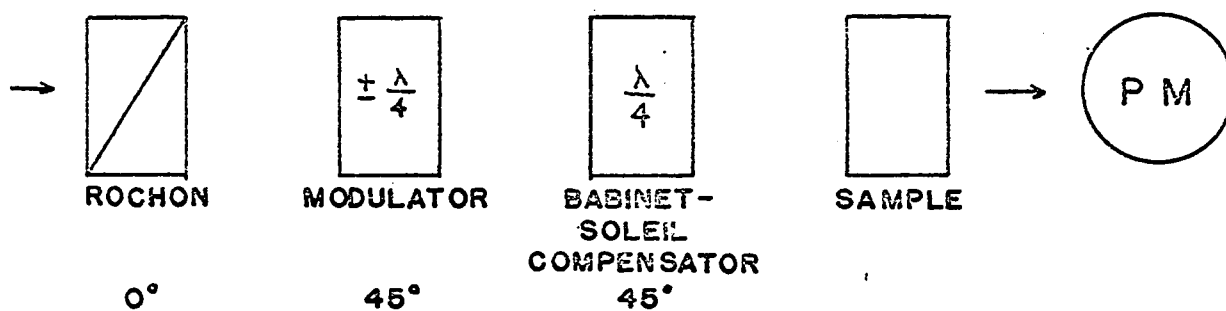
Fig. 5. Dichrograph - CAT hookup



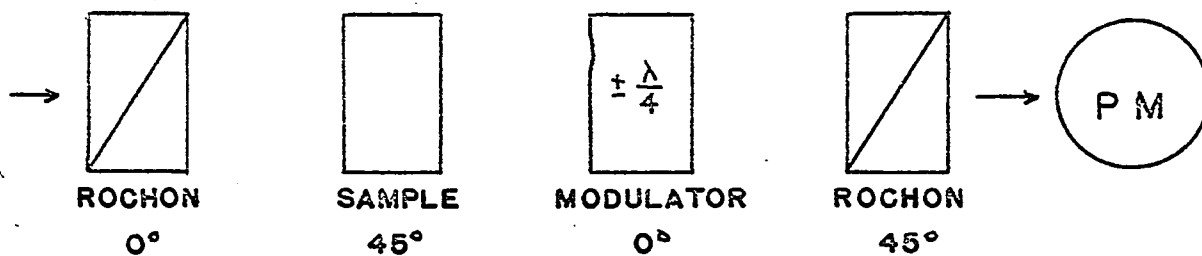Fig. 6. Optics for use of dichrograph to measure linear dichroism



Fig. 7. Optics for use of dichrograph to measure linear birefringence

Cotton-Mouton effect), although the sensitivity is not presently available. The optical arrangements needed for these measurements are shown in Figs. 6 and 7.

In designing these arrangements it is necessary to know the state of polarization of the light beam at each point along the path, and to make certain that the signal emerging from the photomultiplier tube actually contains the information which one wishes to measure. Two particularly helpful aids which greatly simplify the optical analyses are the Poincare sphere and the Jones calculus. This will be illustrated for the operation of the dichrograph in its normal mode for the measurement of circular dichroism.

Points on the Poincare sphere represent polarized light of any degree of ellipticity (16, p. 15)(17). In Fig. 8 the poles represent right and left circular light, the equator represents the various azimuthal angles of plane polarized light as shown and all other points represent some other degree of ellipticity. If we begin with plane polarized light of azimuthal angle 0° (Fig. 9) from the dichrograph polarizer (P) and next introduce a variable retardance (R) at an angle of 45°, the effect of the retarder will be to rotate the sphere about the axis CR to a degree depending on the retardation (i.e., depending on the modulation voltage). If the retardation is 1/4 λ, circularly polarized light will be obtained. Actually, because of the detection system used, the dichrograph modulator is made to retard somewhat more than 1/4 λ at maximum voltage, therefore at this point the light beam is elliptically polarized (18). The Poincare sphere makes it simple to visualize the state of the light entering the
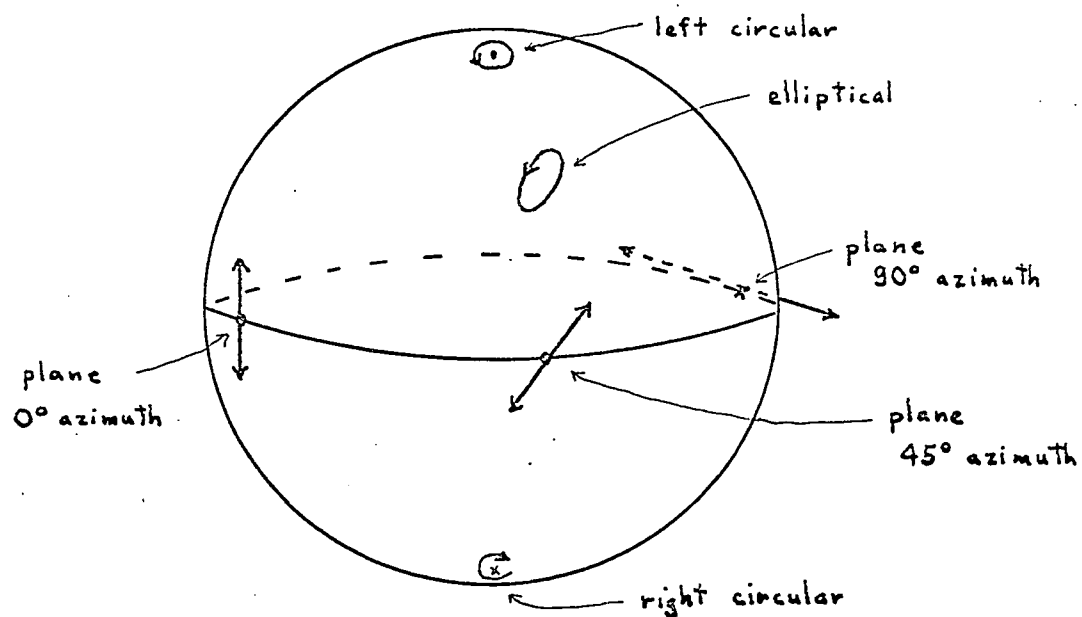
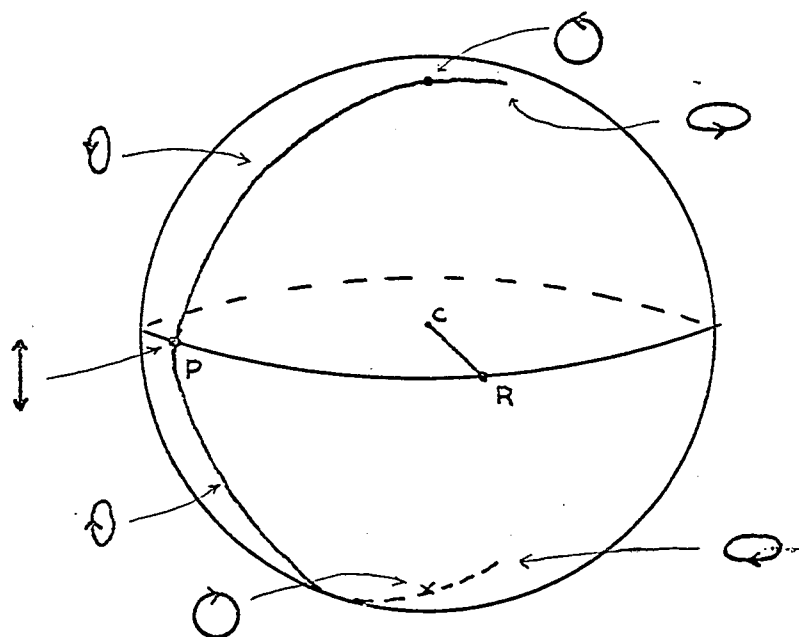Fig. 8. The Poincaré sphere



Fig. 9. Polarization of light during modulation cycle of dichrograph

sample at any point in the modulation voltage cycle.

The voltage as seen at the photomultiplier output is shown in Fig. 10 for various types of samples. This may also be seen easily by using the Jones calculus (16, p. 118)(19). The initial state of polarization of the light beam is represented by a column matrix and each optical component by a square matrix. The matrices are then lined up from right to left in the same order as the components are seen by the light beam. Then the matrices are multiplied from right to left and the resulting matrix yields the state of the emerging light. This is illustrated below for the case of a circularly dichroic sample.

State of polarization = [S] [M] [P]

where $[P] = \begin{bmatrix} 1 \\ 0 \end{bmatrix}$, the column matrix for plane polarized light at an azimuthal angle of $90°$.

$$[M] = \begin{bmatrix} \cos^2\theta \ e^{i\frac{\delta}{2}} + \sin^2\theta \ e^{-i\frac{\delta}{2}} & \cos\theta \ \sin\theta \ 2i \ \sin\frac{\delta}{2} \\ \cos\theta \ \sin\theta \ 2i \ \sin\frac{\delta}{2} & \cos^2\theta \ e^{-i\frac{\delta}{2}} + \sin^2\theta \ e^{i\frac{\delta}{2}} \end{bmatrix},$$

the matrix for the modulator with a retardation $\delta = 1.98 \sin \omega t$ and azimuthal angle of $\theta = 45°$.

$$[S] = \begin{bmatrix} d_1 + d_2 & -i(d_1 - d_2) \\ i(d_1 - d_2) & d_1 + d_2 \end{bmatrix},$$

the matrix for an optically active sample with $d_1 = 10^{-2A_1}$ and $d_2 = 10^{-2A_r}$. $A_1$ and $A_r$ are the respective absorbances for left and right circular light. Then we have

$$[S] \ [M] \ [P] = \frac{1}{2} \begin{bmatrix} (d_1 + d_2) \cos\frac{\delta}{2} + (d_1 - d_2) \sin\frac{\delta}{2} \\ i(d_1 - d_2) \cos\frac{\delta}{2} + i(d_1 + d_2) \sin\frac{\delta}{2} \end{bmatrix} \begin{matrix} A_x \\ A_y \end{matrix}$$
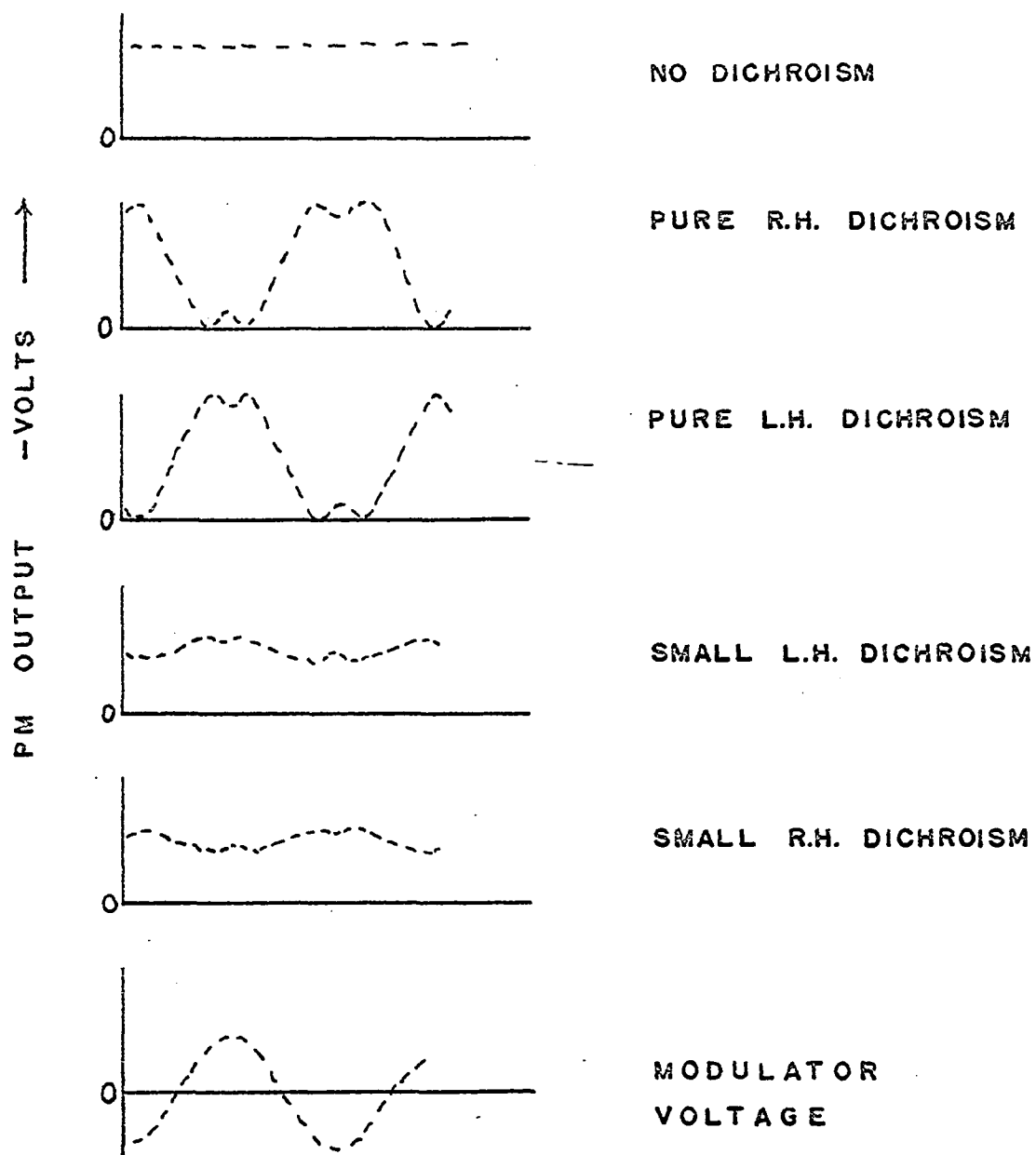
Fig. 10. Photomultiplier output for different types of circularly dichroic samples

where Ax and Ay are the amplitudes in the x and y directions. Now since the intensity I is equal to the square of the amplitude, or

$I = AxAx^* + AyAy^*$,

$$I = Io \; \frac{1}{2}[(d_1^2 + d_2^2) + (d_1^2 - d_2^2) \sin \delta]$$

where $\sin \delta = \sin(\delta_o \; \omega t)$. The first term in the bracket represents the time independent part of the light intensity due to the ordinary absorption and the second term is the time dependent part resulting from the circular dichroism of the optically active sample. So it is seen that the method of the Jones calculus gives quickly an easily visualized expression typifying the intensity of the light which the phototube will observe. Further analysis of the signal as it is processed by the machine follows exactly that given by Velluz et al. (18, p. 60).

## III.   A SIMPLIFIED THEORY OF MCD

The classical and quantum mechanical theories of the molecular Faraday effect have been known for several decades.  However it is only within the last few years that the theory has been developed in a practical form for molecular systems.  Unfortunately little of the quantum mechanical theory of MCD has been stated explicitly in a language which those relatively unfamiliar with the methods and notation can readily grasp.  (The recent thesis of Dratz (10) handles certain aspects of the theory in a very lucid manner.)  Therefore the purpose of this section will be to present the theory as clearly as possible, to indicate references which have been particularly helpful, and to use this simple theory to predict the type of information MCD might provide, especially for molecules of biological interest.  Appendix I contains a second-order perturbation theory derivation for MCD, also presented with considerable explanation of the techniques and mathematical methods used.

A considerable amount of the MCD effect can be understood in terms of the inverse Zeeman effect.  Here "inverse" pertains of the absorption of circularly polarized light rather than emission as is usually used to study the Zeeman effect.  The inverse Zeeman effect is a change in the frequencies at which right and left circular light is absorbed, caused by the action of an external magnetic field upon moving electrons in a substance.  Intuitively one would expect that for two charges orbiting in opposite directions an external magnetic field should favor one direction and retard the other.  This will change the kinetic energies of the charges and therefore change the resonant frequencies at which they will
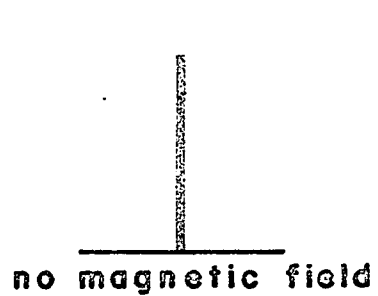
absorb light.  Essentially this is what actually occurs for molecular

electrons.  The effect is observed experimentally by measuring the

absorption of circular light passing through the sample in a direction

parallel to the applied magnetic field.  Fig. 11(a) illustrates this for

sharp absorption lines and Fig. 11(b) for broad bands.  Since MCD is

defined as the result of subtracting right circular absorption from left

circular absorption, a spectrum such as Fig. 11(c) results for broad

bands.

The Zeeman effect is treated nicely in a number of textbooks.

(20,21)  However, to account for the MCD of all molecules it will be

necessary to discuss some quantum mechanical aspects of the circular

absorption process.

## Photons and Transitions

At the beginning it must be realized that single photons always con-

tain one unit ($\hbar$) of angular momentum (spin) (22).  This is true of all

photons, without regard to their frequency or origin.  This angular

momentum may be of either sign, and by convention we will say that a +1

angular momentum means the photon is left-circularly polarized and -1 that

it is a right-circularly polarized photon (23).  Appendix II contains an

explanation of the sign convention used in this thesis and includes the

reasons for the choice of signs.  Fig. 12 shows how the handedness is

defined.  The electric (or magnetic) vector moves clockwise for right-hand

light, counterclockwise for left-hand light as viewed looking toward the

light source.

If a molecule in its ground state absorbs a circularly polarized

(a)

no magnetic field

L R

λ

magnetic field
applied

(b)

no magnetic field

L    R

λ

magnetic field
applied

+

−

λ
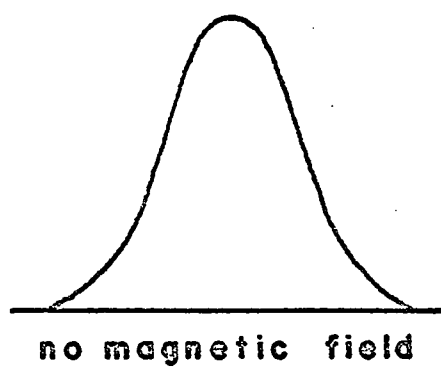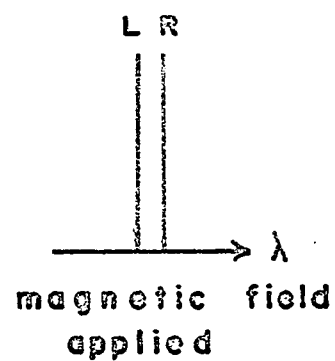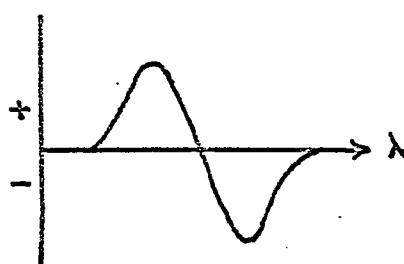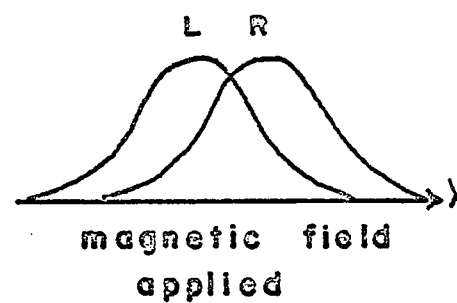
M C D

(c)

Fig. 11.   Inverse Zeeman effect and MCD

RIGHT    LEFT

Fig. 12.   Handedness of circularly polarized light

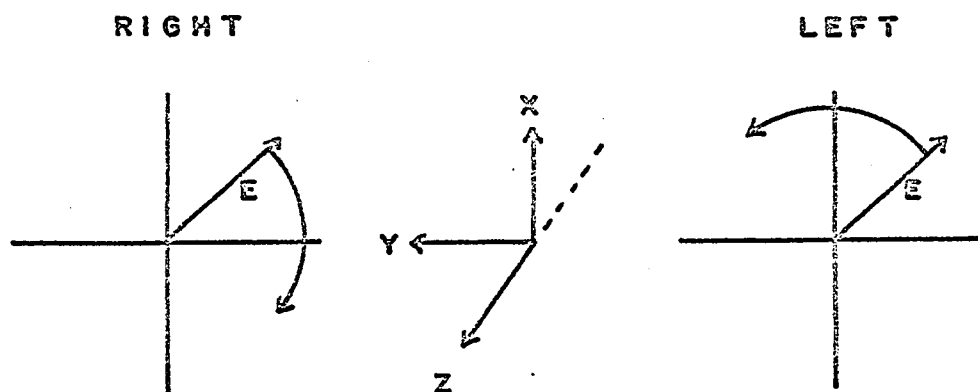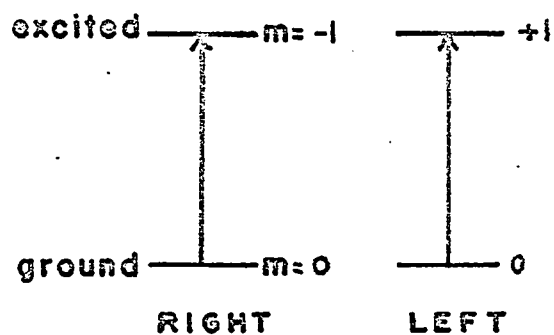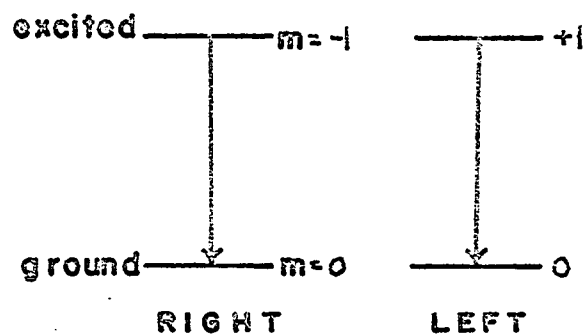Fig. 13.   Absorption of circularly    Fig. 14.   Emission of circularly
polarized light                polarized light

photon, it will gain a unit of angular momentum as shown in Fig. 13 (24).

The quantum number m is used to designate the state of orbital angular

momentum of the electron involved in the transition. If the molecule emits

the energy of the photon, it will release the angular momentum it absorbed,

emitting a photon of the same handedness as it absorbed. This is required

to satisfy the conservation of momentum. Fig. 13 illustrates the "selection

rules" for circularly polarized transitions, for example, the requirement

for right-hand absorption is that $\Delta m = -1$.

## The Quantum Mechanical Language of MCD

One of the primary requisites for understanding quantum mechanical

methods, and indeed for understanding any unfamiliar subject, is to know

the language associated with the subject. Although quantum mechanics is

quite an involved method, individual topics within it can often be

visualized quite easily, a fact not at all obvious from reading most of

the literature. Very often an interpretation or analogy can be found

which will give a "physical feeling" for some concept which has been

written in a compact mathematical manner. Once these "physical feelings"

have been gained the compact language used in quantum mechanical theory

becomes much easier to read.

A number of the terms used in the literature associated with magnetic

circular dichroism, such as "matrix element" and "vector potential", will

be discussed below in an attempt to show why their use is quite natural.

The circular photons which strike our sample may be thought of as

perturbations capable of producing changes in the system. In order to

represent these properties mathematically an expression must be found for

the electromagnetic fields of the photons, for it is these fields which

provide the perturbation.  This could be done by using the electric field

$\overline{E}$ and magnetic field $\overline{H}$ of the photon.  However, for reasons which will

not be discussed, it is mathematically convenient to use a vector function

related to both $\overline{E}$ and $\overline{H}$ called the vector potential $(\overline{A})$.  The relation of

$\overline{A}$ to $\overline{E}$ and $\overline{H}$ is shown in Eqs. 1 (25, p. 108).

$$\overline{E} = -\frac{1}{c}\frac{\partial \overline{A}}{\partial t} - \overline{\nabla}\phi \qquad \text{where} \quad \overline{\nabla} = (\overline{i}\frac{\partial}{\partial x} + \overline{j}\frac{\partial}{\partial y} + \overline{k}\frac{\partial}{\partial z}) \qquad \text{Eq.(1)}$$

$$\overline{H} = \overline{\nabla} \times \overline{A}$$

The scalar potential $\phi$ is associated with an electrostatic field and will

be ignored here since it is assumed that the photon is far from its

electrostatic source.  The electrostatic field is proportional to $\frac{1}{r^2}$,

radiation proportional to $\frac{1}{r}$ and a dipole field is proportional to $\frac{1}{r^3}$.

The vector potential $\overline{A}$ (also called vector magnetic potential) has no real

physical significance.  It cannot be measured experimentally as can $\overline{E}$ and

$\overline{H}$, but is a vector function which yields the magnetic field when the cross

product with $\overline{\nabla}$ is taken.  However we can obtain some feeling for the

function if we examine its definition in Eq. 2.  In this expression

$$\overline{A} = k \int_{\infty} \frac{\overline{J}}{r}\, d\tau \qquad\qquad \text{Eq.(2)}$$

$\overline{A}$ at some point in space at a distance r from the electrostatic source

is proportional to the integral over all space of the current density $\overline{J}$

at the source.  Fig. 15 shows an oscillating dipole $\overline{P}$ (a changing current)

as the source producing an oscillating vector function $\overline{A}$ at some point in

space. ( 26 )  The current traveling back and forth in the dipole is $\overline{J}$.

$$\overline{P} \longleftarrow\!\!\!\!\!\!\xrightarrow{\quad r \quad} \overline{A}$$
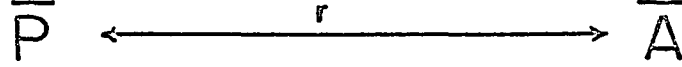
Fig. 15. Vector potential ($\overline{A}$) produced by a dipole ($\overline{P}$)

From the vector potential $\overline{A}$ the fields $\overline{E}$ and $\overline{H}$ may be found using Eqs. 1 .

The vector potential for a circular photon traveling in the z direction can be considered a combination of the vector potentials from dipoles escillating in the x and y directions as in Eq. 3.

$$\overline{A}_r = \overline{i} A_x + i \, \overline{j} \, A_y$$
$$\overline{A}_\ell = \overline{i} A_x - i \, \overline{j} \, A_y$$

Eq.(3)

The imaginary quantity i in Eq. 3 represents a 90° phase factor. The +i in $A_r$ implies that $A_y$ is 90° ahead of $A_x$, the -i in $A_l$ means $A_y$ is behind $A_x$ by 90°.

Without going into the derivation of the perturbation operator, it is obvious that the vector potential $\overline{A}$ does not fully describe the perturbing force. A force ($F = ma = e(\overline{E} + \frac{1}{c}[\overline{V} \times \overline{H}])$) should be related to the mass, charge and velocity of the particles in the substance being illuminated. When the derivation has been accomplished (25,27) the perturbation is found to be

$$H = \frac{e}{mc} \, \overline{A} \cdot \overline{p}$$

where $\bar{p}$ is the momentum operator $- i\ h(\bar{i}\ \frac{\partial}{\partial x} + \bar{j}\ \frac{\partial}{\partial y} + \bar{k}\ \frac{\partial}{\partial z})_0$. Now H

contains the field, mass charge and particle velocity ($\frac{\partial}{\partial x}$ etc). The

expression is considerably simplified by making two approximations. First,

the size of the wavelength of light is considered to be much greater than

the size of the molecule being perturbed, and therefore A is constant over

the molecule. This approximation cannot be made for the perturbation

operator concerned with natural circular dichroism. Essentially this first

approximation will mean that only the first term in an expansion of the

space part of the vector potential $(e^{i\bar{K}\cdot\bar{Z}})$ is needed, and the first term

is unity $(e^{i\bar{K}\cdot Z} \simeq 1 + i\bar{K}\cdot\bar{Z} + \cdots)$. Second, the so-called dipole approxi-

mation will be made in which we assume that the molecule absorbs radiation

as a dipole. This allows $\bar{p}$ to be written in the form $\bar{p} \propto i(\bar{i}x + \bar{j}y + \bar{k}z)$

(25,28). This is equivalent to saying that the velocity of the perturbed

charge and the distance which it moves from its equilibrium point are

directly related.

Now if for simplicity we exclude the constants involved, we see that

the form of the right-hand perturbation operator will be

$$H_r = \bar{A}_r\cdot\bar{p} = (\bar{i}\ A_x + i\ \bar{j}\ A_y) \cdot i(\bar{i}x + \bar{j}y) = A i\ (x+iy)$$

since $A_x = A_y$ for circular light. Doing likewise for the left-hand case

gives $H_1 = Ai(x-iy)$ (29).

It will be convenient to transform the operators from cartesian to

spherical coordinates, since integration will be simpler in this

coordinate system. One finds that $x \pm iy$ transforms as $r\ \sin\ \theta\ e^{\pm i\phi}$.

Again for simplicity only the essential part of this expression will be

used so that for $H_r$ we will use $e^{+i\phi}$ and for $H_l$ use $e^{-i\phi}$.

We are now interested in learning what effect the perturbation of a circular photon has upon a particular molecule. Since the electrons in a molecule exhibit a wave-like behavior, the state of a molecule is represented by wave functions $\psi$. We will represent the perturbation of the ground state of a molecule by a right circular photon as $H_r \psi_1$. This may have some affect upon the wave function and thereby change it slightly.

We would like to know whether the perturbation is capable of causing a transition of the molecule from state $\psi_1$ to a higher state $\psi_2$. In order for this to occur there must be some similarity in spatial configuration between the perturbed state $H_r \psi_1$ and $\psi_2$. One can think of this similarity as an overlap of the regions where an electron in state $H_r \psi_1$ resides with the region it would occupy in state $\psi_2$. This can be determined by calculating the integral $\int \psi_2 H_r \psi_1^* d\tau$, where $d\tau$ means to integrate over all space. This integral gives the average or "expectation" value for the operation $H_r$ when the states $\psi_1$ and $\psi_2$ are involved. The form of the average value is dictated by a law of quantum mechanics (28). Since the perturbation operator in this case contains the dipole moment and may result in a transition, the integral is commonly called a "transition moment". If the result of the calculation is non-zero the transition is said to be "allowed", if zero it is "forbidden".

As an example of evaluating a transition moment we can ask the question, "what is the possibility of changing the state of a molecule from m=0 to m=1 using right-hand or left-hand photons?" We will use only

the parts of the wave functions describing the orbital angular momentum

for simplicity. These parts can be written in the form $e^{im\phi}$ to make the

integrals for transition moment easy to evaluate.

right-hand $\int_{0}^{2\pi} e^{+i\phi} e^{+i\phi} e^{0} \, d\phi = \int_{0}^{2\pi} e^{+2i\phi} \, d\phi = $ zero

left-hand $\int_{0}^{2\pi} e^{+i\phi} e^{-i\phi} e^{0} \, d\phi = \int_{0}^{2\pi} 1 \, d\phi = $ non zero

Therefore only left-hand photons can cause the transition.

The transition moment itself is not proportional to the intensity of

absorption, but rather the product of the transition moment with its

complex conjugate must be taken,

$$\left|\left\langle \psi_2 | H_r | \psi_1 \right\rangle\right|^2 = \left(\int \psi_2 H_r \psi_1^* \, d\tau\right) \left(\int \psi_2^* H_r^* \psi_1 \, d\tau\right)$$

This has its analog classically in that the rate of energy absorption is

proportional to the square of the dipole moment (28, p. 554). Quantum

mechanically the need for the square results from the fact that the states

are set up in such a way that the probability of a system being in the

state $\bar{\psi}$ is $\bar{\psi}^* \bar{\psi}$. This topic is explained clearly by Barrow (30, p. 68).

It should also be noted at this point that the transition moment

$\left\langle \psi_2 | H_r | \psi_1 \right\rangle$ is not observable experimentally. This is apparent mathematical-

ly by the presence of the complex operator containing $ie^{i\phi}$ which will

always result in imaginary answers. Imaginary quantities are not ob-

servable, a corollary of quantum mechanics (28, p. 169). The product of

the transition · moment with its complex conjugate will always result in

a real quantity and will therefore be observable.

Integrals with a form such as $\left\langle \psi_2 | H | \psi_1 \right\rangle$ are commonly called "matrix

elements" (31, p. 87). This results from the fact that it is convenient to use matrix methods to solve equations involving transition moments for a molecular system. The equations to be solved (32) are of the type $d_j = \sum_i \langle \psi_j | Op | \psi_i \rangle \, c_i$, which for the operator Op and the system in Fig. 16 is
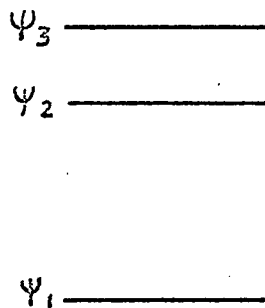
$$\Psi_3 \underline{\hspace{2cm}}$$

$$\Psi_2 \underline{\hspace{2cm}}$$

$$\Psi_1 \underline{\hspace{2cm}}$$

Fig. 16. System of levels

$$\begin{pmatrix} d_1 \\ d_2 \\ d_3 \end{pmatrix} = \begin{pmatrix} \langle \psi_1|Op|\psi_1\rangle & \langle \psi_1|Op|\psi_2\rangle & \langle \psi_1|Op|\psi_3\rangle \\ \langle \psi_2|Op|\psi_1\rangle & \langle \psi_2|Op|\psi_2\rangle & \langle \psi_2|Op|\psi_3\rangle \\ \langle \psi_3|Op|\psi_1\rangle & \langle \psi_3|Op|\psi_3\rangle & \langle \psi_3|Op|\psi_3\rangle \end{pmatrix} \begin{pmatrix} c_1 \\ c_2 \\ c_3 \end{pmatrix} \qquad \text{Eq.(4)}$$

where Op is the operator which will give the average (expectation) values for a particular property. The individual terms $\langle \psi_j | Op | \psi_i \rangle$ are called matrix elements. For the case of electric dipole absorption only those off-diagonal elements in the lower left are of interest. In MCD matrix elements representing magnetic dipole transitions (using Op = $\mu$) and electric dipole transitions (using Op = m) are needed.

In order to simplify the writing of matrix elements the Dirac notation is often used. In this notation reversal of the order of the wave functions indicates a complex conjugate,

$$\langle a|A|b \rangle = \langle b|A|a \rangle^* \qquad (33, \text{ p. } 307) \qquad .$$

We may write the intensity for a right hand transition as

$$k \langle a|x + iy|b \rangle \quad \langle b|x - iy|a \rangle$$

following Dirac. This indicates that the matrix element is being multiplied by its complex conjugate.

It is often stated that only Hermetian operators may be used in quantum mechanics (28, p. 156). However, the operator $x \pm iy$ or $e^{\pm i\phi}$ is not Hermetian since the requirement

$$\langle \psi^*|A|\phi \rangle = \langle \phi|A^*|\psi^* \rangle$$

is not met. This also means the expectation value is not necessarily real, a requirement for an observable. This does not matter to us since it is the product of the expectation value with its complex conjugate that we use, it will be real and therefore will be observable.

## The Atomic Case

To illustrate the theory of MCD we will begin with some simple cases, the most elementary of which are transitions between s and p atomic orbitals as shown in Fig. 17. The orbitally degenerate p levels have
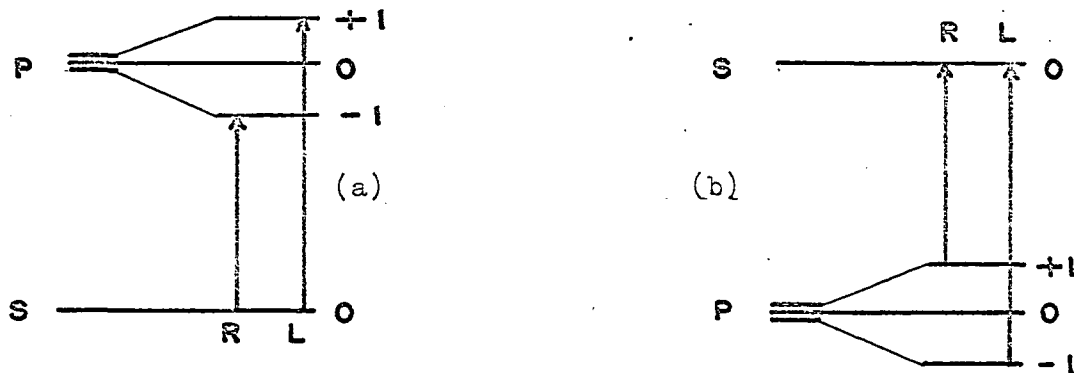


Fig. 17. Circularly polarized transitions for s → p

different energies when a magnetic field is applied, in this case in the

z direction. This change of energies is called Zeeman splitting. The

splitting will be of a magnitude proportional to the magnetic moment of

the electron involved and the external magnetic field $\Delta E = \mu \bar{H}$. The

magnetic moment results from the magnetic field developed by the orbiting

electron, and therefore depends upon the angular momentum of the orbital.

The diagonal terms of Eq. 4 (such as $\langle \psi_1 | L_z | \psi_1 \rangle$ ) are used to evaluate

the magnetic moment of a state.

The $p_x$ and $p_y$ orbitals may now be thought of as containing electrons

orbiting around the z axis, but circulating in opposite directions for

$p_x$ and $p_y$. Before the magnetic field was applied it was not possible to

distinguish between the orbitals $p_x$, $p_y$ and $p_z$ (34, p. 113). After the

field is established the energies of these three orbitals attain a value

depending upon their orbital angular momentum (m). This means it is now

necessary for the $p_x$ and $p_y$ wave functions to be written including the

complex quantity $e^{im\phi}$, (35, p. 8) which designates the value of m. Or

conversely, a wave function which must be written with such a complex

quantity possesses orbital angular momentum. The angular parts of these

wave functions are shown in Eq. 5. It can be seen that these are of the

form $e^{\pm i\phi}$ and therefore we can calculate which circularly polarized

transitions are permitted to each of the states by evaluating the transi-

tion moments. Since circularly polarized transitions are forbidden for

$\Delta m = 0$, we will not be interested in that case.

$$\psi_{p_x} = \frac{x + iy}{2} \qquad \psi_{p_y} = \frac{x - iy}{2} \qquad \text{Eq.(5)}$$

If the transitions are now represented by absorption bands with

Gaussian shape as in Fig. 18, the MCD resulting will be that of Fig. 19.

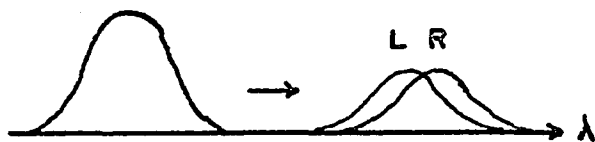This particular type of MCD is called "A term" MCD, and is the result of

Zeeman splitting.



Fig. 18.  Excited state splitting
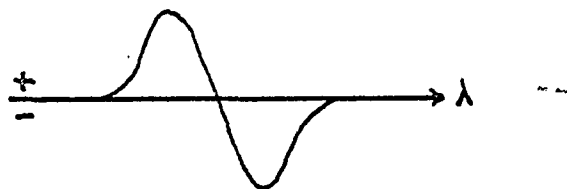


Fig. 19.  A term MCD

Both situations a and b in Fig. 17 will show A term MCD, but in addi-

tion b will have another effect since the ground state is degenerate.  This

effect occurs because the Zeeman splitting will change the energies of the

orbital components of the ground state (36, p. 204).  They will no longer

be populated thermally to the same extent, but rather their populations

will depend on the Boltzmann relation $N = N_o e^{-\frac{E}{KT}}$ .  This leads to the

results shown in Figs. 20 and 21.  The effect due to the populations of



Fig. 20.  Ground state splitting



Fig. 21.  A plus C term MCD

the levels is called "C term" MCD.

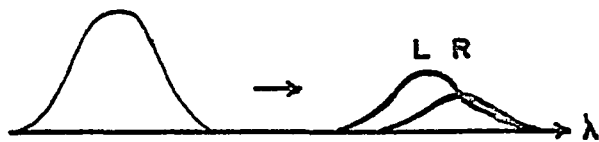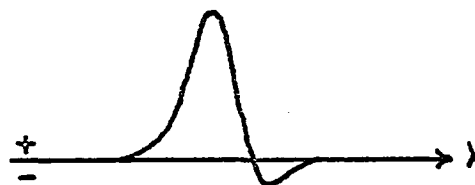So far nothing has been said about electron spin. However, in the event that there is no interaction between electron spin and orbit (approximately true for light atoms), it can be shown that spin has no effect on MCD. The splitting due to spin will be of the same magnitude in both ground and excited states as shown in Fig. 22. The result is
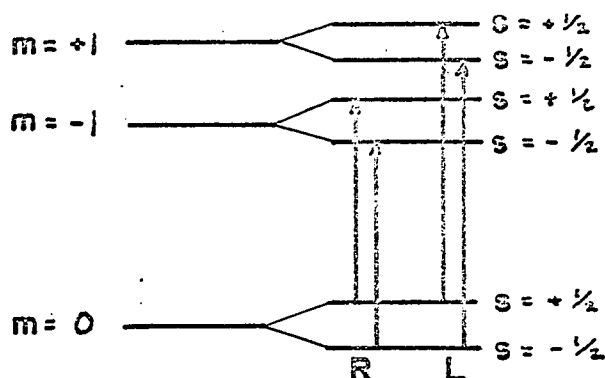


Fig. 22. Effect of spin on MCD

that the frequencies of the transitions are unaffected. Transitions in which the spin quantum number changes (such as $m=0$, $s = -\frac{1}{2} \longrightarrow m=+1$, $s = +\frac{1}{2}$) are highly forbidden, so they do not contribute in Fig. 22.

Other examples of simple atoms could be shown, such as transitions between p and d levels, or between d and f levels. However, the results for these are almost identical to those for the s $\rightarrow$ p case described (36, p. 104).

## The Molecular Case

Unfortunately the MCD of the compounds we will consider is not so simple as that of atoms. We take as an example a case which approaches more closely the situation in biologically interesting molecules.

Suppose an atom with p orbitals has arranged around it charges (e.g., a crystal field or ligands) such that the degeneracy of the p levels is now lifted electrostatically (35, pp. 65-78). The moving electrons in the p orbitals interact strongly with the perturbing charges and may be
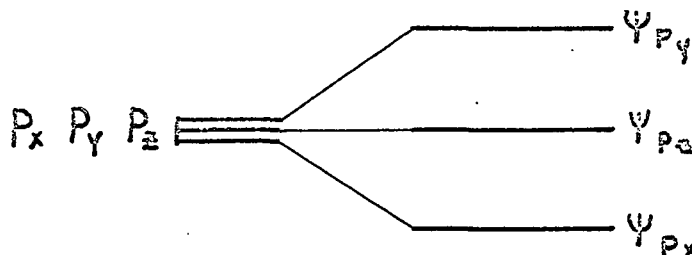


Fig. 23. Electrostatic splitting of p levels

considered to exchange angular momentum with the particles which bear the charges (28, p. 259). This exchange erases any trace of an exact orbital angular momentum (m) for the orbitals. Mathematically this is stated by writing the angular parts of the states $\psi_{px}$ and $\psi_{py}$ as linear combinations of the m=+1 and m=-1 states. The z state is not of interest to us. It can be seen that these states

$$\psi_{px} = \frac{1}{\sqrt{2}} \left[ \frac{x + iy}{\sqrt{2}} + \frac{x - iy}{\sqrt{2}} \right]$$

$$\psi_{py} = \frac{i}{\sqrt{2}} \left[ \frac{x - iy}{\sqrt{2}} - \frac{x + iy}{\sqrt{2}} \right]$$

can now be described by real functions, that is $\psi_{px} = x$ and $\psi_{py} = y$. Since these states are not complex, they no longer may be considered to possess orbital angular momentum. It is said that the orbital angular momentum

is "quenched". There is as much electron circulation in one direction around the z axis as the other. There will be just as many right hand transitions as left hand transitions to each state and therefore no circular dichroism.

Now when a magnetic field is applied, there are no orbital degeneracies to split, so there is no possibility of A or C terms. But the magnetic field does have an effect in this case which tends to "unquench" the angular momentum to an extent linear with the external magnetic field strength.

If there is a possibility of a magnetic transition between two states, in this case between the $\psi_{px}$ and $\psi_{py}$ wave functions, there can be mixing of some of the $\psi_{py}$ into the $\psi_{px}$ and some of the $\psi_{px}$ into the $\psi_{py}$, unquenching the orbital angular momentum somewhat. This leads to a probability of more right hand transitions to one state, more left hand transitions to the other. MCD resulting from this effect is called "B term" MCD, and will be most important for the compounds which will be discussed.

The sign of the mixing term will depend upon the direction of the magnetic dipole transition, that is for the levels in Fig. 24 it depends upon whether the transition is x→y or y→x. The signs will be opposite, $M_{xy} = -M_{yx}$ (37). This shows mathematically that the B terms associated with the two interacting levels will be of opposite sign.

If the x and y transitions are now represented by Gaussian bands, the resulting MCD is shown in Fig. 24.

From the perturbation derivation (See Appendix I) it is seen that the form of the B term is
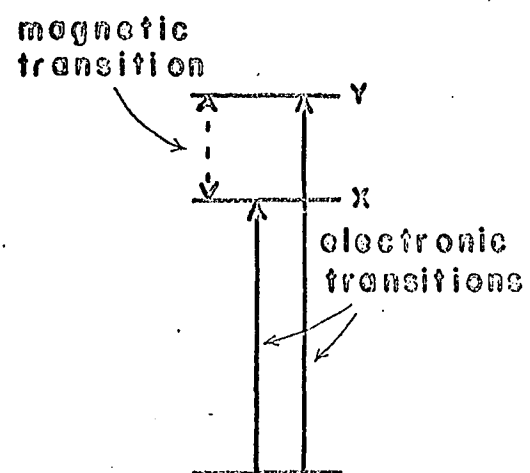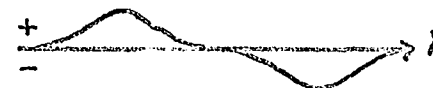
Fig. 24. B term MCD from two interacting levels

$$\frac{\overline{M} \cdot (\overline{R} \times \overline{R}')}{\Delta E} \quad \text{where } \overline{M} = k\langle \psi_x | L_z | \psi_y \rangle \qquad\qquad Eq.(6)$$

$$L_z = \text{ang. mom. operator } (x\frac{\partial}{\partial y} - y\frac{\partial}{\partial x})$$

where $\overline{M}$ is a magnetic dipole transition between two of the levels and $\overline{R}$ and $\overline{R}'$ are two electric dipole transition moments separated in energy by $\Delta E$. Note that $\overline{M}$ is an off-diagonal matrix element of the type in Eq. 4 . From Eq. 6 we can see that certain features are required in order to have a B term:

1. Two electric transitions with some perpendicular component.

2. An allowed magnetic transition between states common to $\overline{R}$ and $\overline{R}'$ and possessing a component perpendicular to the plane containing $\overline{R}$ and $\overline{R}'$.

It should be noted that the constant coefficients in $\overline{M}$ and $\overline{R}$ contain the charge of the particle, therefore the sign of the B term will depend on the sign of the charge.

As the electrostatic splitting of the two bands becomes smaller, the unquenching of the orbital angular momentum by the magnetic field becomes more efficient. In the limit that the two bands are orbitally degenerate we have returned to the A or C term case. Fig. 25 shows what the B term for two interacting bands looks like as the energy difference between the transitions is reduced. At a certain point it becomes impossible to tell B term from A term MCD.

We will now show by a simple derivation that when two states (j and k) are magnetically mixed B term MCD will result. The initial states (see Fig. 26) are assumed real and therefore possess no orbital angular
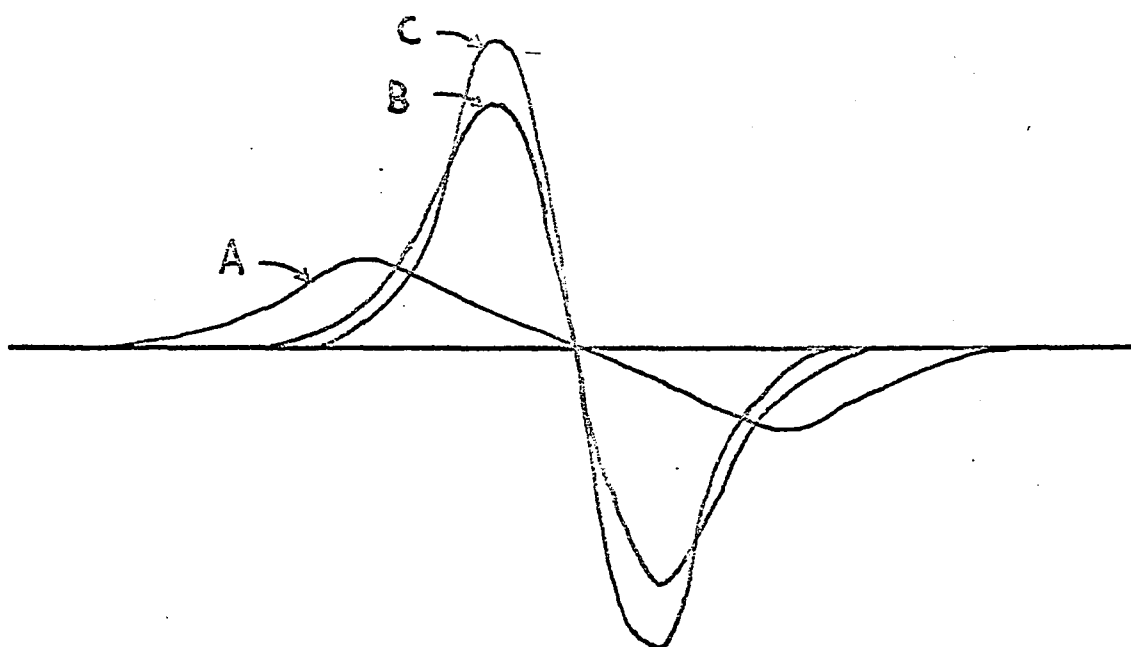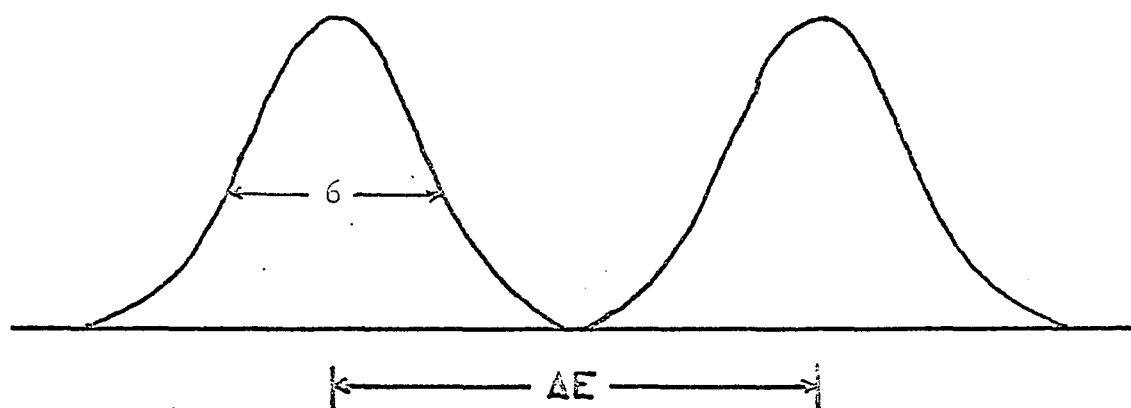
Fig. 25. B term for two identical interacting bands with various energy differences

momentum. The transition moments for right hand and left hand cases are
written for the $g \rightarrow j$ transition, squared to obtain intensities, and then
the right hand absorption is substracted from left hand absorption to
yield MCD. The result is a real quantity as all observables must be. The
magnetic mixing factor is written $\overline{M}=ia$ in order to make it easier to
follow manipulation of the imaginary number i. Terms containing $a^2$ are
dropped because they are very small and because we are interested only
in the terms linear in a magnetic field.

$$\text{—————} \quad k \rightarrow k + iaj$$

$$\text{—————} \quad j \rightarrow j + iak$$

$$\text{—————} \quad g$$
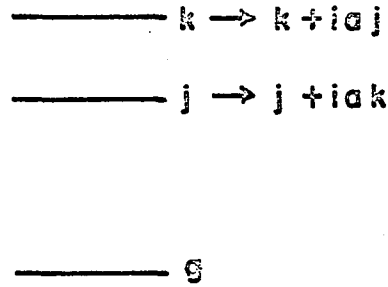
Fig. 26. Levels for B term derivation

right hand transition moment

$$\langle g|Ai(x+iy)|j-iak\rangle \; \langle j+iak|-Ai(x-iy)|g\rangle$$

$$= (Ai[gxj + igyj - iagxk + agyk])$$

$$x(Ai[-jxg + ijyg - iakxg - akyg]) =$$

$$\begin{bmatrix} -gxjjxg - igyjjxg + iagxkjxg - agykjxg \\ + igxjjyg - gyjjyg + agxkjyg + iagykjyg \\ - iagxjkxg + agyjkxg - a^2gxkkxg - ia^2gykkxg \\ - agxjkyg - iagyjkyg + ia^2gxkkyg - a^2gykkyg \end{bmatrix} \quad x[-A^2]$$

Here the term gxjjxg is shorthand for $\langle g|x|j\rangle \langle j|x|g\rangle$ .

left hand transition moment

$\langle g|Ai(x-iy|j - iak\rangle \langle j + iak|- Ai(x+iy)|g\rangle$

$= (Ai[gxj - igyj - iagxk - agyk])$

$x(Ai[-jxg - ijyg - iakxg + akyg])$

$$\begin{bmatrix} - gxjjxg + igyjjxg + iagxkjxg + agykjkg \\ - igxjjyg - gyjjyg - agxkjyg + iagykjyg \\ - iagxjkxg - agyjkxg - a^2gxkkxg + ia^2gykkxg \\ + agxjkyg - iagyjkyg - ia^2gxkkyg - a^2gykkyg \end{bmatrix} x[-A^2]$$

Left hand - Right hand intensities $= - A^2[4agxjkyg - 4agyjkxg]$

$= - 4 A^2 a[gxjkyg - gxkjyg]$

$= - (-i) 4 A^2(ia)[gxjkyg - gxkjyg]$

$= i 4 A^2 \overline{M}[gxjkyg - gxkjyg]$

MCD $= i 4 A^2 \overline{M}[\langle g|x|j\rangle \langle k|y|g\rangle - \langle g|x|k\rangle \langle j|y|g\rangle]$

### d-d Transitions

Another somewhat more complicated molecular arrangement which gives

additional insight into the origin of MCD is provided by transition metal

complexes.  The spectra of these compounds are characterized by transitions

between the d orbitals of the metal ions, transitions which are normally

forbidden but slightly allowed by vibrations which mix in other states

with the d states.

The d orbitals of the free metal ion are degenerate, this has already

been mentioned in the atomic case.  But the ligands of a metal-ligand

complex will affect the energies of the various d orbitals to different

degrees, partially or perhaps completely destroying the degeneracy.  We

will illustrate using complexes of octahedral symmetry which split the d orbitals as shown in Fig. 27 (38, p. 53).
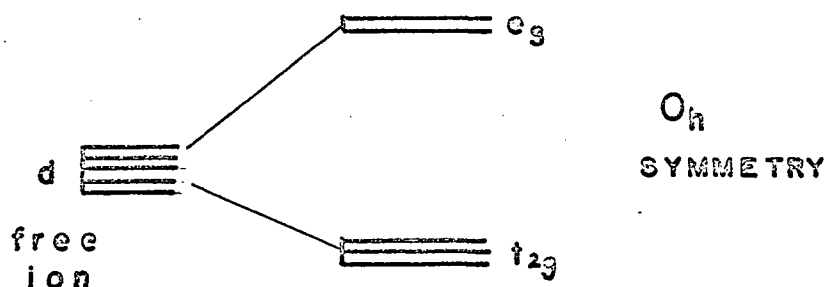


Fig. 27. d shell less than half filled

The angular parts of the five d orbitals are listed below as they may be written before electrostatic splitting occurs (39, p. 63).

$$d_{+2} = \sqrt{\tfrac{3}{8}}\,(x + iy)^2$$

$$d_{+1} = -\sqrt{\tfrac{3}{2}}\,(x + iy)z$$

$$d_{o} = \tfrac{1}{2}\,(3z^2 - r^2)$$

$$d_{-2} = \sqrt{\tfrac{3}{2}}\,(x - iy)z$$

$$d_{-1} = \sqrt{\tfrac{3}{8}}\,(x - iy)^2$$

After the splitting they must be written as below. The reasons for writing them in this way are similar to the case described above for the electrostatic splitting of p orbitals.

$$t_{2g}{}^{o} = \frac{1}{\sqrt{2}}\,(d_2 - d_{-2}) = \frac{1}{\sqrt{2}}\,[\sqrt{\tfrac{3}{8}}\,(x+iy)^2 - \sqrt{\tfrac{3}{8}}\,(x-iy)^2]$$

$$t_{2g}{}^{-} = d_{-1} \qquad\qquad = \sqrt{\tfrac{3}{2}}\ (x-iy)z$$

$$t_{2g}{}^{+} = d_{+1} \qquad\qquad = -\sqrt{\tfrac{3}{2}}\ (x+iy)z$$

$$e_{g}{}^{a} = d_{o} \qquad\qquad = \tfrac{1}{2}\ (3z^{2}-r^{2})$$

$$e_{g}{}^{b} = \sqrt{\tfrac{1}{2}}\ (d_{2}+d_{-2}) \qquad = \frac{1}{\sqrt{2}}\ [\ \sqrt{\tfrac{3}{8}}\ (x+iy)^{2} + \sqrt{\tfrac{3}{8}}\ (x-iy)^{2}]$$

If now the matrix elements for transitions between $e_{g}$ and $t_{2g}$ levels
are evaluated, we find that although both right-hand and left-hand transi-
tions are allowed for $t_{2g}{}^{\pm} \to e_{g}$, right-hand transitions are predominant
for $t_{2g}{}^{-} \to e_{g}$ and left-hand transitions are predominant for $t_{2g}{}^{+} \to e_{g}$. So
we are left with the situation as shown in Fig. 28.

Fig. 29 shows the same case for the d levels split by an octahedral
field, but with the d shell more than half-filled, that is $d^{n}$, (n=6,7,8,9).
The levels are inverted (24, p.146) and it can be seen now that the sign
(handedness) of the longest wavelength band should change sign. The MCD
expected from this is shown in Fig. 30.

The reason for the inversion of levels for a more- than- half-filled
shell is that the system now acts as though positive holes occupy the d
shell, changing the sign of the charge and therefore of the magnetic
moment as in Eq. 7 (39, p. 69).

$$\mu = \frac{ep}{2m} \qquad \begin{array}{l} p - \text{ang. mom. } \hbar \text{ of particle} \quad \text{of mass m} \\ e - \text{charge of particle} \end{array} \qquad\qquad Eq.(7)$$

## Cylindrical Symmetry

In the case of diatomic molecules, or more complex molecules with
cylindrical symmetry (such as benzene or metallo-porphyrin) there is the
possibility that a component of orbital angular momentum may still remain
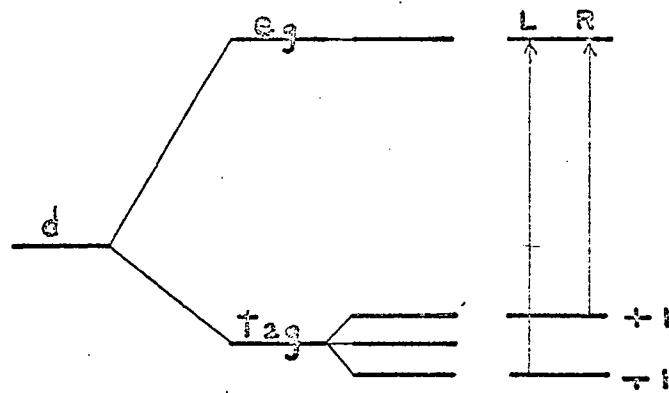
Fig. 28. Circularly polarized transitions, shells less than half filled
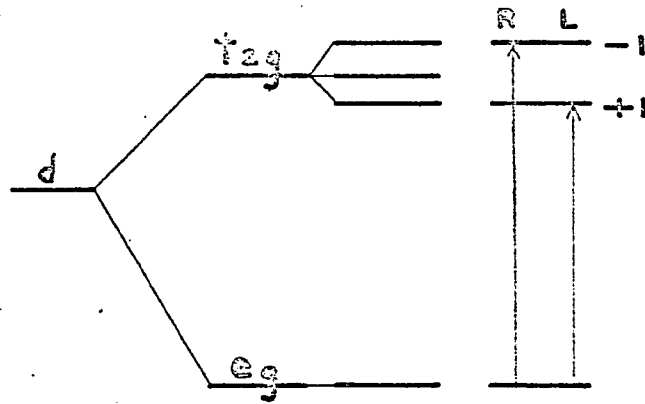


Fig. 29. Circularly polarized transitions, shells more than half filled
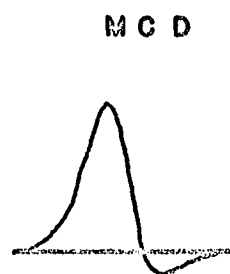
ABSORPTION

MCD

ABSORPTION

MCD

$t_{2g} \longrightarrow e_g$

$e_g \longrightarrow t_{2g}$

A + C
TERM

A TERM ONLY

(a)

(b)

42
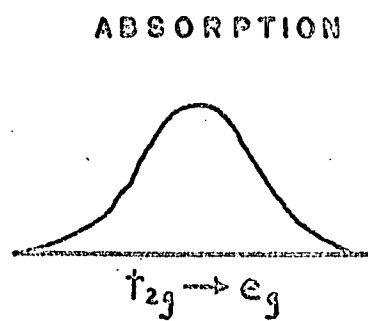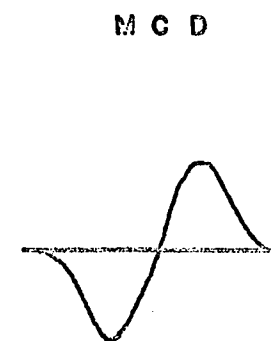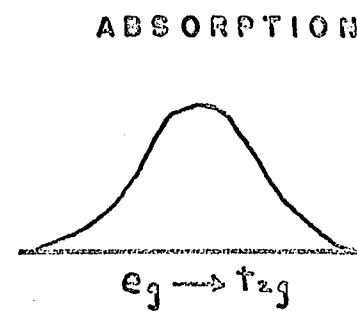
Fig. 30.   MCD from d levels

(a) less than half filled

(b) more than half filled

unquenched (40).  The angular momentum may be defined with respect to the axis of the cylinder.  In Fig. 31 this is illustrated by the $Cl_2^-$ ion (35, p. 199).

From the figure it can be seen that the x and y orbitals remain essentially undisturbed and there is no reason for them to lose their exact quantum number m.  The z orbitals point in such a direction that there will be maximum interaction between the electrons and nuclei, quenching any discrete angular momentum they may have possessed before the molecule was formed.

Sigma bonding and antibonding orbitals are formed by the $z_1$ and $z_2$ atomic orbitals and pi bonding and antibonding orbitals come from the $y_1, y_2, x_1$, and $x_2$ orbitals.  The $\pi_u$ and $\pi_g$ states are both orbitally degenerate, but since they are also occupied no C term MCD would be expected, only A term.

## Polyatomic Molecules

For most of the molecules of biological interest the orbital angular momentum is quenched (30, p. 267).  The orbits of the electrons cannot be determined exactly, although they can be known well enough to be characterized by their symmetry.  It is in terms of these symmetries that we can best discuss the electronic structures of polyatomic molecules.

Exceptions to the quenching of orbital angular momentum in nonlinear molecules have been mentioned above.  This may be expected to occur with molecules of sufficiently high symmetry such as the cylindrical symmetry of the metallo-porphyrins.

It should also be emphasized that the microsymmetry of the area
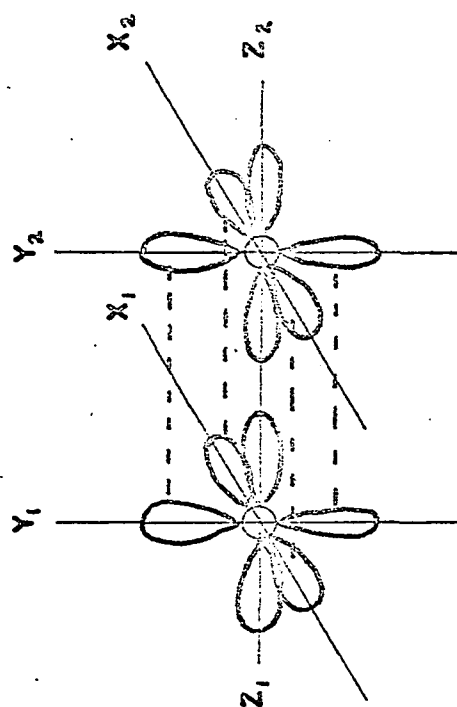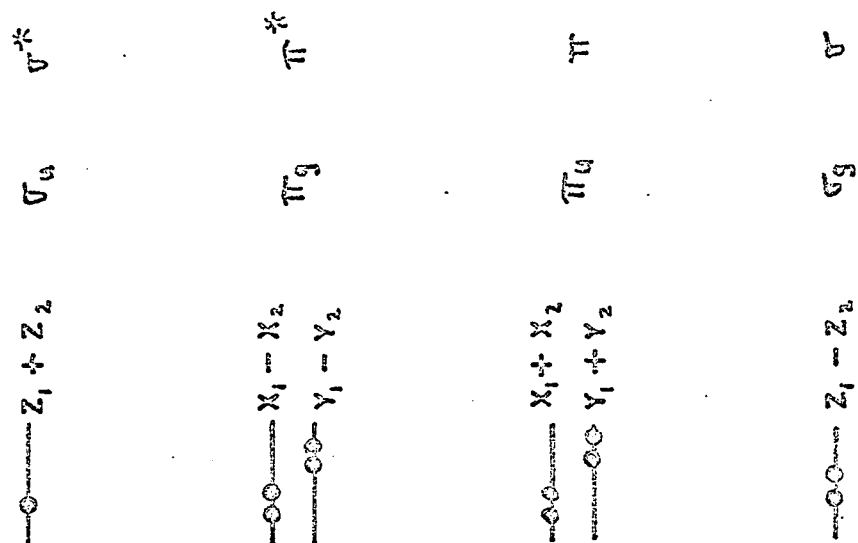
Fig. 31. The $Cl_2^-$ ion

surrounding the chromophore is of the most importance in determining

whether quenching occurs. For instance, an -R substitution destroying

the cylindrical symmetry of the complete metallo-porphyrin molecule has

minor effects on both the absorption and MCD spectra (38, p. 90).

Since there is no orbital angular momentum associated with most

polyatomic molecules, there is no spin-orbit coupling, A-term or C

term MCD to consider. The electrons are usually in orbits which may be

classified as belonging to σ, or π bonds or n non-bonding orbitals.

There is the possibility of magnetic mixing between all energy levels as

discussed above, leading to B term effects. This could lead to MCD spectra

too complex to be useful. Some knowledge about which levels are mixing

may be inferred by studying several types of experimental and theoretical

information. These are:

1. The observed sign and shape of the MCD.

2. The energy differences between the levels.

3. The symmetry permitted magnetic transitions between the levels.

4. The area under the MCD band.

5. Known directions of transition moments.

## Summary

From the theory above we can make several observations and

predictions:

1. The sign of the MCD should depend on the sign of the charge

   involved in the transition.

2. MCD should be useful for the study of orbital angular momentum

   quenching effects and spin-orbit interactions.

3. Degeneracies in the ground state can be observed by studying the temperature dependence of MCD.

4. Some information about the relative directions of transitions moments is available from MCD.

# IV. RESULTS AND DISCUSSION

## The Rare Earths

The temperature dependence of MCD for a rare earth (didymium) glass reveal clear examples of A and C term MCD. The advantages and disadvantages of using didymium glass are given below.

Advantages

1. The rare earths exhibit narrow band spectra of transitions between their f electron levels. As seen from Fig. 18, the narrower the bandwidth for any absorbance and splitting, the greater will be the MCD. Therefore the MCD of the rare earths is easy to obtain experimentally.

2. Didymium glass contains a number of rare earths.

3. The glass is easy to handle for temperature measurements, no problems of freezing, boiling or bubble formation are encountered as when using solutions.

4. The large number of transitions increases the possibility that several different types of MCD effects may be observed with one sample.

Disadvantages

1. The rare earths have so many transitions so close together that it has not been possible to assign the energy levels with any degree of certainty. Therefore it is not possible to know which levels possess orbital degeneracy.

2. With absorption bands very close together or on top of one another it is difficult to distinguish two C term effects
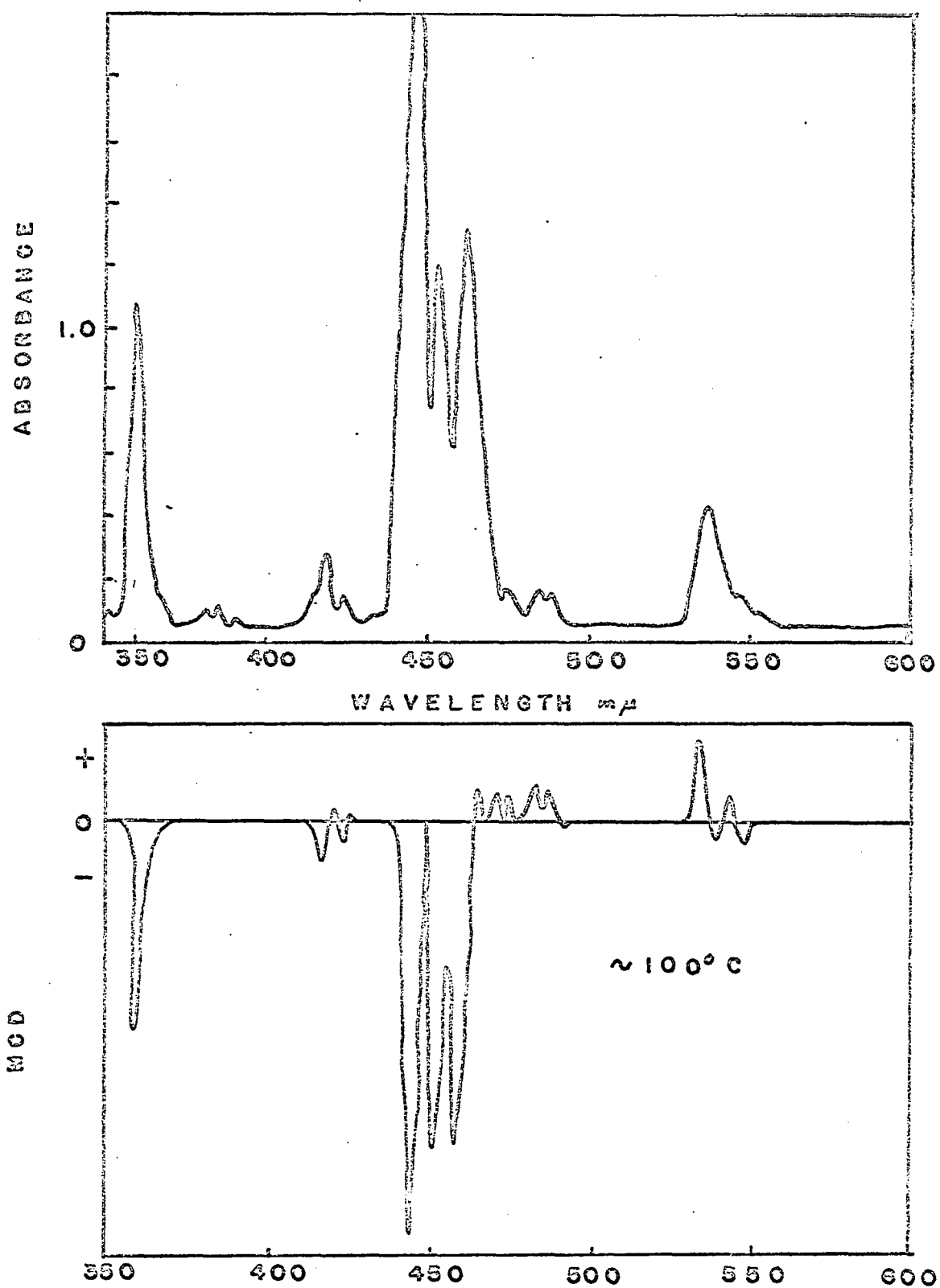
Fig. 32.  Absorbance and high temperature MCD of didymium glass
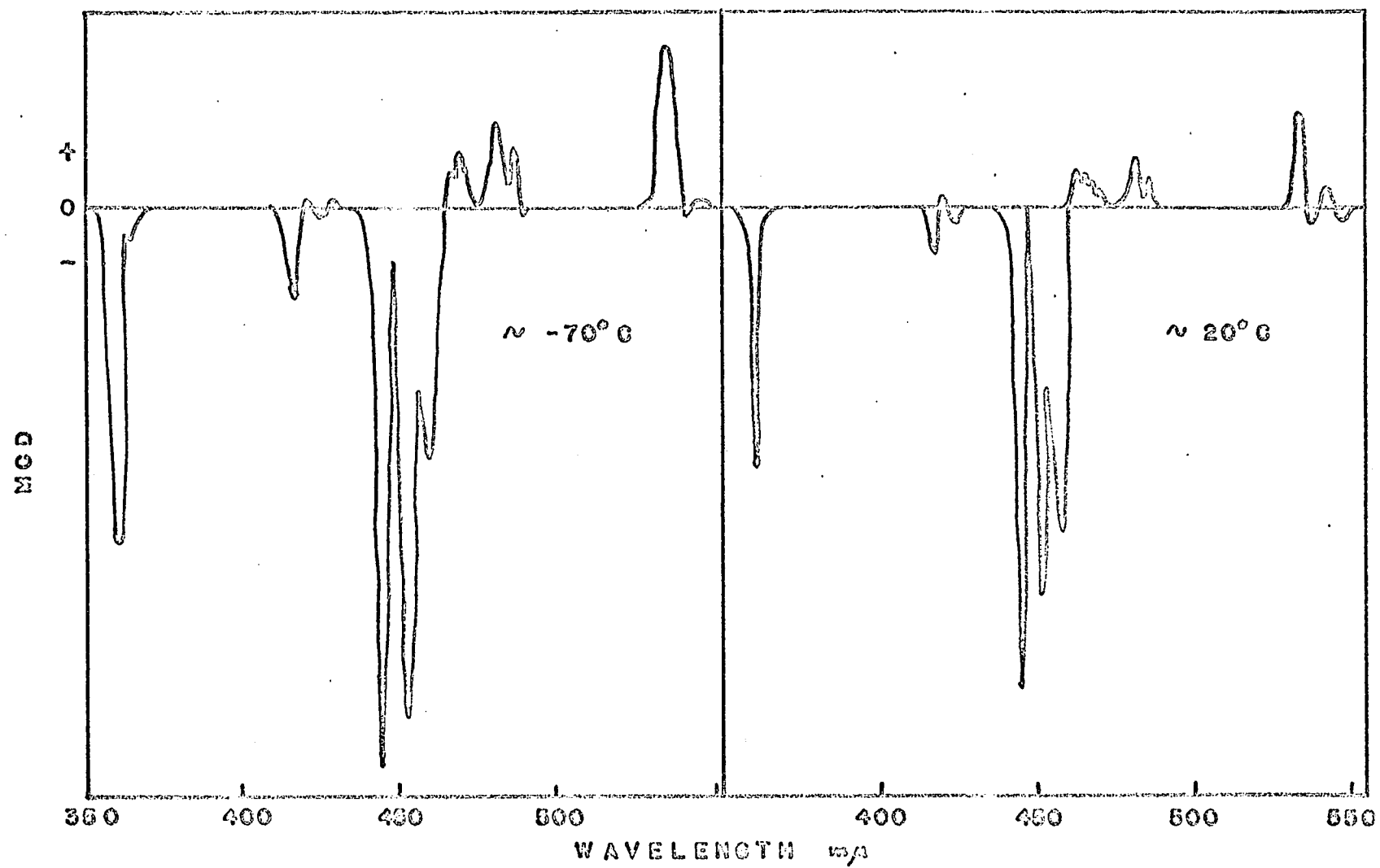
Fig. 33. Room and low temperature MCD of didymium glass

of opposite sign from a single A term.

3. Since the rare earth atoms are in a condensed state, random crystal field effects will tend to broaden the absorption bands. However, this is not serious since the f electrons are shielded by two other outer electron shells.

Interpretation of results

1. The bands all appear to be temperature dependent, the magnitudes vary roughly as 1/T. From this we can conclude:

a) B terms are relatively small or non-existent

b) The transitions originate in degenerate ground states.

2. As the temperature increases, the populations of the ground state levels tends to become equalized. Therefore the C terms should become smaller while the A term remains the same. This should result in spectra at higher temperatures with more of an A term appearance. This appears to be happening for the absorption bands at 419 mμ and 537 mμ.

3. There is an _increase_ in MCD with increasing temperature for the bands appearing at 540-550 mμ. This can be accounted for by the population of a low-lying electronic level. If this level exists, and transitions take place to an excited state common with the 540 mμ absorption, the level would be expected to lie about 30 cm$^{-1}$ above the ground state. This state would be approximately 90% populated at the temperatures used.

Inorganic Systems

Temperature dependence

The absorbance and temperature dependence of the MCD of $K_3Fe(CN)_6$ are shown in Fig. 34. The graph in Fig.35 indicates that the MCD of ferricyanide ion follows very closely a 1/T dependence. This may be interpreted as meaning B terms are quite small for these bands. Only the 425 mμ band indicates some slight leveling off of the MCD as temperature is increased, evidence of some B term contribution. It seems therefore that the spectra are almost exclusively C terms. This is more likely to occur with wide band widths, as for any given Zeeman splitting the A terms will decrease as the band is made broader.

Further temperature dependence data is given in the table below.

Table 1. Temperature dependence data for the MCD of cobalt and nickel ions

| Ion | λ mμ | Temp. Range | MCD change | 1/T change |
|---|---|---|---|---|
| $Co(H_2O)_6^{+2}$ | 520 | 3°C---63°C | 12% | 18% |
| $Ni(H_2O)_6^{+2}$ | 385 | 5°C---60°C | 15% | 17% |

It appears that the cobalt ion may exhibit a significant amount of B term MCD for the 520 mμ band, whereas the nickel probably has little or no B term effect.

Tetrachloroplatinate (II) ion

Another inorganic system was investigated in an attempt to assign one of the excited state energy levels associated with the band at 330 mμ. The absorption and MCD of tetrachloroplatinate are shown in Fig. 36.
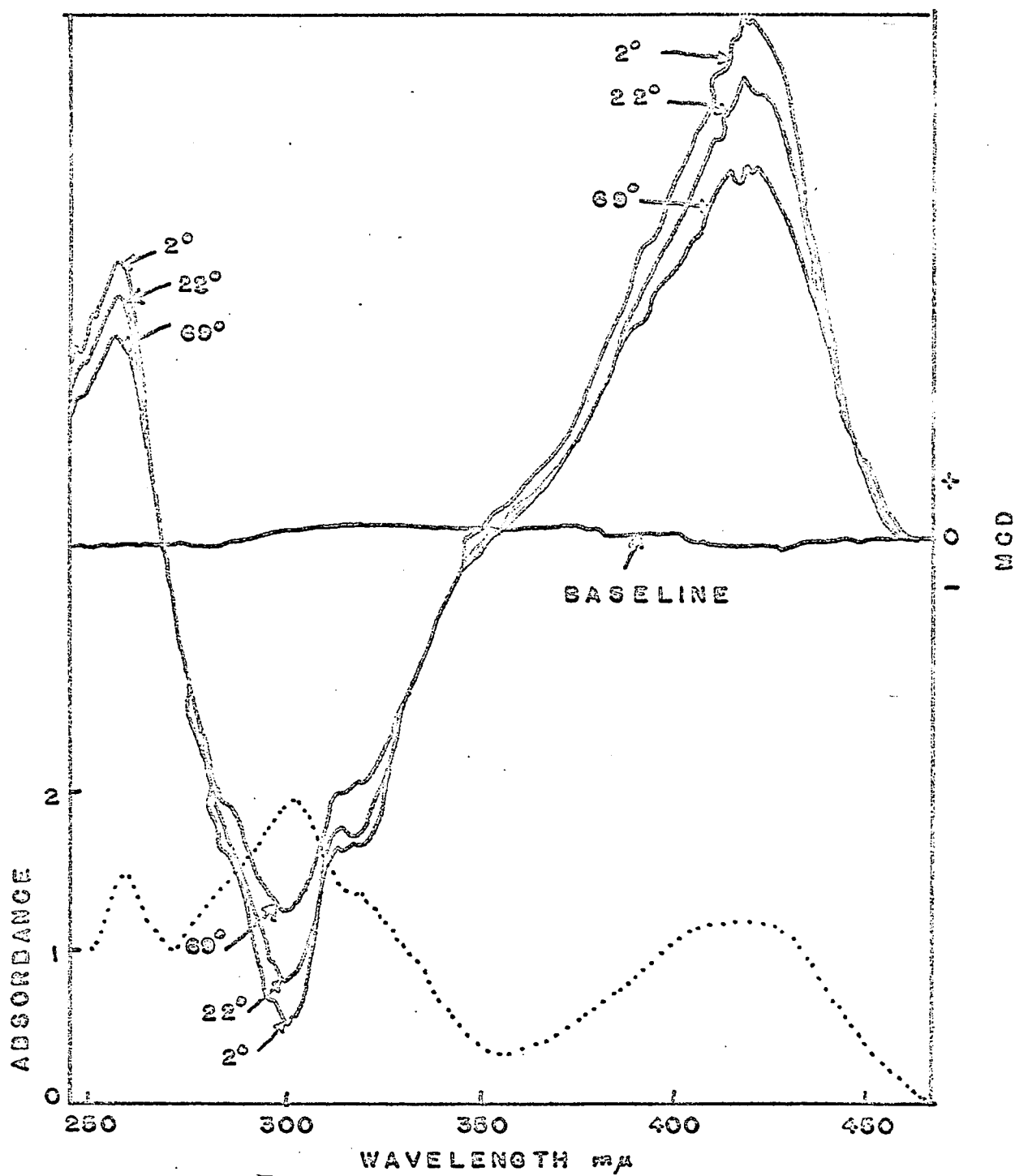
Fig. 34. Absorbance (· · · · · · · · · ·) and MCD (————) for $K_3$ Fe(CN)6
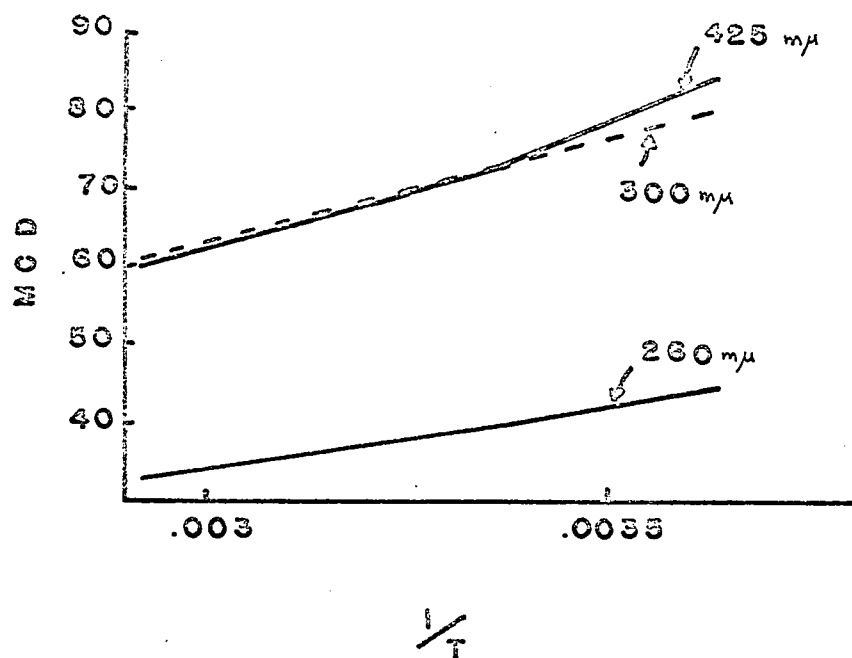
Fig. 35. Temperature dependence of MCD for $K_3$ $Fe(CN)_6$ at three wavelengths
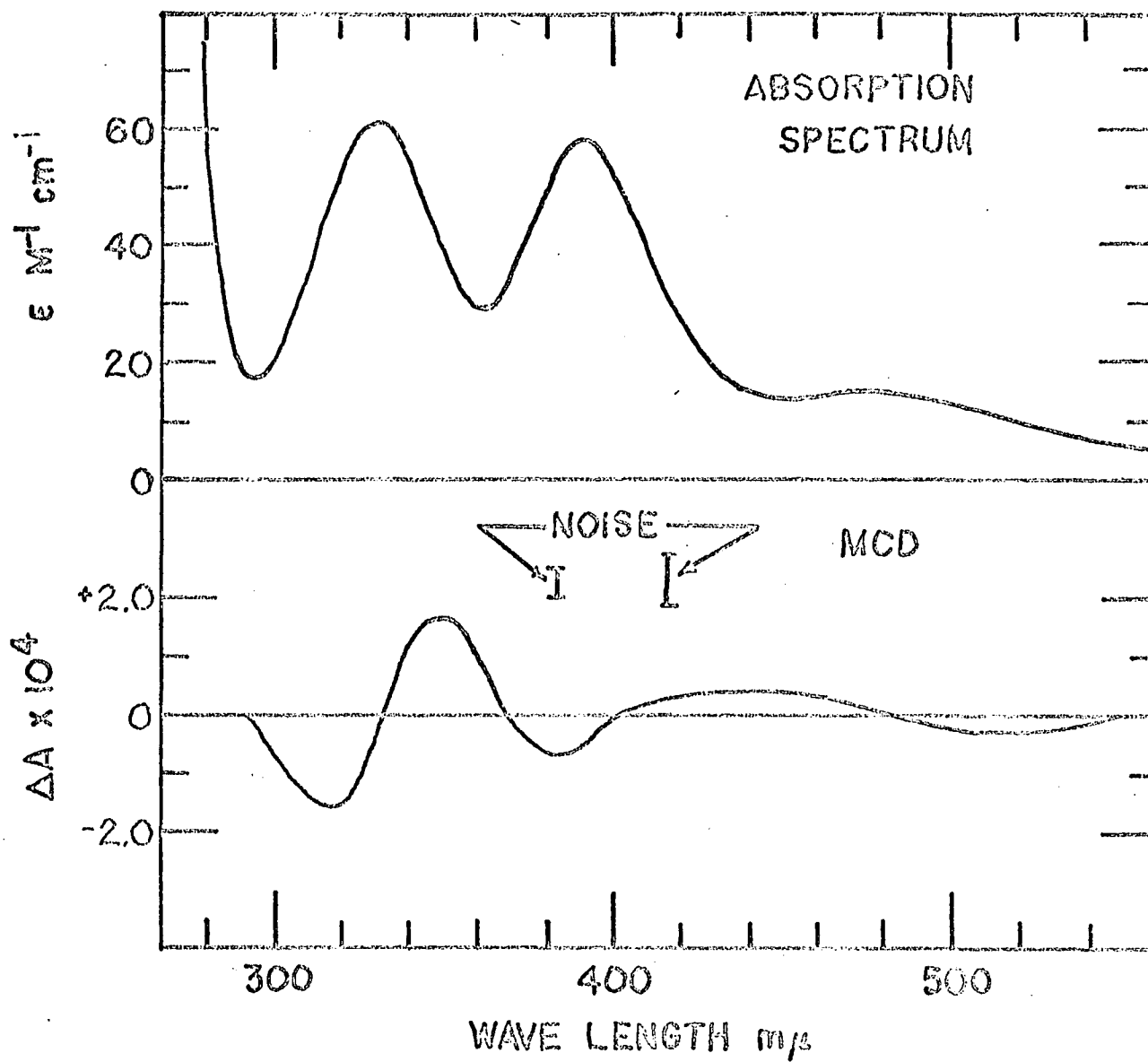
Fig. 36. Absorption and MCD for tetrachloro platinate ion

The band at 330 mµ presents an A term appearance in the MCD which indicates excited state degeneracy. If this degeneracy is broken by a magnetic field each Zeeman component will be changed in energy by an amount δ for a total splitting of 2 δ. The splitting may take place in either the ground or excited state, giving δg and δm respectively. A computer program was written using a least squares method to fit the experimental MCD to separate values of δg and δm. The results gave δg = 0.00 cm$^{-1}$ and δm = 0.45 cm$^{-1}$.

The lack of a Zeeman splitting of the ground state agrees with the assignment of the state to $^1A_{1g}$. The presence of a splitting of the excited state supports the assignment as $^1Eg$. (12) Also, the magnetic moment of $^1Eg$ level would be expected to be one Bohr magneton. The experimental value of δm corresponds to a magnetic moment of 0.8 Bohr magnetons, the correct order of magnitude for the expected moment.

$$\Delta E = H \, n \, \beta$$

$$0.45 \text{ cm}^{-1} = (12 \times 10^3 g)(n)(4.67 \times 10^{-5} \text{ cm}^{-1} g^{-1} \text{dipole}^{-1})$$

$$n = \frac{0.45}{0.56} = 0.8 \text{ Bohr magnetons}$$

Sign of MCD

In the theoretical section the effects of changing from an electron to a hole formalism were discussed. Essentially this would be expected to change the sign of MCD if holes rather than electrons are involved in the transitions. There is some experimental evidence from the inorganic systems that this does indeed occur.

Fig. 37 illustrates again the arrangement of levels and MCD to be expected if the states are inverted. This is, of course, a much simplified
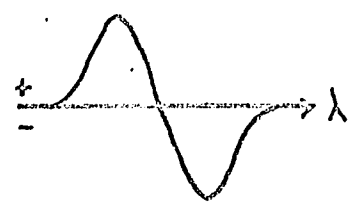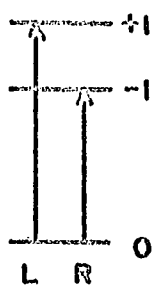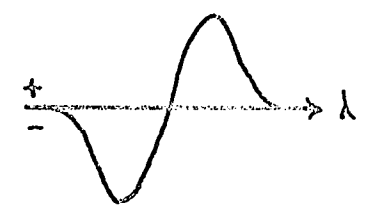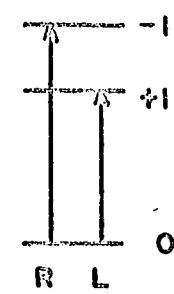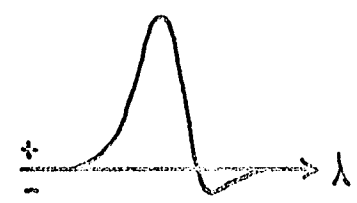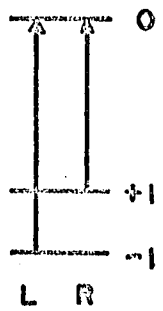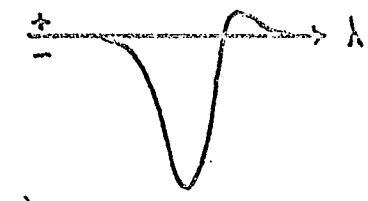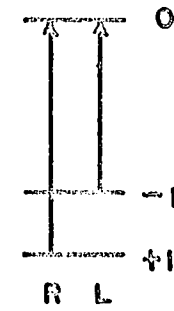
Fig. 37.  MCD resulting from inverted levels

view of the true situation. However, the inversion of levels will still have essentially these effects.

Examples of case (a) in Fig. 37 are not available. The results of Stephens, Schatz, et al. (41) on the Cr(III) complexes with $NH_3$, $H_2O$ and CN give examples of the (c) case. Since Cr(III) is a $d^3$ system, the electron formalism holds. Case (b) is represented by the $K_2PtCl_4$ MCD discussed above. The tetrachloroplatinate ion has the $d^8$ configuration corresponding to two holes. Case (d) includes $Co(H_2O)_6^{+2}$ which is a $d^7$ system, and the 395 m$\mu$ band of $Ni(H_2O)_6^{+2}$, a $d^8$ system. The MCD spectrum of the latter ion is shown in Fig. 38.

The ideal system in which to look for the sign change would be $d^1$ vs. $d^9$ configurations. These are represented by $Ti(H_2O)_6^{+3}$ and $Cu(H_2O)_6^{+2}$, respectively. Unfortunately Ti(III) exhibits no MCD for the 495 m$\mu$ band representing the $t_{2g} \rightarrow e_g$ excitation of the single d electron. This may be due to a Jahn–Teller distortion which always tends to remove the degeneracy needed to have orbital angular momentum. Likewise, the $e_g$ ground state of Cu(II) is distorted by the Jahn–Teller effect. Possibly some $d^1$ and $d^9$ systems exist which exhibit MCD, but this will be left for experts in inorganic chemistry to determine.
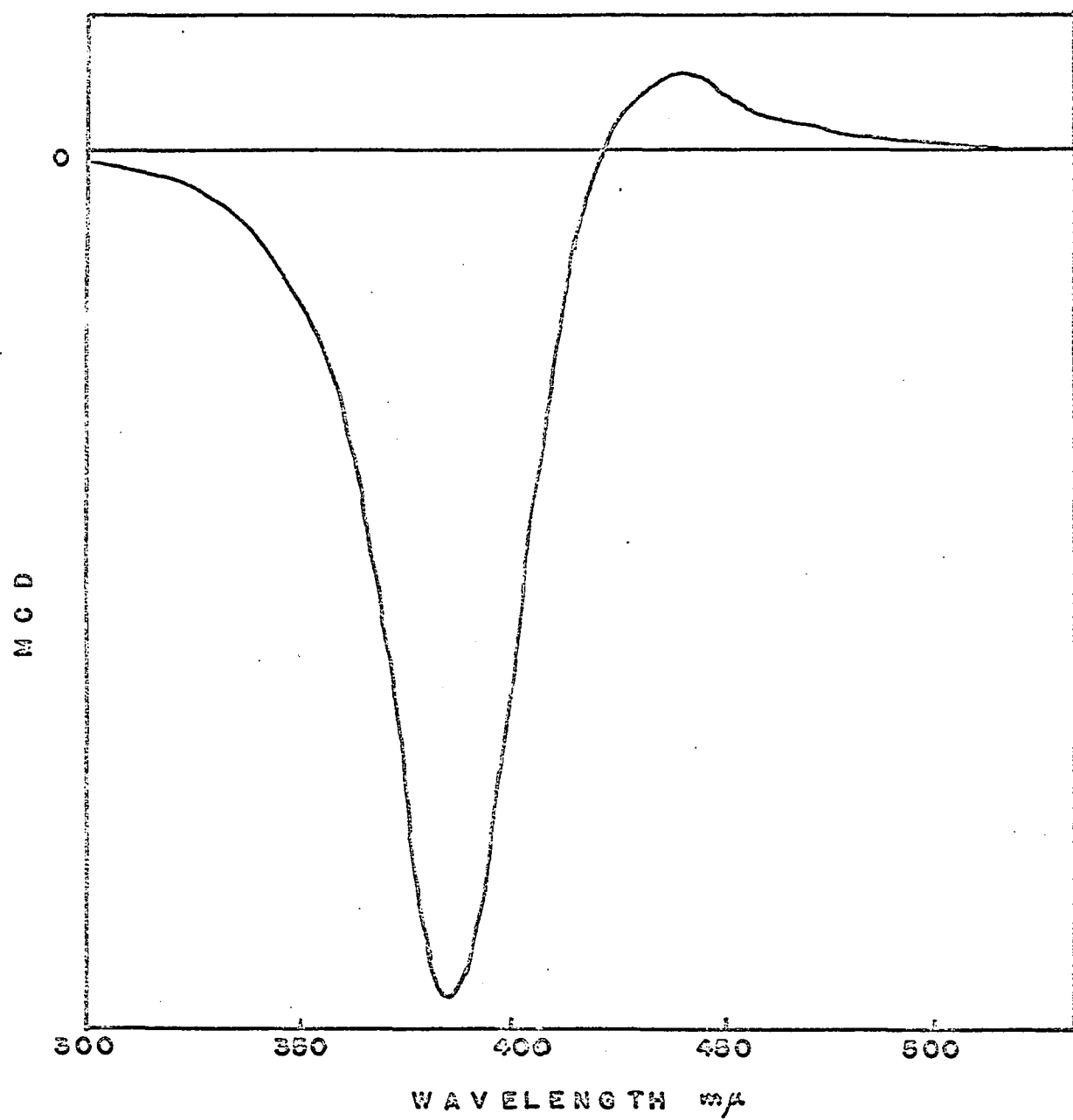
Fig. 38. MCD of $Ni(H_2O)_6^{+2}$

The Substituted Benzenes

A very important part of the spectroscopy of biological compounds

deals with the absorption of light by aromatic structures. Many

biologically interesting molecules contain such groups and the spectra

are in an easily accessible region.

The spectral effects observed in the more complex aromatic structures

are often correlated with those found in simple benzene derivaties, there-

fore the substituted benzenes can serve as models. However, there still

exist some uncertainties in understanding the spectra of even these simple

molecules, notably in assigning transitions to certain symmetry changes

and in direction of transition moments. These difficulties hamper the use

of aromatic spectral properties to help solve biological problems. There-

fore the first step should be to find what MCD can tell us about the model

compounds.

From the theory discussed above, it was seen that if two bands mix

and MCD occurs, then certain conditions must have been met. From this we

can infer certain properties for the electronic structure of the molecule.

In view of this possibility, it was decided to study the MCD of the sub-

stituted benzenes in an attempt to shed some new light on their electronic

properties. This seemed particularly feasible after several randomly

picked benzene derivatives showed easily measurable and interesting MCD

spectra. A portion of the results in this section has been reported

previously (14).

The ultraviolet absorption

The UV absorption of benzene is characterized by three bands, the

$A_{1g} \rightarrow B_{2u}$ ($L_b$) band at 256 mμ, the $A_{1g} \rightarrow B_{1u}$ ($L_a$) band at 203 mμ, and the $A_{1g} \rightarrow E_{1u}$ band at 180 mμ. The $L_a$ and $L_b$ bands are forbidden, the $A_{1g} \rightarrow E_{1u}$ band is allowed. The transitions correspond to changes in the electronic structure of the molecule as shown in Fig. 40. The signs correspond to the signs of the electronic wavefunctions as seen on one side of the molecular plane.

The $A_{1g} \rightarrow B_{1u}$ transition involves changes in the wave functions at the positions of the _atoms_, so is called L_a_. The signs of the wave functions change in the _bond_ region for $A_{1g} \rightarrow B_{2u}$ and are termed L_b_ (42). The direction of the transition moment for the $L_a$ transition is considered to be through the atoms, the transition moment for the $L_b$ band is through the bonds (see Fig. 41).

Origin of MCD

There are a number of reasons for believing the MCD of the $L_b$ band is due primarily to mixing between the $B_{1u}$ and $B_{2u}$ levels. None of these reasons alone proves conclusively that such is the case, but taken together they suggest strongly that this is the correct interpretation.

The levels closest to the $B_{1u}$ and $B_{2u}$ levels are those for the ground state ($A_{1g}$) and the next higher excited state ($E_{1u}$). Therefore the $B_{1u}$ and $B_{2u}$ levels could be mixing with either or both of these, or with another level even higher in energy than $E_{1u}$. However, when two energy levels are mixing with another level which is higher or lower in energy than either of them, they should both have the same MCD sign while the level they are mixing with should have the opposite sign (see the Simple Theory). This is not the case for the $L_a$ and $L_b$ bands, they always have opposite signs.
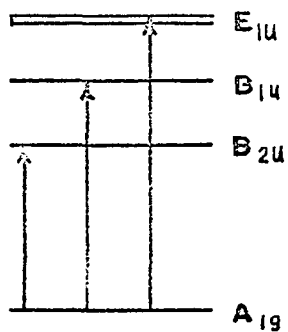
Fig. 39. The benzene electronic energy levels
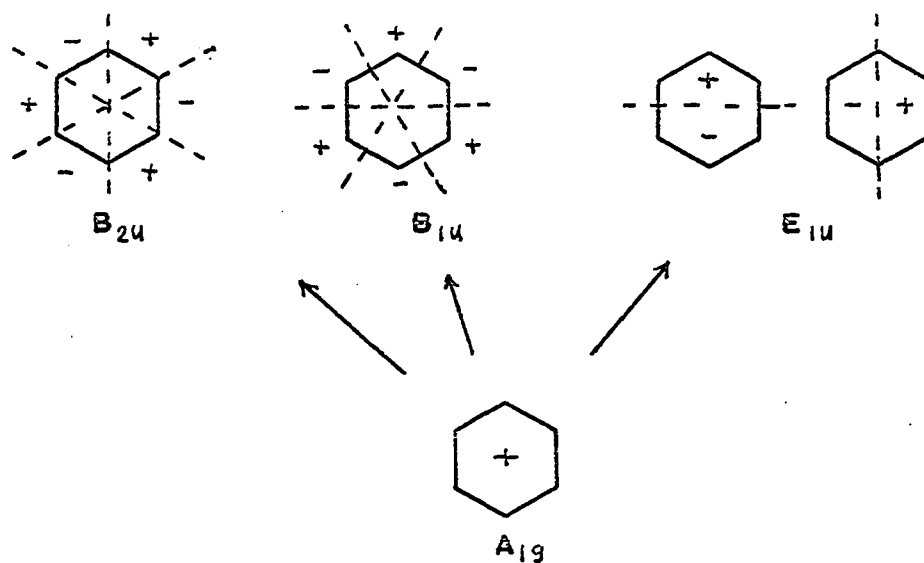


Fig. 40. Symmetry changes for benzene transitions
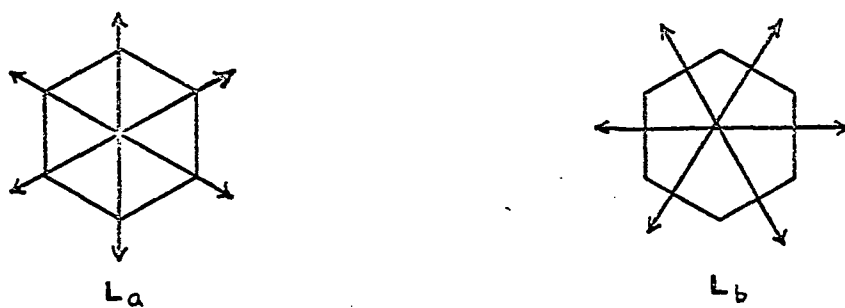


Fig. 41. Direction of transition moments for $L_a$ and $L_b$ bands

The MCD is inversely proportional to the energy difference between the mixing levels. These differences are

$E_{01}$ $(B_{2u} - A_{1g}) \cong 38000$ cm$^{-1}$      $E_{23}$ $(E_{1u} - B_{1u}) \cong 7500$ cm$^{-1}$

$E_{02}$ $(B_{1u} - A_{1g}) \cong 48000$ cm$^{-1}$      $E_{13}$ $(E_{1u} - B_{2u}) \cong 17500$ cm$^{-1}$

$E_{12}$ $(B_{1u} - B_{2u}) \cong 10000$ cm$^{-1}$

The MCD is also proportional to the vector product of the electronic transition moments. We use the square roots of the $\varepsilon$ values for the transition moments and these are

$$R_{01} \ (A_{1g} \quad B_{2u}) \ \alpha \ 15$$
$$R_{02} \ (A_{1g} \quad B_{1u}) \ \alpha \ 85$$
$$R_{03} \ (A_{1g} \quad E_{1u}) \ \alpha \ 200$$

The three mixing possibilities are shown in Fig. 42. The dotted lines represent magnetic transitions, the solid lines are electric transitions.

Assuming for the moment that the magnetic transition moments are the same for the substituted benzenes (some evidence that this may be true comes later), we can calculate how the MCD is proportional to the R and E values using

$$MCD \ \alpha \ \frac{R_i \ x \ R_j}{E_{ij}}$$

For the case of Fig. 42(a) we cannot calculate the MCD expected since the order of magnitude of the electric transition moment between states 1 and 2 is not known. However since the $R_{01}$ and $R_{02}$ values are relatively small and $E_{01}$ and $E_{02}$ are relatively large, this contribution might be expected to be smaller than for the cases in Fig. 42(b and c).

For mixing between states 1 and 2
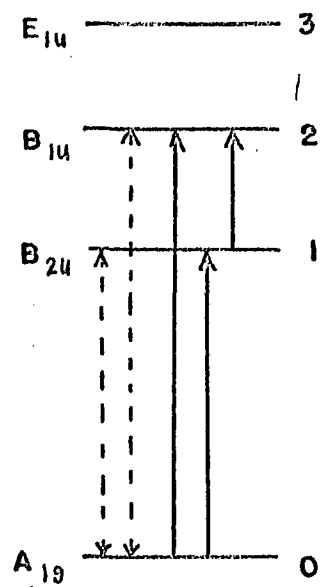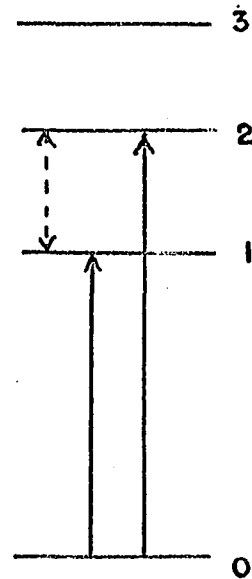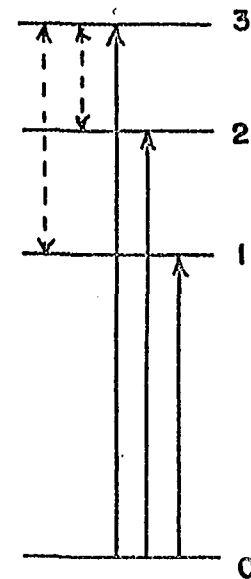
Fig. 42. Magnetic (- - - -) and electronic (———) transition possibilities for benzene levels

$$\text{MCD } \alpha \ \frac{(R_{01})(R_{02})}{E_{12}} = 0.13.$$

For the case of Fig. 42(c)

$$\text{MCD } \alpha \ (\frac{1}{E_{13}} + \frac{1}{E_{23}}) \ (R_{03})(R_{01} + R_{02})$$

$$= R_{03} \ (\frac{R_{01}}{E_{13}} + \frac{R_{01}}{E_{23}}) + R_{03} \ (\frac{R_{02}}{E_{13}} + \frac{R_{02}}{E_{23}})$$

$$= 0.57 + 3.23 = 3.90$$

Now we can draw hypothetical MCD spectra to illustrate what we would

expect to see in each case. These are shown in Fig. 43.

The MCD spectra observed look most like Fig. 43(b) both in regard to

signs and magnitudes.

A further argument against the likelihood of Fig. 42(c) being correct

is the fact that the magnetic transitions are symmetry forbidden for the

planar substituted benzenes.

The MCD for both $L_a$ and $L_b$ bands of aniline is shown in Table 2 (see

below). The larger value for the $L_a$ band suggest that the $B_{1u}$ state may

be interacting with more than one energy level, but the general appearance

of the MCD spectrum (Fig. 48) is very like that of Fig. 43(b).

As the $L_a$ and $L_b$ bands approach each other in energy, as happens in

certain compounds, the MCD values tend to be equal in magnitude and

opposite in sign, just what would be expected for mixing of $B_{1u}$ and $B_{2u}$

bands.

MCD data

Data related to the MCD of the substituted benzenes is listed in
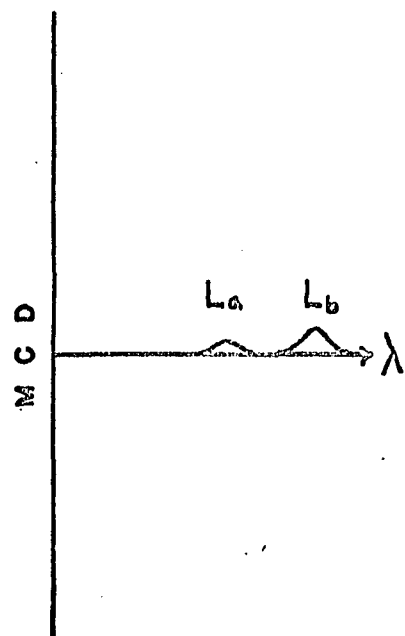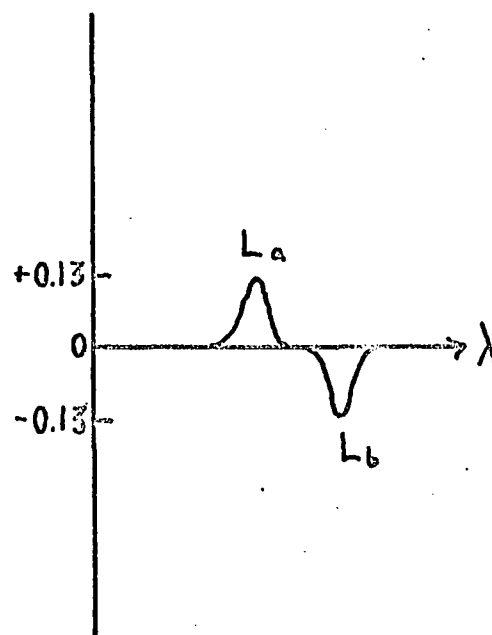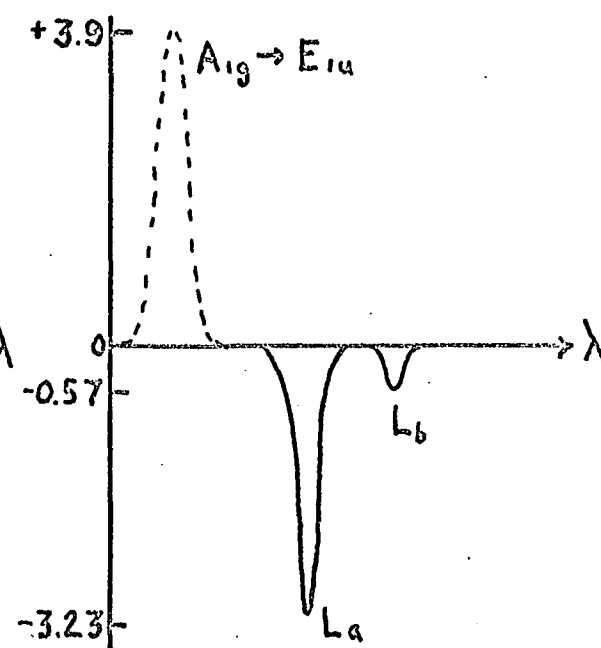
Fig. 43. MCD expected from hypothetical mixing cases

Table 2.

The values for $\sigma_p$ in Table 2 are from Ferguson (43, p. 415). These were determined from chemical data. The signs for the $\sigma_p$ of the halogens were changed when it was found that this greatly improved the fit of a plot of MCD vs $\sigma_p$ for a number of compounds (see below). It is realized that there is no strong justification for this sign change. However, there are some reasons for thinking the spectral and chemical properties might be of opposite sign for the halogens. For instance, the halogens are considered to be electron releasing by resonance and electron with-drawing by inductive effects. The $\sigma_p$ may be considered to consist of two contributions of opposite sign, related to resonance ($\sigma_R$) and induction ($\sigma_I$). The $\sigma_R$ effect is negative for the halogens (43, p. 394). The $\sigma_p$ for the benzenes with more than two substituents are calculated by a simple addition of the $\sigma_p$ of the groups, again considering the halogens as having a negative sign.

Several references were used to obtain extinction coefficients ($\varepsilon$) (44, p. 257)(45,46). Since there is some disagreement between sources for $\varepsilon$ values, they should be considered no more accurate than 10%. The square roots of the $\varepsilon$'s are proportional to the magnitudes of the transition moments.

The energies at the peak maxima for the $L_a$ and $L_b$ bands are needed for calculations, but are also listed since there is sometimes disagreement on the assignment of the $L_b$ band. When no other guidance was available, the most reasonable bands were chosen as $L_a$ and $L_b$. In cases where the $L_a$ and $L_b$ bands seemed to be almost degenerate, no attempt was made to

Table 2. Experimental data for the mono-substituted benzenes

| Group | CN | COOH | CHO | F |
|---|---|---|---|---|
| $\sigma_p$ | +0.66 | +0.45 | +0.23 | -0.06 |
| $\varepsilon L_b$ | 1000 | 970 | 1000 | 1280 |
| $\sqrt{\varepsilon L_b}$, $(R_1)$ | 31.5 | 31.1 | 31.5 | 35.7 |
| $\varepsilon L_a$ | 13000 | 11600 | 11400 | 7950 |
| $\sqrt{\varepsilon L_a}$, $(R_2)$ | 113 | 108 | 106.5 | 88.8 |
| $E_1$ cm$^{-1}$, $L_b$ | 36900 | 36500 | 35400 | 38500 |
| $E_2$ cm$^{-1}$, $L_a$ | 44700 | 43500 | 40800 | 4900 |
| $E_2 - E_1$, $(E_{12})$ | 7800 | 7000 | 5400 | 10500 |
| $(R_1)(R_2)/E_{12}$ | 0.456 | 0.48 | 0.62 | 0.30 |
| [MCD] | +0.377 | +0.276 | +0.305 | 0 |
| solvent | EtOH | 1N HCl-EtOH | 95% EtOH | EtOH |
| symmetry | $C_{2v}$ | $C_{2v}$ | $C_{2v}$ | $C_{2v}$ |
| Fig. 44 no. | 1 | 2 | 3 | 4 |

Table 2. (Continued)

| Group | $C_2H_5$ | $CH_3$ | I | Cl | Br |
|---|---|---|---|---|---|
| $\sigma_p$ | -0.15 | -0.17 | -0.18 | -0.22 | -0.23 |
| $\epsilon L_b$ | 160 | 225 | 700 | 190 | 192 |
| $\sqrt{\epsilon L_b}$, $(R_1)$ | 216 | 15 | 26.4 | 13.7 | 13.8 |
| $\epsilon L_a$ | 32000 | 7000 | 7000 | 7400 | 7900 |
| $\sqrt{\epsilon L_a}$, $(R_2)$ | 178 | 83.2 | 83.2 | 85.5 | 88.5 |
| $E_1$ cm$^{-1}$, $L_b$ | 38600 | 38500 | 38900 | 38000 | 38500 |
| $E_2$ cm$^{-1}$, $L_a$ | 48500 | 48300 | 47500 | 47500 | |
| $E_2 - E_1$, $(E_{12})$ | 9900 | 10000 | 9400 | 9500 | 9000 |
| $(R_1)(R_2)/E_{12}$ | 0.39 | 0.124 | 0.233 | 0.125 | 0.136 |
| [MCD] | -0.0276 | -0.0283 | -0.044 | -0.065 | -0.071 |
| solvent | EtOH | 95% EtOH | EtOH | EtOH | 95% EtOH |
| symmetry | $C_{2v}$ | $C_{2v}$ | $C_{2v}$ | $C_{2v}$ | $C_{2v}$ |
| Fig. 44 no. | 5 | 6 | 7 | 8 | 9 |

Table 2. (Continued)

| Group | OH | $NH_2$ | H<br>(benzene) | $OCH_3$ |
|---|---|---|---|---|
| $\sigma_p$ | -0.37 | -0.66 | 0 | -0.27 |
| $\varepsilon L_b$ | 1450 | 1430 | 200 | 1480 |
| $\sqrt{\varepsilon L_b}$, $(R_1)$ | 38 | 37.6 | 14.1 | 38.3 |
| $\varepsilon L_a$ | 6200 | 8600 | 7400 | 6400 |
| $\sqrt{\varepsilon L_a}$, $(R_2)$ | 78.3 | 92.3 | 85.6 | 79.7 |
| $E_1$ cm$^{-1}$, $L_b$ | 37100 | 35800 | 39000 | 37300 |
| $E_2$ cm$^{-1}$, $L_a$ | 47500 | 43500 | 49000 | 46000 |
| $E_2 - E_1$, $(E_{12})$ | 10400 | 7700 | 10000 | 8700 |
| $(R_1)(R_2)/E_{12}$ | 0.286 | 0.45 | 0.12 | 0.35 |
| [MCD] | -0.224 | -0.417 | $\pm 0.0096$ | -0.266 |
| solvent | 0.1NHCl | 95% EtOH | cyclohexane | EtOH |
| symmetry | $C_{2v}$ | $C_{2v}$ | D6h | $C_{2v}$ |
| Fig. 44 no. | 10 | 11 | 12 | 13 |

69

Table 2. (Continued)

| Group | N,N di-Me aniline | $COO^-$ | $SO_3H$ | $SO_2NH_2$ | $SO_2Cl$ |
|---|---|---|---|---|---|
| $\sigma_p$ | -0.83 | -- | -- | -- | --- |
| $\epsilon L_b$ | 15500 | 560 | 290 | 740 | 1260 |
| $\sqrt{\epsilon L_b}$, $(R_1)$ | 124 | 23.6 | 17 | 27.1 | 35.5 |
| $\epsilon L_a$ | 30000 | 8700 | 7800 | 9700 | 12000 |
| $\sqrt{\epsilon L_a}$, $(R_2)$ | 173 | 93 | 88 | 98 | 109 |
| $E_1$ $cm^{-1}$, $L_b$ | 40000 | 37400 | 38000 | 37800 | 37000 |
| $E_2$ $cm^{-1}$, $L_a$ | 50000 | 44700 | 47000 | 45800 | 47700 |
| $E_2 - E_1$, $(E_{12})$ | 10000 | 7300 | 9000 | 8000 | 10700 |
| $(R_1)(R_2)/E_{12}$ | 2.15 | 0.30 | 0.166 | 0.332 | 0.360 |
| [MCD] | +2.28 | +0.224 | +0.0432 | +0.178 | +0.346 |
| solvent | EtOH | 0.1N NaOH | $Cl_2$ water | $NH_4OH$ | EtOH |
| symmetry | $C_{2v}$ | $C_{2v}$ | $C_{2v}$ | $C_{2v}$ | $C_{2v}$ |
| Fig. 44 no. | 14 | -- | -- | -- | -- |

Table 2. (Continued)

| Group | $NH_3^+$ | $NO_2$ | 1-NH$_2$ 2-OH | 1-NH$_2$ 3-Cl | 1-NH$_2$ 3-Br | 1-CH$_3$ 3-OH |
|---|---|---|---|---|---|---|
| $\sigma_p$ | -- | +0.78 | -1.03 | -0.88 | -0.89 | -0.54 |
| $\varepsilon L_b$ | 160 | -- | 3300 | 2100 | 2400 | 1600 |
| $\sqrt{\varepsilon L_b}$, ($R_1$) | 12.6 | -- | 57.3 | 45.9 | 48.8 | 40 |
| $\varepsilon L_a$ | 7500 | 10000 | 7100 | 8500 | 7800 | -- |
| $\sqrt{\varepsilon L_a}$, ($R_2$) | 86 | -- | 84 | 91.7 | 88 | -- |
| $E_1$ cm$^{-1}$, $L_b$ | 39400 | -- | 34800 | 34700 | 34500 | 36300 |
| $E_2$ cm$^{-1}$, $L_a$ | 49400 | 39700 | 42600 | 42100 | 42100 | -- |
| $E_2 - E_1$, ($E_{12}$) | 10000 | -- | 7800 | 7400 | 7600 | -- |
| $(R_1)(R_2)/E_{12}$ | 0.109 | -- | 0.62 | 0.569 | 0.567 | -- |
| [MCD] | -0.0057 | +0.586 | -0.411 | -0.522 | -0.491 | -0.19 |
| solvent | 1N HCl | cyclohexane | EtOH | EtOH | EtOH | 95% EtOH |
| symmetry | $C_{2v}$ | $C_{2v}$ | $C_s$ | $C_s$ | $C_s$ | $C_s$ |
| Fig. 44 no. | -- | 15 | 16 | 17 | 18 | 19 |

Table 2. (Continued)

| Group | 1-CH$_3$ 2-CH$_3$ | 1-CH$_3$ 3-CH$_3$ | 1-CH$_3$ 4-CH$_3$ | 1-NO$_2$ 4-CHO | 1-CH$_3$ 2-I | 1-Br 3-F |
|---|---|---|---|---|---|---|
| $\sigma_p$ | -0.34 | -0.34 | -0.34 | +1.01 | -0.35 | -0.29 |
| $\epsilon L_b$ | 260 | 280 | 520 | 3020 | -- | 1000 |
| $\sqrt{\epsilon L_b}$, ($R_1$) | 16.1 | 1.67 | 22.7 | 54.8 | -- | 31.5 |
| $\epsilon L_a$ | 9000 | 8000 | 7500 | 14400 | 12000 | 8000 |
| $\sqrt{\epsilon L_a}$, ($R_2$) | 94.4 | 89 | 86.2 | 119 | 109 | 89 |
| $E_1$ cm$^{-1}$, $L_b$ | 38000 | 37800 | 36600 | 33100 | -- | 37500 |
| $E_2$ cm$^{-1}$, $L_a$ | 47900 | 47000 | 47100 | 37600 | 43000 | 47000 |
| $E_2 - E_1$, ($E_{12}$) | 9900 | 9200 | 10500 | 4500 | -- | 9500 |
| ($R_1$)($R_2$)/$E_{12}$ | 0.154 | 0.162 | 0.187 | 1.45 | -- | 0.295 |
| [MCD] | -0.046 | -0.038 | -0.090 | +0.757 | 0 | 0 |
| solvent | EtOH | EtOH | 95% EtOH | EtOH-H$_2$O | EtOH | EtOH |
| symmetry | C$_{2v}$ | C$_{2v}$ | D2h | C$_{2v}$ | C$_s$ | C$_s$ |
| Fig. 44 no. | 20 | 21 | 22 | 23 | 24 | 25 |

Table 2. (Continued)

| Group | 1-OH 2-COOH | 1-NH$_2$ 4-COOH | 1-Cl 4-OH | 1-Br 4-NO$_2$ |
|---|---|---|---|---|
| $\sigma_p$ | -0.12 | -0.21 | -0.59 | +0.55 |
| $\varepsilon L_b$ | 4000 | 18600 | 1600 | 9000 |
| $\sqrt{\varepsilon L_b}$, (R$_1$) | 6.3 | 136 | 40 | -- |
| $\varepsilon L_a$ | 32000 | 8900 | 8900 | 13000 |
| $\sqrt{\varepsilon L_a}$, (R$_2$) | 178 | 94 | 94 | -- |
| $E_1$ cm$^{-1}$, $L_b$ | 32700 | 34600 | 35700 | -- |
| $E_2$ cm$^{-1}$, $L_a$ | 48900 | 45500 | 44500 | -- |
| $E_2 - E_1$, (E$_{12}$) | 16200 | 10600 | 8800 | -- |
| (R$_1$)(R$_2$)/E$_{12}$ | 0.692 | 1.20 | 0.428 | -- |
| [MCD] | 0 | -2.24 | -0.357 | +0.648 |
| solvent | 95% EtOH | EtOH | H$_2$O | EtOH-H$_2$O |
| symmetry | C$_s$ | C$_{2v}$ | C$_{2v}$ | C$_{2v}$ |
| Fig. 44 no. | 26 | 27 | 28 | 29 |

Table 2. (Continued)

| Group | 1-Br 4-Br | 1-Br 4-Cl | penta- methyl | hexa- chloro | 1,3,5 tri- methyl | hexa- ethyl |
|---|---|---|---|---|---|---|
| $\sigma_p$ | -0.46 | -0.45 | -0.85 | -1.32 | -0.51 | -0.90 |
| $\epsilon L_b$ | 315 | 415 | 20 | 210 | 200 | 470 |
| $\sqrt{\epsilon L_b}$, $(R_1)$ | 17.7 | 20.4 | 4.45 | 14.5 | 14.1 | 21.6 |
| $\epsilon L_a$ | 15000 | 13500 | --- | --- | --- | 8450 |
| $\sqrt{\epsilon L_a}$, $(R_2)$ | 122 | 116 | --- | --- | --- | 92 |
| $E_1$ cm$^{-1}$, $L_b$ | 38500 | 36500 | 37000 | 34400 | 37700 | 36700 |
| $E_2$ cm$^{-1}$, $L_a$ | 43700 | 44700 | --- | --- | --- | 45500 |
| $E_2 - E_1$, $(E_{12})$ | 5200 | 8200 | --- | --- | --- | 8800 |
| $(R_1)(R_2)/E_{12}$ | 0.416 | 0.29 | --- | --- | --- | 0.226 |
| [MCD] | -0.203 | -0.218 | -0.00247 | +0.0338 | 0 | +0.029 |
| solvent | EtOH | EtOH | EtOH | EtOH | 95% EtOH | EtOH |
| symmetry | D2h | $C_{2v}$ | $C_{2v}$ | D3d | D3h | D6h |
| Fig. 44 no. | 30 | 31 | 32 | 33 | 34 | 35 |

Table 2. (Continued)

| Group | $CH_2OH$ | $O^-$ | $1-NH_2^+$ 4-COOH | $1-Br$ 2-$CH_3$ | $1-OCH_3$ 2-COOH |
|---|---|---|---|---|---|
| $\sigma_p$ | -- | -- | -- | -0.40 | +0.18 |
| $\varepsilon L_b$ | 480 | 2600 | 1000 | 460 | 2950 |
| $\sqrt{\varepsilon L_b}$, $(R_1)$ | 21.9 | 51 | 31.5 | 21.4 | 54 |
| $\varepsilon L_a$ | 8000 | 9400 | 11500 | 10000 | 7950 |
| $\sqrt{\varepsilon L_a}$, $(R_2)$ | 89 | 96.6 | 107 | 100 | 89 |
| $E_1$ cm$^{-1}$, $L_b$ | 38500 | 34900 | 37000 | 37400 | 35500 |
| $E_2$ cm$^{-1}$, $L_a$ | 47600 | 42500 | 44200 | 48000 | 43700 |
| $E_2 - E_1$, $(E_{12})$ | 9100 | 7600 | 7200 | 10600 | 8200 |
| $(R_1)(R_2)/E_{12}$ | 0.214 | 0.647 | 0.467 | 0.201 | 0.586 |
| [MCD] | -0.00529 | -0.717 | +0.273 | -0.0743 | 0 |
| solvent | $H_2O$ | 0.1N NaOH | 0.1N HCl | EtOH | $H_2O$ |
| symmetry | $C_{2v}$ | $C_{2v}$ | $C_{2v}$ | $C_s$ | $C_s$ |
| Fig. 44 no. | -- | -- | -- | 36 | 37 |

Table 2. (Continued)

| Group | 1-F 3-COOH | 1-OH 4-COCH$_3$ | 1-NO$_2$ 4-NH$_2$ | 1-Br 3-NO$_2$ |
|---|---|---|---|---|
| $\sigma_p$ | +0.39 | +0.33 | +0.12 | +0.55 |
| $\varepsilon L_b$ | 1700 | -- | -- | |
| $\sqrt{\varepsilon L_b}$, (R$_1$) | 41 | -- | -- | |
| $\varepsilon L_a$ | 11300 | 15000 | -- | |
| $\sqrt{\varepsilon L_a}$, (R$_2$) | 106 | -- | -- | |
| E$_1$ cm$^{-1}$, L$_b$ | 34900 | -- | -- | |
| E$_2$ cm$^{-1}$, L$_a$ | 43500 | 40500 | -- | |
| E$_2$ - E$_1$, (E$_{12}$) | 8600 | -- | -- | |
| (R$_1$)(R$_2$)/E$_{12}$ | 0.507 | -- | -- | |
| [MCD] | +0.304 | + | 0 | + |
| solvent | H$_2$O | EtOH | EtOH | EtOH |
| symmetry | C$_s$ | C$_{2v}$ | C$_{2v}$ | C$_s$ |
| Fig. 44 no. | 38 | -- | -- | -- |

estimate their relative energies or extinction coefficients.

The quantity [MCD] is the molar magnetic circular dichroism (the $\Delta A$ which would be observed for a 1 molar solution with a 1 cm path length) normalized to a 10 kgauss field. It is calculated using the peak height for the MCD band. According to the theory, the area of an MCD band rather than its maxima should be used in the calculation. However, most of the $B_{2u}$ bands for the substituted benzenes have band widths within a few hundred wave numbers of 3300 $cm^{-1}$, and therefore peak heights are very nearly proportional to areas. In those cases where the band width is considerably larger than 3300 $cm^{-1}$ it is usually caused by a contribution from some absorption not related to the $B_{2u}$ absorption.

The symmetries given in the table are the local symmetries as seen by the benzene ring. For example, any monosubstituted benzene, regardless of the symmetry of the substituent, is called $C_{2v}$.

Table 3 shows a correlation of the MCD of a number of monosubstituted benzenes with their directing properties. The order of the substituents was found by dividing them into ortho-para and meta directing groups and then arranging them in order of their effect on the wavelength of the $B_{1u}$ band relative to benzene (44, p. 257). For all of the compounds except $NO_2$ the energy difference between the $B_{1u}$ and $B_{2u}$ bands is roughly of the same order.

The correlation in Table 3 is very good semiquantitatively with the exception of benzonitrile. However, even in this case the sign is correct. It appears that if a substituent is meta-directing it will have a positive sign for the MCD of the $L_b$ band, if it is ortho-para directing the sign

Table 3.  MCD and wavelength change of $L_a$ band for mono-substituted benzenes

| | Group | $\Delta\lambda$ mµ | [MCD] |
|---|---|---|---|
| | $NO_2$ | 60 | +0.586 |
| | CHO | 46.5 | +0.305 |
| | COOH | 26.5 | +0.276 |
| | COO- | 20.5 | +0.224 |
| meta | CN | 14.5 | +0.377 |
| | $SO_2NH_2$ | 14 | +0.178 |
| | $NH_3^+$ | 0 | -0.0057 |
| | $CH_3$ | 3 | -0.0283 |
| | Cl | 6 | -0.065 |
| Ortho- | Br | 6.5 | -0.071 |
| para | OH | 7 | -0.224 |
| | $OCH_3$ | 14 | -0.266 |
| | $NH_2$ | 26.5 | -0.417 |
| | O- | 31.5 | -0.717 |
| | $N(CH_3)_2$ | ? | +2.28 |

Table 4.  MCD and percent meta substitution for some mono-substituted benzenes

| Group | % Meta | [MCD] |
|---|---|---|
| $NO_2$ | 93.3 | +0.586 |
| CN | 81 | +0.377 |
| COOH | 80.2 | +0.276 |
| CHO | 79 | +0.305 |
| H | (40) | +0.0096 |
| $CH_3$ | 4.4 | -0.0283 |
| I | 2.1 | -0.044 |
| $OCH_3$ | 2.0 | -0.266 |
| Br | 1.2 | -0.071 |
| Cl | 0.9 | -0.065 |
| F | 0.5 | 0 |
| OH | 0 | -0.417 |
| $NH_2$ | 0 | -0.224 |

will be negative.  Compared to unsubstituted benzene, the ortho-para

directors result in a net increase of electron density in the ring, the

meta directors produce a net decrease.  Since there are fewer electrons

than spaces for electrons in the latter case, one may speak of positive

holes as circulating in the ring.  The experimental evidence suggests that

the sign of the charge carrier determines the sign of the MCD.

Table 4 is a correlation of MCD with the respective percent of meta

substitution (43, p. 431).  The quantitative agreement is poor but again

the signs are positive for m-directors and negative for o-p directors.

Although the sign of the MCD seems to have a reasonable explanation,

the magnitude of the MCD is not so easily resolved.  The form of the B

term equation suggests that the magnitude of the charge carrier (holes

or excess electrons) should affect the size of the MCD effect.  However,

there is no independent measurement for the magnitude of the charge

carrier to relate to the MCD.  Tables 3 and 4 are attempts in this

direction but the amount of charge carrier is not necessarily directly

related to either correlation.

Fig. 44 shows a plot of MCD versus $\sigma_p$.  The heavy rings indicate

points for monosubstituted benzenes.  31 out of the 38 compounds plotted

follow an approximate straight line relationship which appears to be

quite good considering experimental error.

It is somewhat surprising that nitrobenzene ⑮ fits in the straight-

line region since it is not an example of a compound with well separated

$B_{1u}$ and $B_{2u}$ bands.  The MCD and absorption spectra of $NO_2$-benzene are

shown in Fig. 45.  In view of the circumstances, the fit of nitrobenzene
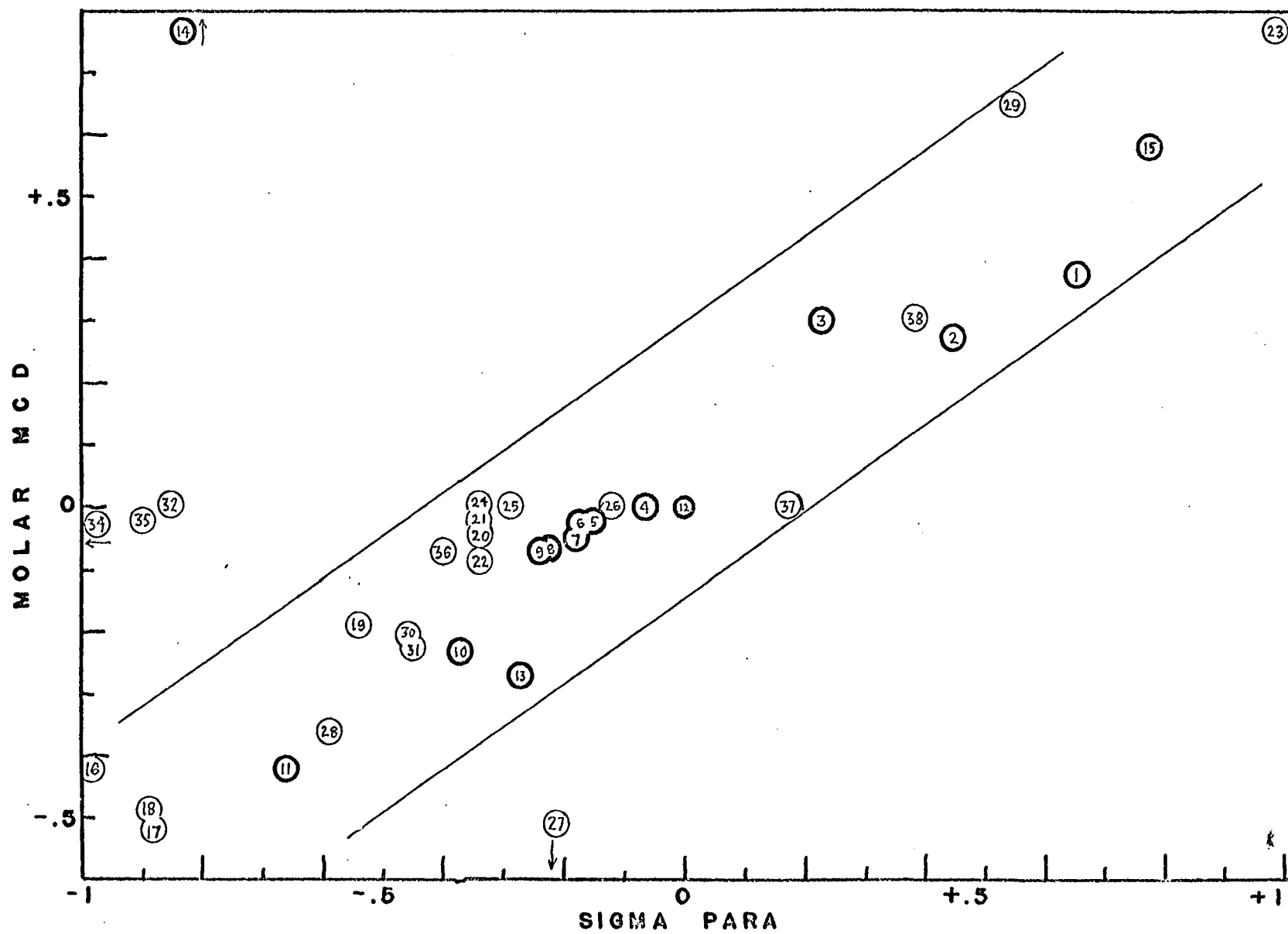
Fig. 44. MCD vs. Hammett's sigma para
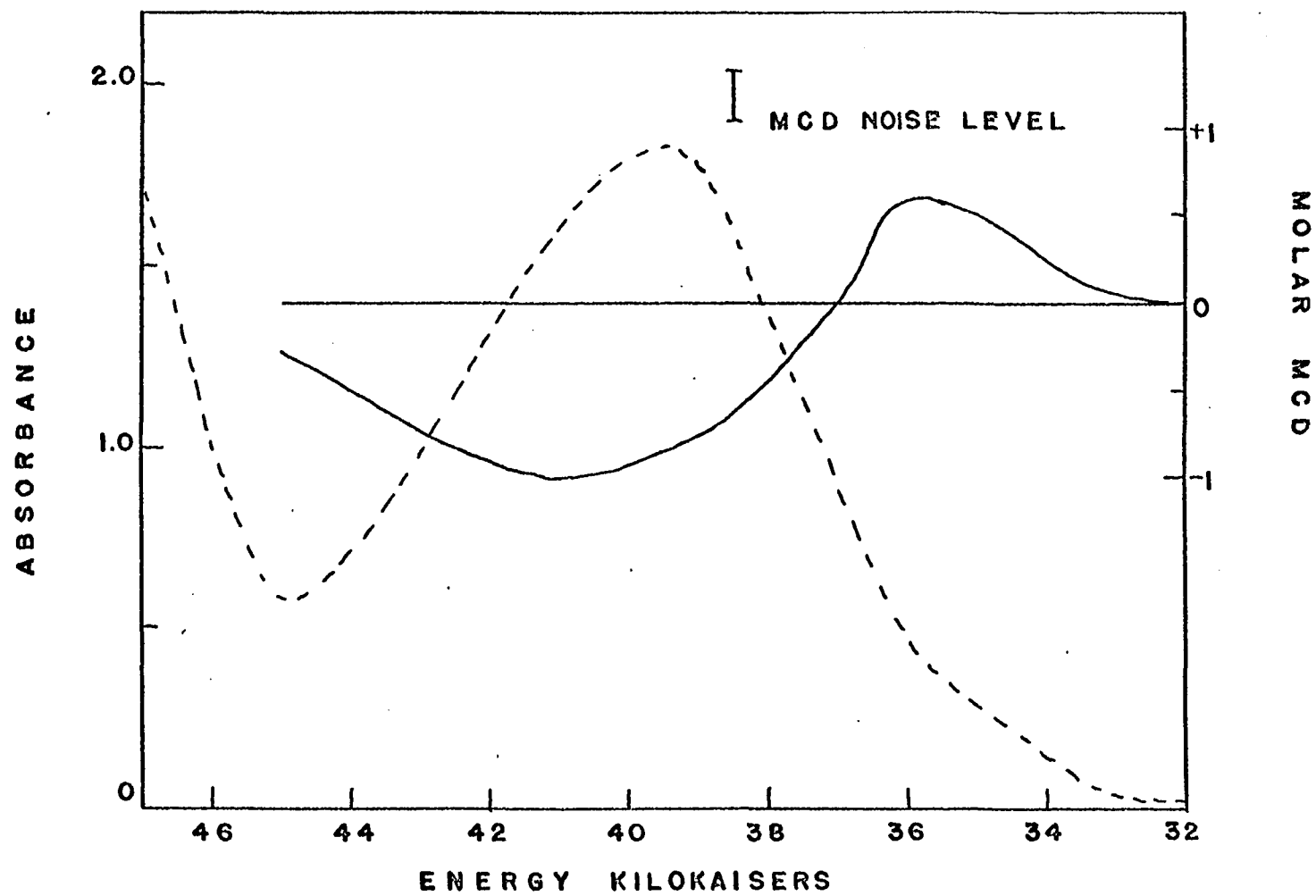
Fig. 45. Absorption (- - - -) and MCD (———) of nitrobenzene

in Fig. 44 may be fortuitous. The shape of the absorption spectrum

indicates that a single band is present with a maximum at 252 mμ. How-

ever, the drastic electron-withdrawal of the nitro group is expected to

move the $A_{1g} \rightarrow B_{1u}$ band to approximately the same position as the

$A_{1g} \rightarrow B_{2u}$ band. One would expect a wider bandwidth in this case, and

this occurs, the bandwidth is about 6600 $cm^{-1}$, or about twice the normal

value. However it is not really obvious that the two bands are almost

degenerate until one sees the MCD spectrum. The shape of the MCD makes

it clear that two bands very close in energy are interacting. It is

still not possible to determine the relative energies of the interacting

bands, for the one with lowest energy will always give the same sign.

But the usefulness of MCD for determining when an accidental degeneracy

has taken place is quite evident.

N,N dimethyl aniline (see Fig. 46) seems to have some mixing with an

$n \rightarrow \pi^*$ band at lower energy (300 mμ) than the $B_{2u}$ band. This may be the

reason that neither the sign nor magnitude of the MCD fit the plot of

Fig. 44. Para-amino benzoic acid is another example where the $L_a$ and $L_b$

bands may be almost degenerate (see Fig. 47). The spectra for $p-NH_3^+$

benzoic acid are included in Fig. 47 to indicate the change which is

brought about simply by putting a proton on the amino group.

The spectra of aniline are given in Fig. 48 as an example showing

the MCD of both the $L_a$ and $L_b$ transitions. In most cases the $L_a$ band

was too low in wavelength to give dependable experimental results,

although the sign could usually be determined.

The points 32-35 are poor-fitting, the reason seems to be related
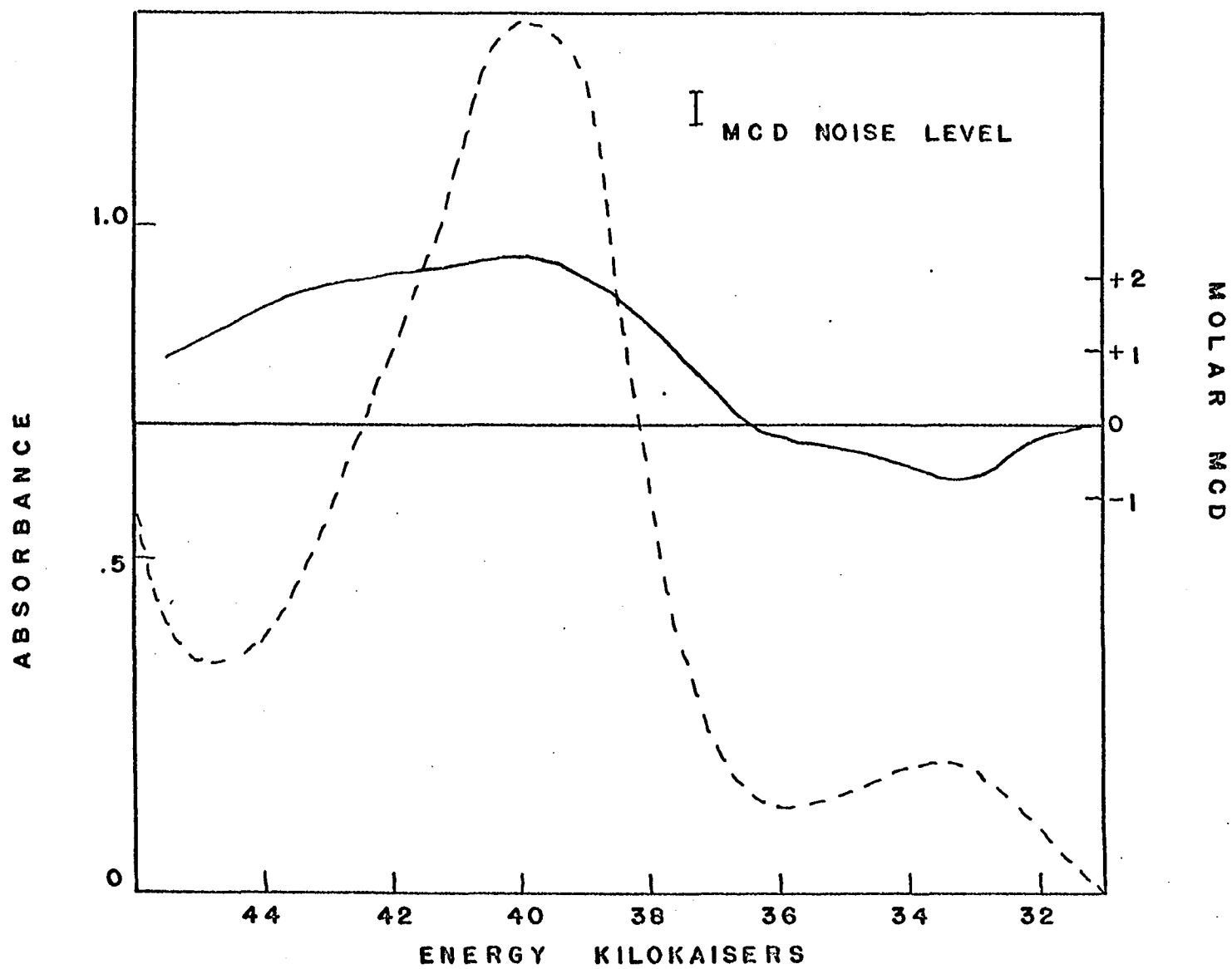
Fig. 46. Absorption (- - - -) and MCD (———) of N,N dimethyl aniline
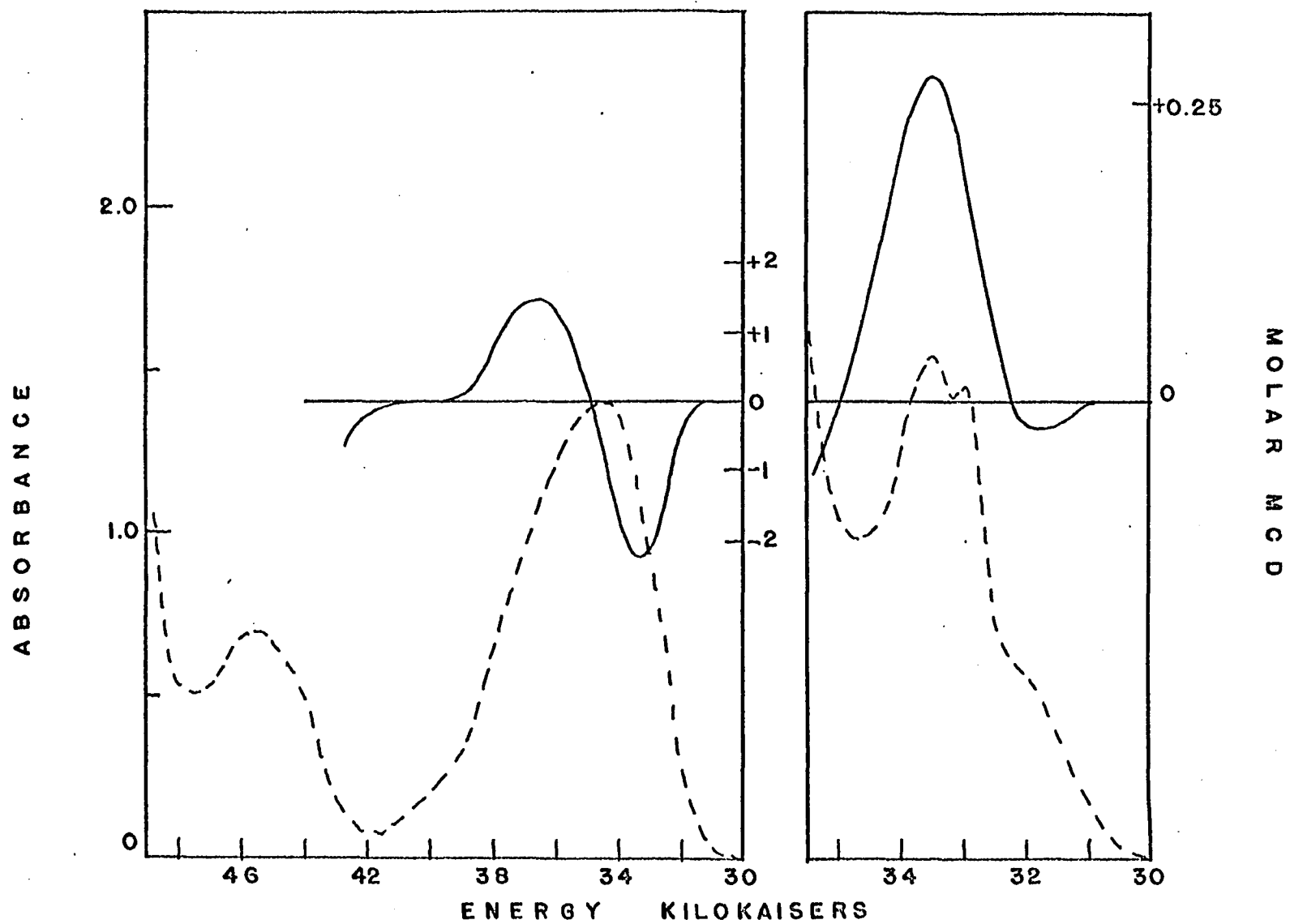
Fig. 47. Absorption (------) and MCD (———) of p-amino benzoic acid in (left) ethanol and (right) acidic solution
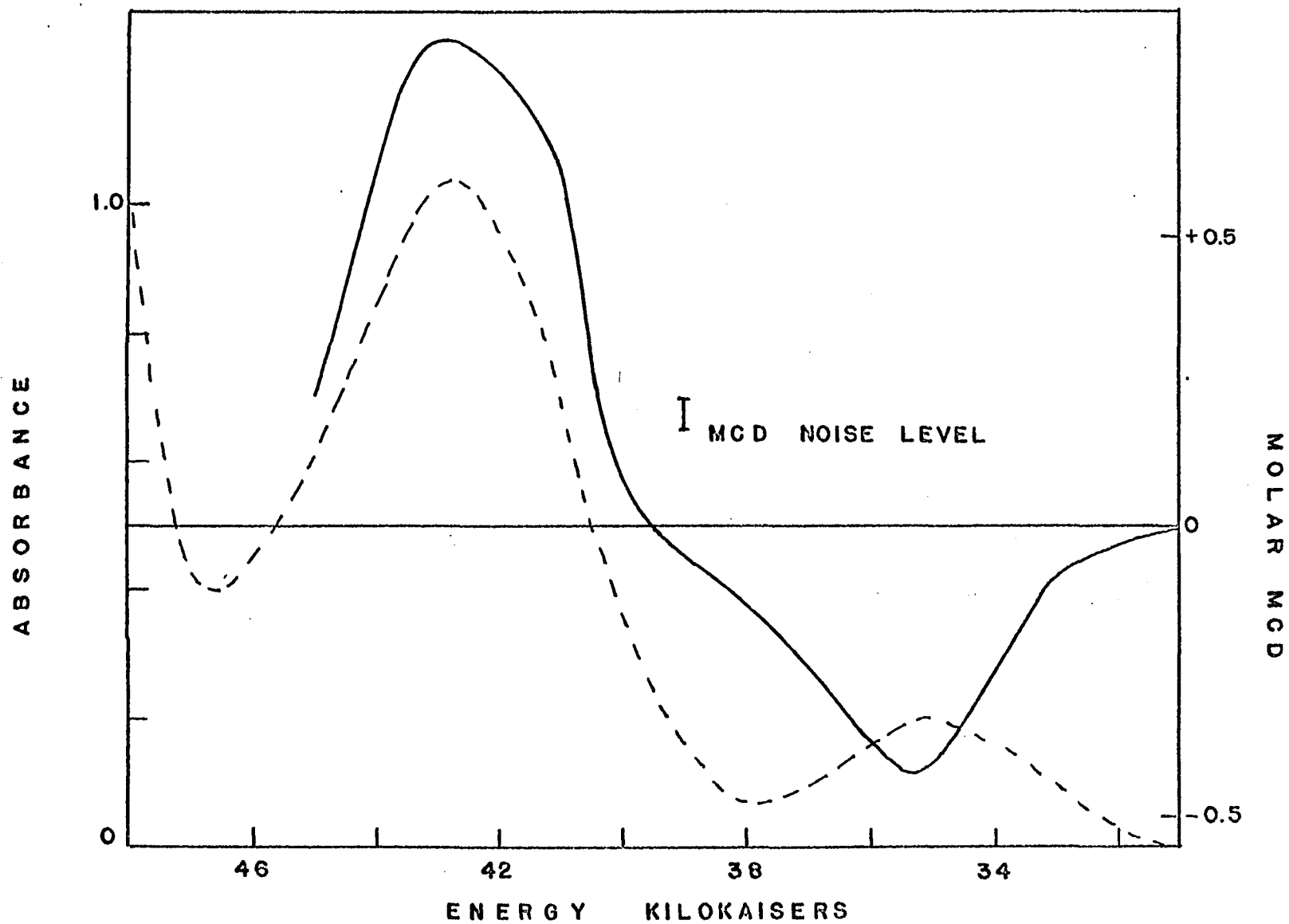
Fig. 48. Absorption (- - - - -) and MCD (————) of aniline

to the symmetry of these compounds and will be discussed below.

In general, Fig. 44 indicates a good relationship for compounds in which the $L_a$ and $L_b$ bands are well-separated and in which no interfering bands mix with them. Although it is not possible to make any unambiguous interpretation of the relationship revealed by Fig. 44, there seems to be a clear indication that the sign of the MCD is related to the sign of the charge carrier in the aromatic ring.

Symmetry effects

As mentioned above, symmetry seems to play a part in determining the MCD of some of the substituted benzenes. Four of the points which did not fit well on the graph in Fig. 44 are highly symmetrical compounds.

Table 5 indicates the symmetry conditions for transitions of the substituted benzenes. The groups correspond to molecular types as follows: D6h for benzene and hexa-substituted benzenes, C2v for mono-substituted benzenes, D3h for 1,3,5 tri-substituted benzenes, Cs for any planar benzene derivative not of higher symmetry, D3d for the "puckered" molecule hexachlorobenzene, and D2h for para disubstituted benzenes.

The symmetry groups which correspond to $A_{1g}$, $B_{1u}$ and $B_{2u}$ were taken from correlation tables (47). Then the selection rules were evaluated from character tables (48). An 0 means the transition is forbidden by symmetry, + means it is allowed. The coordinate convention used is shown in Fig. 49.

From the form of the B term one can see that the relative directions are important since vectors are involved, $B \propto \overline{M}_{12} \cdot \overline{R}_1 x \overline{R}_2$. In order to have an MCD there must be some perpendicular component between the two

Table 5. Symmetry relations for substituted benzenes

| Group | D6h Correlations | | | $B_{1u} \leftrightarrow B_{2u}$ Magnetic | | | $L_a$ Electronic | | | $L_b$ Electronic | | |
|---|---|---|---|---|---|---|---|---|---|---|---|---|
| | | | | x | y | z | x | y | z | x | y | z |
| D6h | $A_{1g}$ | $B_{1u}$ | $B_{2u}$ | 0 | 0 | + | 0 | 0 | 0 | 0 | 0 | 0 |
| $C_{2v}$ | $A_1$ | $A_1$ | $B_1$ | 0 | + | 0 | 0 | 0 | + | + | 0 | 0 |
| D3h | $A_1'$ | $A_1'$ | $A_2'$ | 0 | 0 | + | 0 | 0 | 0 | 0 | 0 | 0 |
| $C_s$ | A' | A' | A'' | + | + | 0 | + | + | 0 | 0 | 0 | + |
| D3d | $A_{1g}$ | $A_{1u}$ | $A_{2u}$ | 0 | 0 | + | 0 | 0 | 0 | 0 | 0 | + |
| D2h | $A_g$ | $B_{2u}$ | $B_{3u}$ | 0 | 0 | + | 0 | + | 0 | + | 0 | 0 |

Fig. 49. Symmetry coordinate conventions

electronic transition moments $\overline{R1}$ and $\overline{R2}$, and there must be a parallel

component between the magnetic transition moment $\overline{M}_{12}$ and the vector

product of the electronic moments $\overline{R1} \times \overline{R2}$. The ideal situation would be

to have the three transitions allowed in mutually orthogonal directions.

This is possible for the C2v, Cs and D2h symmetries. These are all

represented by molecules with large MCD's.

Benzene has no allowed electronic transitions for the $B_{1u}$ or $B_{2u}$

symmetries. That the $B_{1u}$ and $B_{2u}$ bands are seen at all is due to a

molecular vibration with $E_g$ symmetry which mixes in small amounts of

allowed symmetries. The vibration-permitted transitions are, however,

not necessarily in the directions needed for MCD. Benzene and the other

D6h compound studied, hexaethylbenzene, have small MCD values which may

be caused by their symmetry.

Hexachlorobenzene has a puckered shape (49), and as a result one

direction for the $A_{1g} \longrightarrow B_{2u}$ transition is allowed. It does have a larger

MCD than benzene or hexaethylbenzene but still fits poorly in Fig. 44.

Mesitylene (1,3,5 trimethyl benzene) has the same selection rules

as compounds of D6h symmetry. No MCD was detected for this compound and

symmetry seems to be strongly implicated in this result.

A non-benzenoid molecule with D3h symmetry was examined, it also has a small MCD. The compound is symmetrical-triazine, the spectrum is shown in Fig. 50. The band peaking at 272 m$\mu$ is assigned as an n$\rightarrow\pi^*$ transition, with an obvious vibrational progression stating at about 320 m$\mu$ (50).

The tropylium ion

An obvious test of the hypothesis that the sign of the charge carrier is determining the sign of the MCD is to examine molecules which by their structure should possess either an extra electron or a hole. In 1966 in a private communication, Professor W. Simpson of the University of Washington suggested that good examples to investigate would be the ions tropylium ($C_7H_7^+$) and cyclopentadienide ($C_5H_5^-$). Unfortunately $C_5H_5^-$ seems to have no spectrum in the accessible region.

The MCD and absorption spectra of $C_7H_7BF_4$ in conc. $H_2SO_4$ are shown in Fig. 52. One would expect the long wavelength absorption to be positive if holes circulate in the ring. Some data on the molecule is given in Table 6. The absorption coefficients are given by Ginsberg (51).

Table 6. Optical data for the tropylium ion

Extinction coefficient ($\epsilon$)

$A_1' \rightarrow E_3'$.............4270

$A_1' \rightarrow E_1'$.............40800

Transition energy

$A_1' \rightarrow E_3'$.............36500 cm$^{-1}$

$A_1' \rightarrow E_1'$.............46000 cm$^{-1}$

Molar MCD ([MCD])

at 280 m$\mu$ ..........+1.69
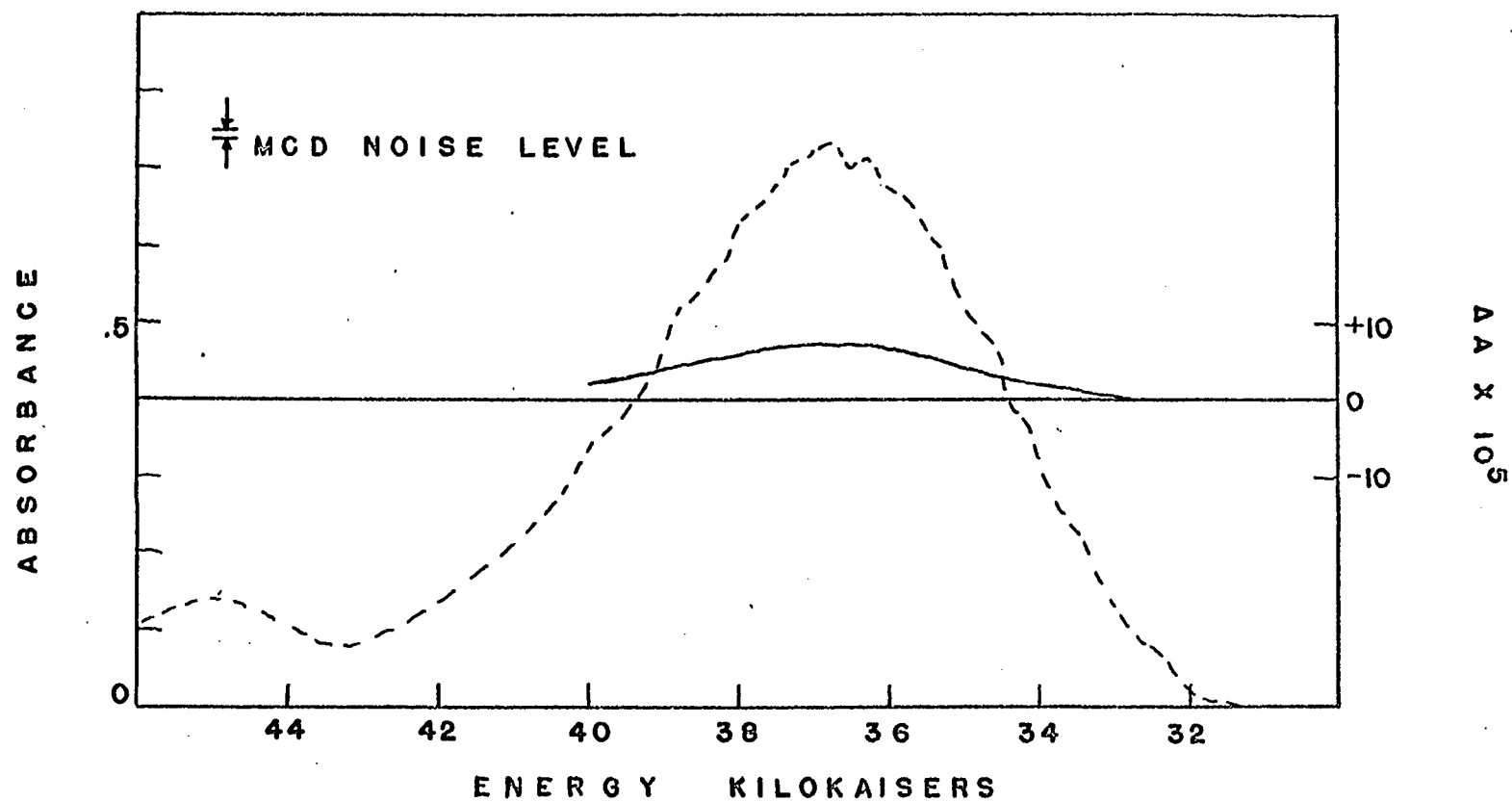
Fig. 50. Absorption (----) and MCD (———) of symmetrical-triazine

Experimental and theoretical work on the tropylium ion have been done by

J. N. Murrell and H. C. Longuet-Higgins, and W. von Doering and L. H.

Knox (52,53). The energy level diagram is shown in Fig. 51 and the

symmetry correlation between D7h and D6h is given by Table 7.
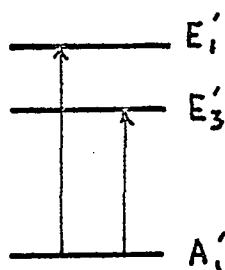


Fig. 51. Tropylium ion energy
levels

Table 7. Symmetry correlations for
the tropylium ion

| D7h | D6h |
|---|---|
| $A_1^1$ | $A_{1g}$ |
| $E_1^1$ | $E_{1u}$ |
| $E_3^1$ | $B_{1u}$, $B_{2u}$ |

The MCD spectrum agrees with that expected from an $A \rightarrow E$ type (doubly

degenerate) transition. If the $E_3^1$ state is truly degenerate the MCD would

be the result of an A term interaction. Another possibility is that the

two levels of the $E_3^1$ state are slightly different in energy as the result

of some perturbation, although still appearing as essentially a single

peak at 37,000 $cm^{-1}$. The MCD in this event would be due to B term inter-

actions. In either case the MCD will have the same appearance. The sign

of the splitting for tropylium agrees with the assumption that a hole is

the charge carrier. The presence of a small negative MCD at the long

wavelength end of the absorption region is somewhat disturbing, for the

lowest energy MCD should be positive. From the position of this small

MCD relative to the absorption band, it may be related to the 0-0
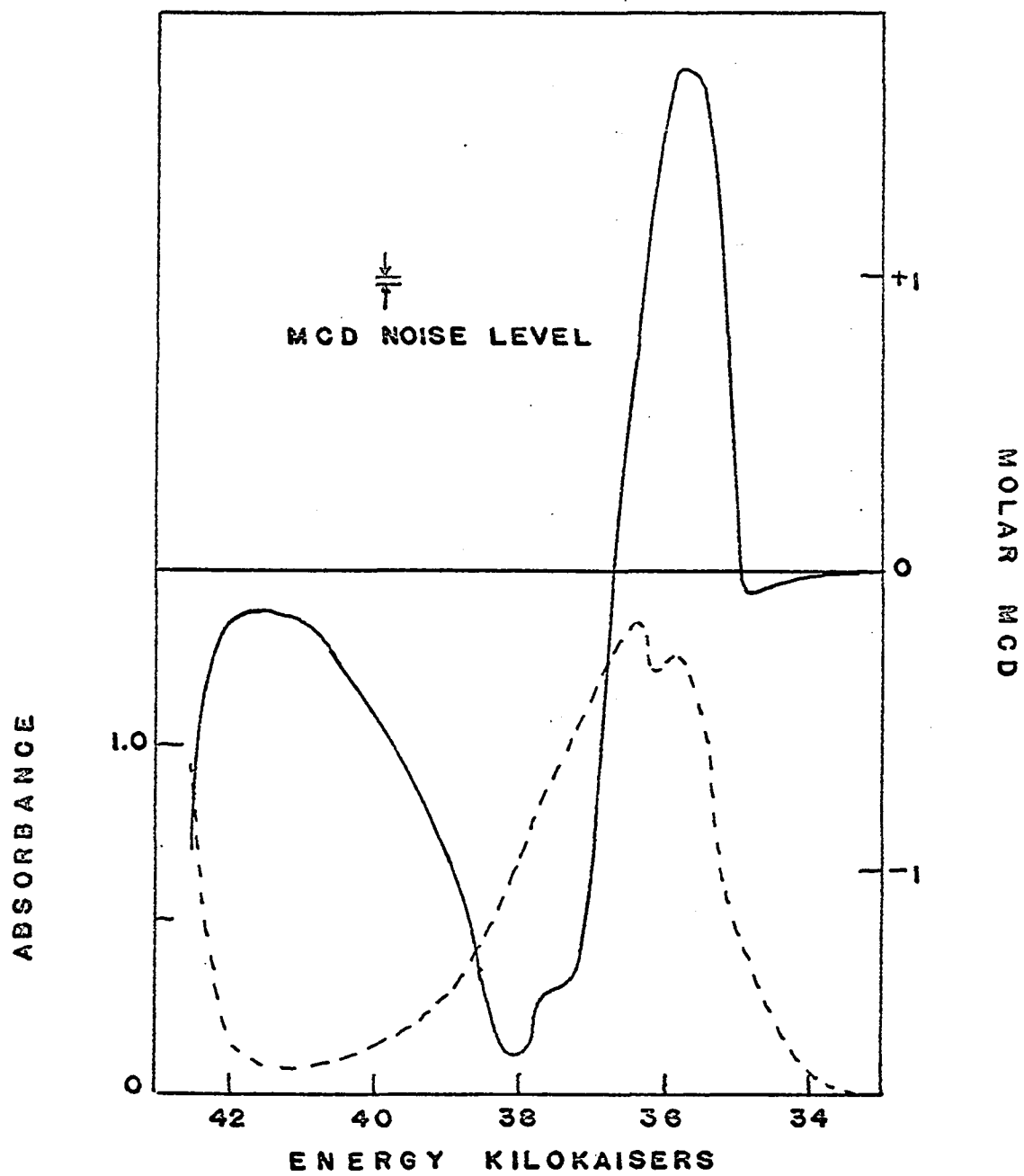
Fig. 52.  Absorption (- - - -) and MCD (———) of
tropylium ion

vibrational transition. This transition is not normally seen in the
electronic spectrum since it is forbidden. However, its MCD may be
permitted by some mechanism exclusive of that allowing the rest of the
band. This sort of situation occurs in natural circular dichroism. More
analysis would be necessary to clarify this case.

## Correlations

The form of the B term

$$MCD \: \alpha \: \frac{\overline{M} \cdot \overline{R}_1 \: x \: \overline{R}_2}{E_{12}}$$

suggests that we plot the data in Table 2 as

$$[MCD] \: vs. \: \frac{\overline{R}_1 \: x \: \overline{R}_2}{E_{12}}$$

in order to determine whether the magnetic transition moment is appreciably
different for the substituted benzenes. Since the relative directions
for the transitions are not known, the vector products cannot be evaluated.
Therefore we will approximate by performing the ordinary multiplication of

$R_1$ and $R_2$. A plot of $[MCD]$ vs. $\frac{(R_1)(R_2)}{E_{12}}$ is shown in Fig. 53.

Considering the approximations made, the graph indicates a definite
trend, suggesting that changes in the magnitude of the magnetic transition
moment are minor between different substituted benzenes. Since the
directions of the transition moments are not known (although they are
probably the same for all monosubstituted benzenes), nothing more definite
can be said.

Another correlation is suggested by the fact that circulating

ABSOLUTE MOLAR MCD

Fig. 53. MCD vs. $\dfrac{(R_1)(R_2)}{E_{12}}$

$\dfrac{R_1 \times R_2}{E_{12}}$
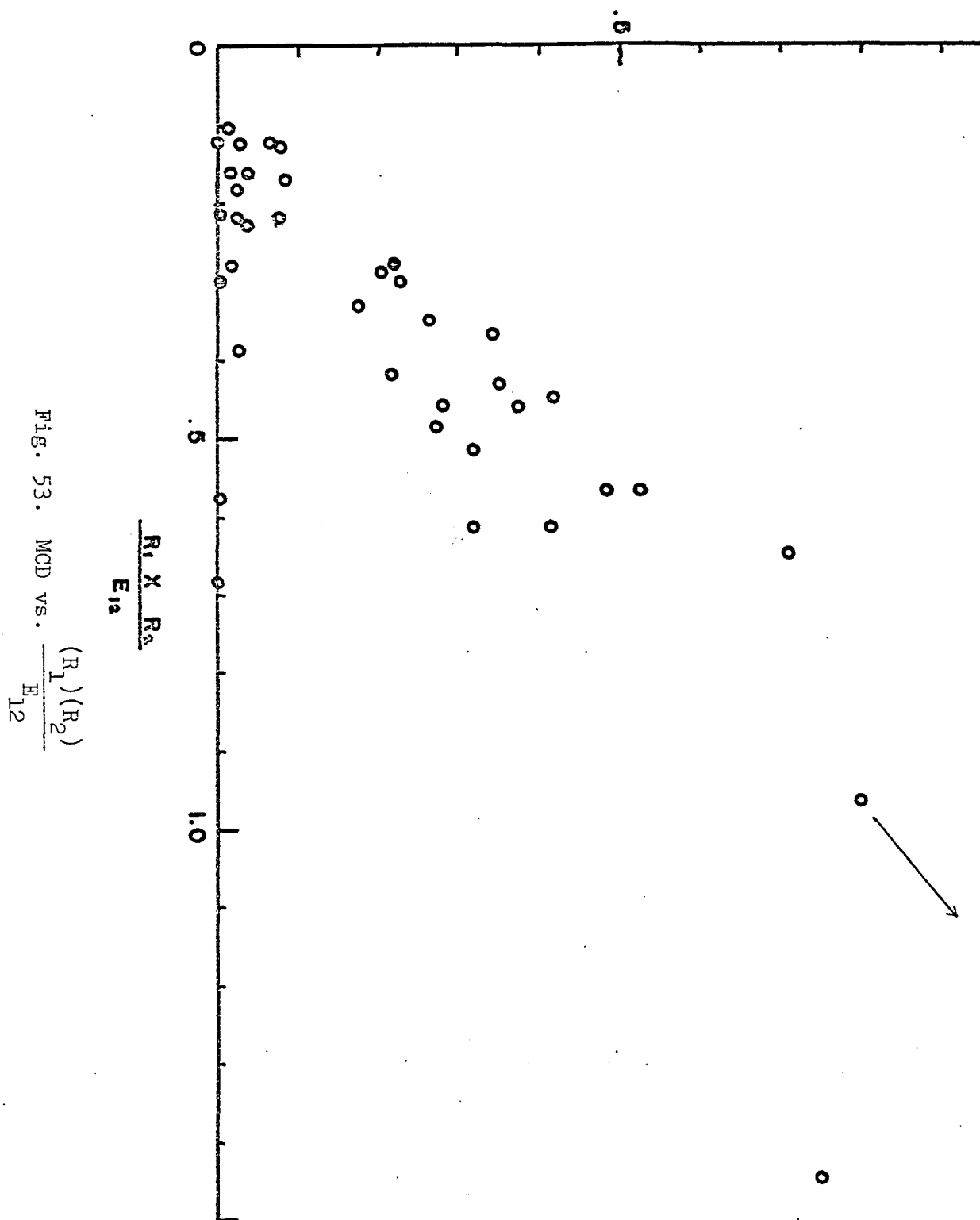
electrons in the benzene ring produce a diamagnetism. If the diamagnetism due to the atoms of the substituents could be determined separately, this could be subtracted from the total diamagnetic susceptibility to yield that due only to the atoms in the ring plus the ring current. The data from these calculations is shown in Table 8. The experimental values are from the literature (54,55,56). Pascal's values were used to evaluate the substituent susceptibilities (43, p. 53). For the disubstituted benzenes the value of the hydrogen atom susceptibility had to be added to obtain the $C_6H_5$ susceptibility.

As the graph of [MCD] vs. $\chi$ shows (see Fig. 54), there are two trends which seem to take place, one for molecules with small MCD (no correlation) and another for those with relatively large MCD (positive correlation). The interpretation of this result is not obvious.

Summary

A number of conclusions resulting from the study of the substituted benzenes are listed below.

1. The $B_{1u}$ and $B_{2u}$ levels mix magnetically in the substituted benzenes, resulting in MCD. This implies that the directions of the two electronic transitions must have some perpendicular component relative to one another.

2. There is a good deal of evidence that the charge carrier in the benzene ring determines the sign of the MCD. This sign is negative if the charge carrier is an electron and is positive if the charge carrier is a hole.

3. Highly symmetrical molecules often exhibit no MCD or very

Table 8. MCD and diamagnetic susceptibility of substitute benzenes

| Group | diamag. susc. | Substit. susc. | C6H5 susc. | MCD |
|---|---|---|---|---|
| H | $-54.86 \times 10^{-6}$ | $-2.93 \times 10^{-6}$ | $-51.93 \times 10^{-6}$ | +0.01 |
| CH3 | -65.54 | -14.79 | -50.75 | -0.028 |
| Et | -77.26 | -26.65 | -50.61 | -0.0276 |
| $NH_2$ | -62.95 | -11.43 | -51.52 | -0.417 |
| $CN$ | -65.19 | -6.74 | -58.45 | +0.377 |
| Cl | -69.97 | -17.00 | -52.97 | -0.065 |
| OH | -60.21 | -7.54 | -52.67 | -0.224 |
| $CH_2OH$ | -71.83 | -19.40 | -52.43 | -0.0053 |
| COOH | -70.28 | -16.90 | -53.38 | +0.276 |
| CHO | -60.78 | -7.21 | -53.57 | +0.305 |
| Br | 078.1 | -26.5 | -51.6 | -0.071 |
| I | -92.00 | -40.50 | -51.50 | -0.044 |
| $OCH_3$ | -72.10 | -19.40 | -52.70 | -0.266 |
| p-Cl, OH | -77.6 | -24.54 | -55.99 | -0.357 |
| m-cresol | -71.90 | -22.33 | -52.50 | -0.19 |
| o-xylene | -77.78 | -29.58 | -51.13 | -0.046 |
| m-xylene | -76.56 | -29.58 | -49.91 | -0.038 |
| p-xylene | -76.81 | -29.58 | -50.16 | -0.090 |
| m-Br, $NH_2$ | -84.89 | -33.90 | -51.00 | -0.491 |

Fig. 54. MCD vs. $\chi_{C_6H_5}$

MOLAR MCD

$\chi_{C_6H_5} \times 10^6$
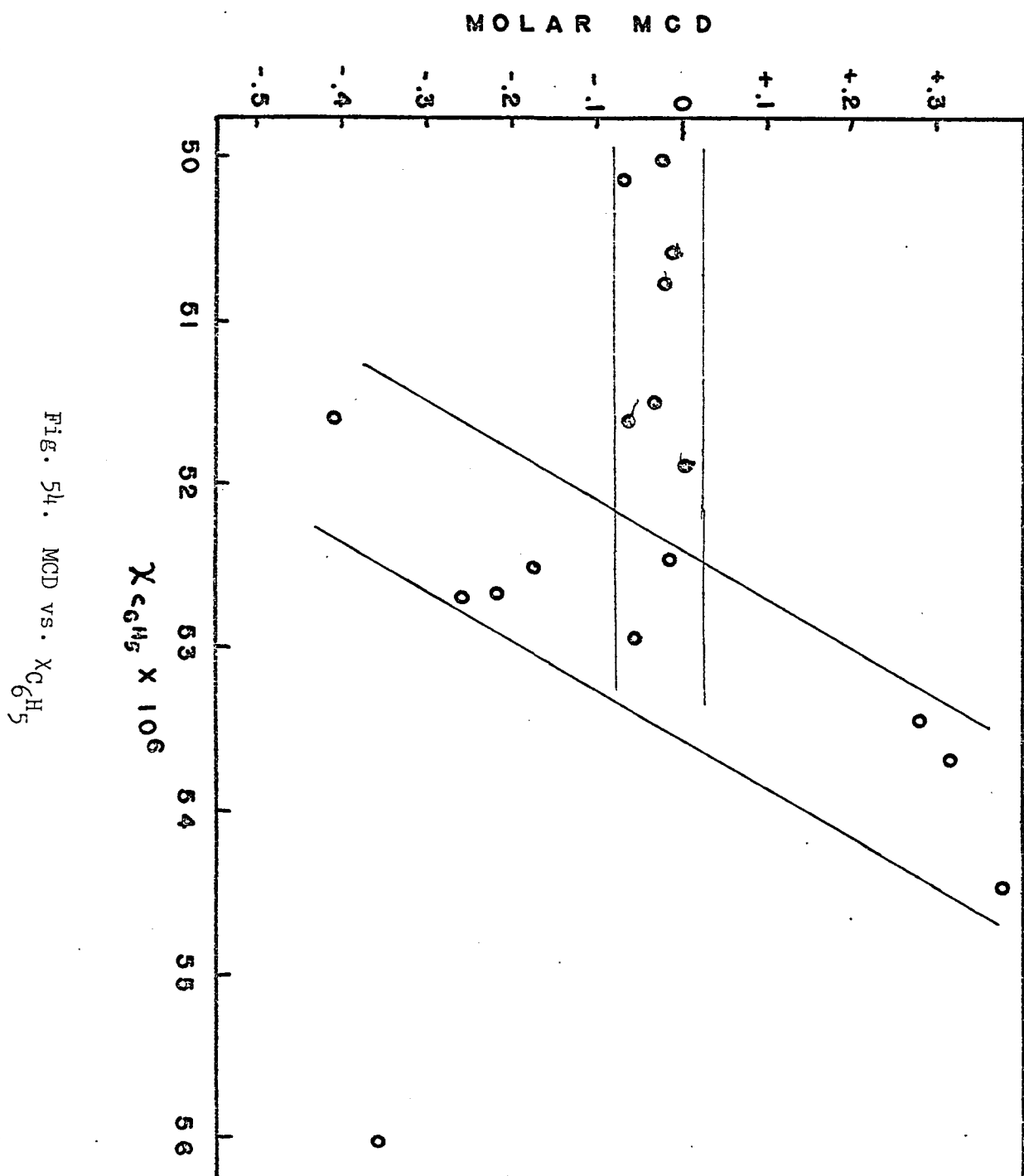
small MCD. This is probably related to the symmetry-forbidden character of the electric or magnetic transitions involved.

4. The shape of the MCD spectrum for several of the compounds studied indicated the presence of near- or accidental degeneracy of absorption bands. This method of detecting accidental degeneracy could be an important supplement to other methods.

5. There is some evidence that the magnetic transition moment is approximately the same for the substituted benzenes.

Benzene and the Catacondensed Aromatics

## Benzene

The ultra-violet spectrum of the benzene molecule has undergone a great deal of study both theoretically and experimentally. There is general agreement that the sharp bands near 260 mμ constitute the electrically forbidden $A_{1g} \rightarrow B_{2u}$ ($L_b$) transition, and that this is partially allowed by an $E_g$ vibration. If there were simply mixing between the $B_{2u}$ and $B_{1u}$ levels the MCD should have the same sign for the entire $L_b$ band, as occurs for almost all of the substituted benzenes studied. This is not the case, as can be seen from Fig. 55. The MCD spectrum suggests that the situation may be quite complex, e.g., possibly more than one type of vibration is involved in permitting the $L_b$ transition. The individual components of each vibronic structure could then partially overlap and interact to give the splittings observed.

The MCD of benzene is very weak and therefore the signal-to-noise ratio is quite small. One method of improving the results is to make many scans of the spectrum and then average them together. This is possible with a Computer of Average Transients (CAT). The spectrum in Fig. 55 represents 50 scans which should give a theoretical overall improvement of signal-to-noise ratio of $\sqrt{50} \cong 7$ times.

## The catacondensed aromatics

Klevens and Platt (57) assigned $L_a$ and $L_b$ bands for the series of catacondensed aromatics: benzene, naphthalene, antheacene, tetracene, pentacene. If their assignments were correct, this offers the interesting possibility of observing the MCD of the $L_a$ and $L_b$ transitions as
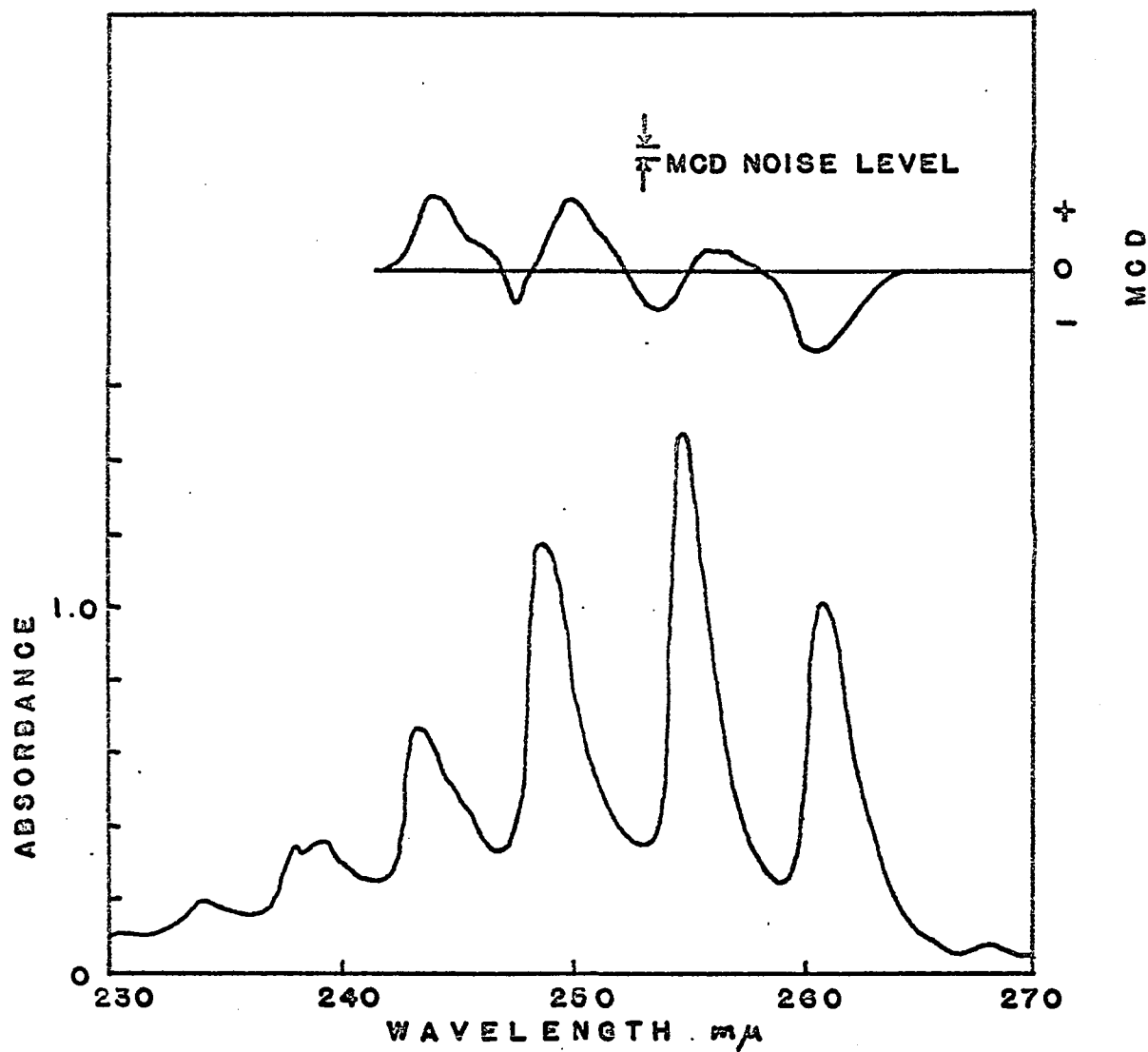
Fig. 55. Absorption and MCD of benzene
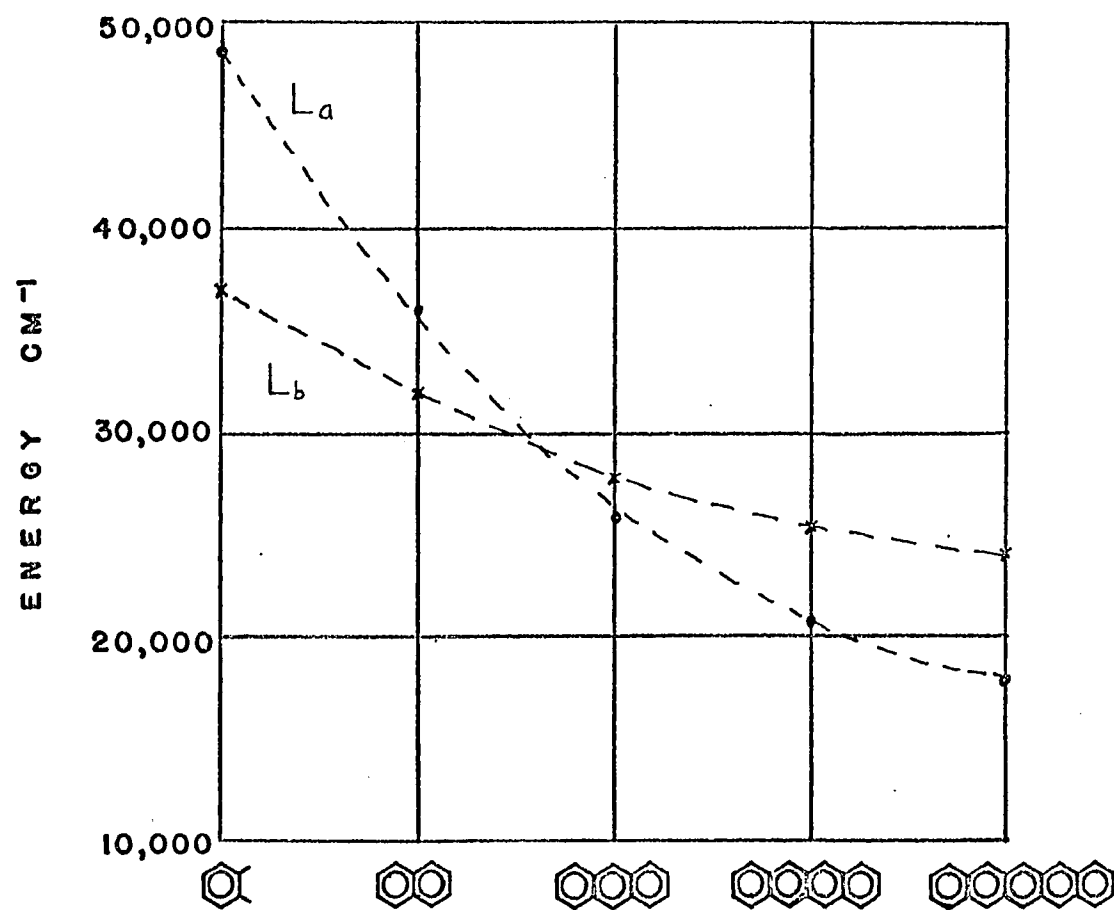
Fig. 56. Proposed energies for the $L_a$ and $L_b$ bands of the catacondensed aromatics

they change position with respect to their energies (see Fig. 56). The

$L_a$ band is expected to be affected in energy to a greater degree by changes

in the skeletal structure of the molecule. This results because the sign

of the wave function changes at the positions of the atoms, so that addi-

tion of a substituent or another ring has a greater perturbation on the

$L_a$ transition than the $L_b$ transition which has nodes at the atoms.

The polarization of the $L_a$ and $L_b$ bands has been determined by effects

of substituents and is illustrated in Fig. 57.
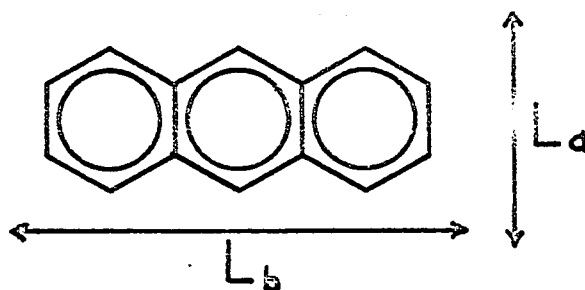


Fig. 57. Polarization of $L_a$ and $L_b$ bands

One might predict that the MCD for the series in Fig. 56 would become

larger in magnitude as the bands approach one another and then decrease

again as they draw apart in tetracene and pentacene. The long wavelength

band would be expected to retain the same sign but an interesting problem

comes up if a narrow band occurs within a broader one. According to

theory, the result should be as shown in Fig. 58(a). Another possibility

which does not agree with theory but might be intuitively expected is in

Fig. 58(b). The situation might well occur for the cases being studied,

for Platt (57) has characterized the $L_b$ band as one with sharp vibrational

structure and a bandwidth of 300 $cm^{-1}$, while the $L_a$ band has a width of approximately 500 $cm^{-1}$.

The experimental results for the MCD of the series of compounds in Fig. 56 are shown in Fig. 59. Unfortunately, problems with oxidation of the pentacene in solution precluded the possibility of measuring the MCD for this compound. In order to make the results of the complicated spectra more easily visible, the molar magnetic circular dichroism of the peaks have been calculated and replotted as lines. The proposed assignments of Klevens and Platt are indicated in the figure and the positions of the main absorption peaks are marked along the abscissa.

As expected, the MCD becomes larger in magnitude as the $L_a$ and $L_b$ bands approach one another in naphthalene and anthracene. The MCD does not decrease again with tetracene in disagreement with the prediction. Also, if the tetracene $L_a$ and $L_b$ bands are mixing, equal and opposite values would be expected for their respective MCD's, whereas the MCD for the $L_a$ bands is of the same sign as the $L_b$ MCD and barely detectable experimentally. These difficulties make the assignment of the tetracene bands questionable. For the naphthalene and anthracene opposite signs are found generally for $L_a$ and $L_b$ MCD although they are not of equal magnitude (nor are the areas under their curves of equal size) suggesting that complex interactions are taking place. Since the vibrational bands are so close together for anthracene it is difficult to compare with the expected MCD of Fig. 58, but there is substantial agreement with Fig. 58 (b), that is, not as expected from theory. In any case, it seems improbable that, merely by coincidence, the only MCD band with a positive sign would be the
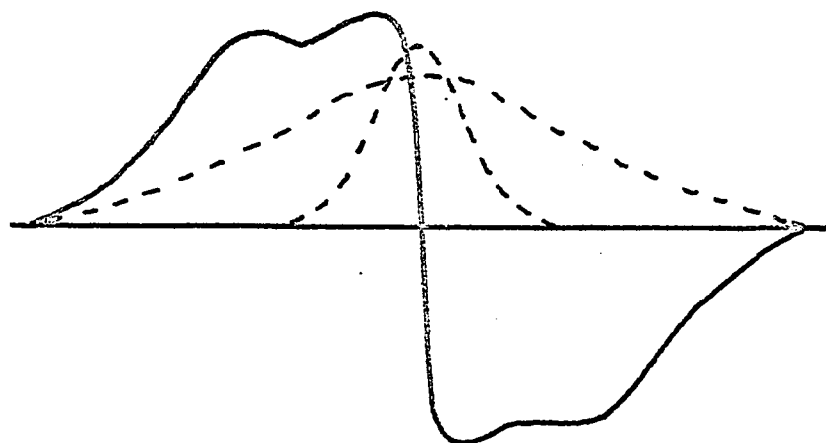
(a)
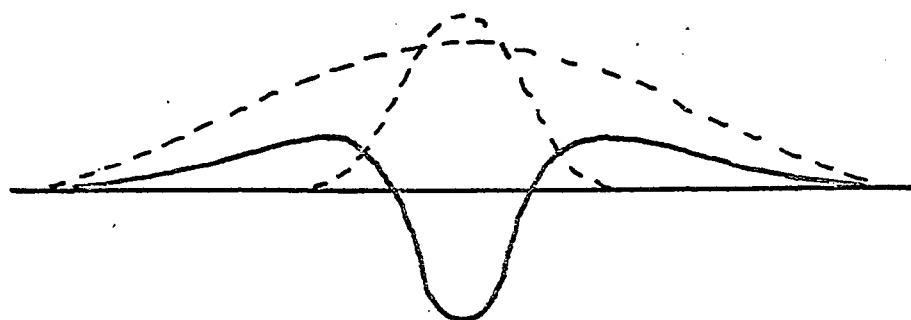
(b)

Fig. 58. Possible MCD (———) resulting from overlapping narrow
and broad absorption bands (— — — —)
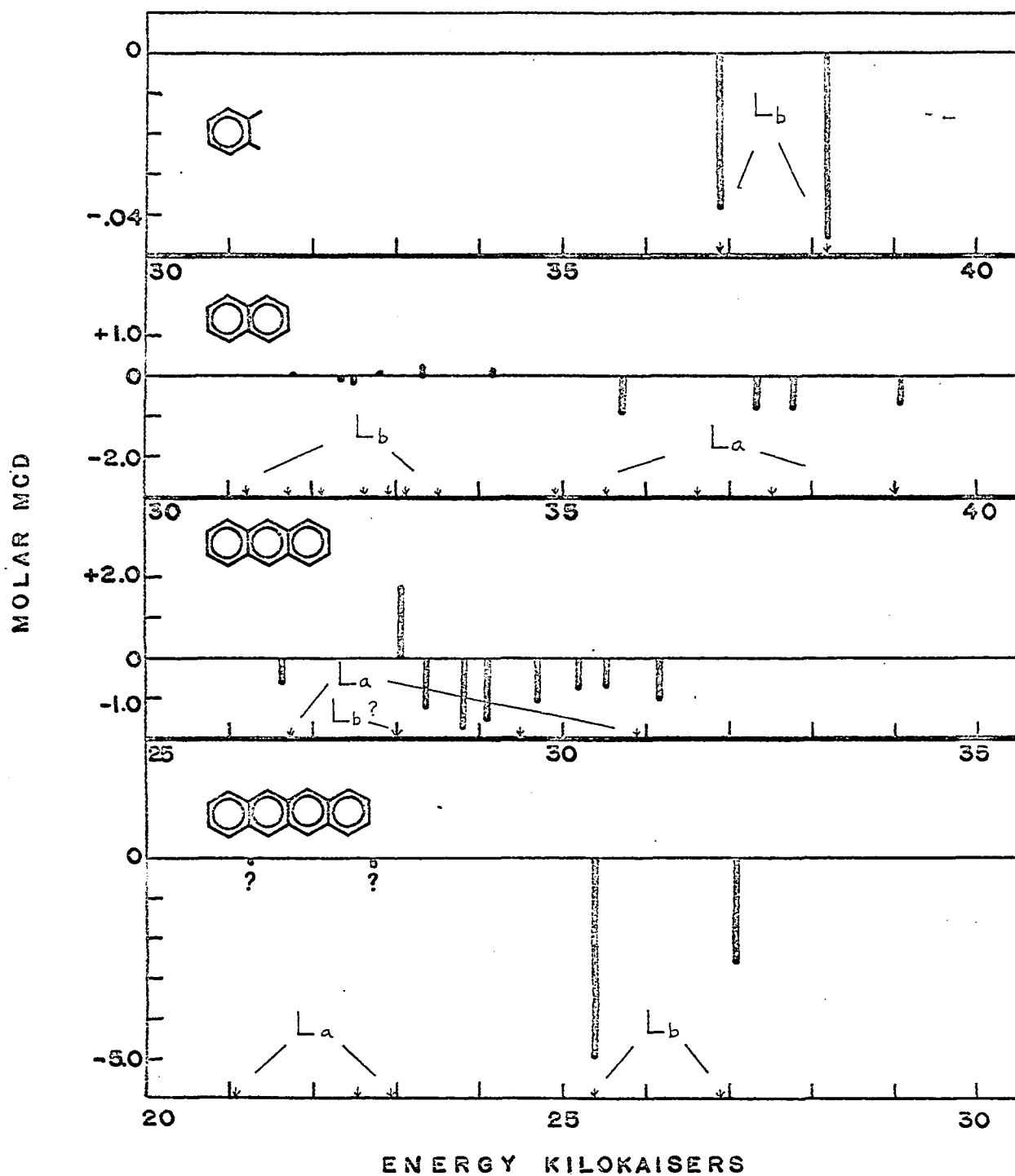
Fig. 59. MCD results for the catacondensed aromatics

predicted $L_b$ band at 28,000 $cm^{-1}$.

## Substituted naphthalenes

The MCD spectra of several substituted naphthalenes were observed in order to compare with the results found with the substituted benzenes. Since the $L_a$ and $L_b$ bands are both accessible experimentally for these compounds, spectra similar to those in Fig. 60 are expected.



(a)                              (b)
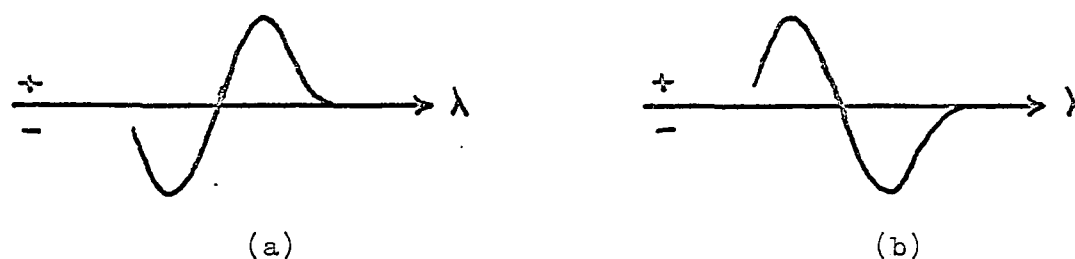
Fig. 60. Expected MCD for the naphthalenes

Several of the substituted naphthalenes gave good examples of the spectra in Fig. 60. The only case of Fig. 60 (a) was α-nitro naphthalene. Examples of Fig. 60 (b) were the molecules with -OH or $-NH_2$ in the α position, 1,5 naphthalene diol and $5-NH_2-1$-naphthol. Once again the classification of substituents as electron-withdrawing and electron-donating correlates with the sign of the longest wavelength MCD.

Naphthalenes with β substituents gave weak, complex MCD spectra for which no interpretation will be offered.

The Quinolines

## The ultraviolet spectra

The electronic absorption spectrum of quinoline is very similar to that of naphthalene (44, p. 379). From Fig. 61 it may be seen that several sharp bands appear at the longer wavelengths from 300-320 m$\mu$, and a broad band system peaks at about 270 m$\mu$. By noting the effects of substituents the former bands have been assigned as the $L_b$ transition and the latter as the $L_a$ transition. The intensity of the $L_b$ band is higher than for naphthalene, probably a result of the reduced symmetry. As with naphthalene, the polarization of the $L_b$ transition moment is along the long axis of the molecule, the $L_a$ moment is along the short axis. There are no recognizable n$\rightarrow\pi^*$ transitions for the quinolines, a situation often encountered for hetero-aromatics with only one ring nitrogen (58, p. 301).

The ring nitrogen (=N-) is electron-attracting for the $\pi$ electrons (58, p. 34). Hammett $\sigma$-values have been calculated for the quinoline molecule and are positive for all but the 8 position (59).

The substituted quinolines also have absorption spectra very similar to the corresponding substituted naphthalene. The most common result of substitution is a bathochromic shift of the $L_a$ band while the $L_b$ band moves very little. This effect is represented by the compounds in Figs. 63 and 64.

Addition of a proton to quinoline seems to lower the intensity of the $L_a$ transition and shift it to the red (44, p. 369). The $L_a$ band may be partially covered by the $L_b$ absorption. The absorption spectrum of
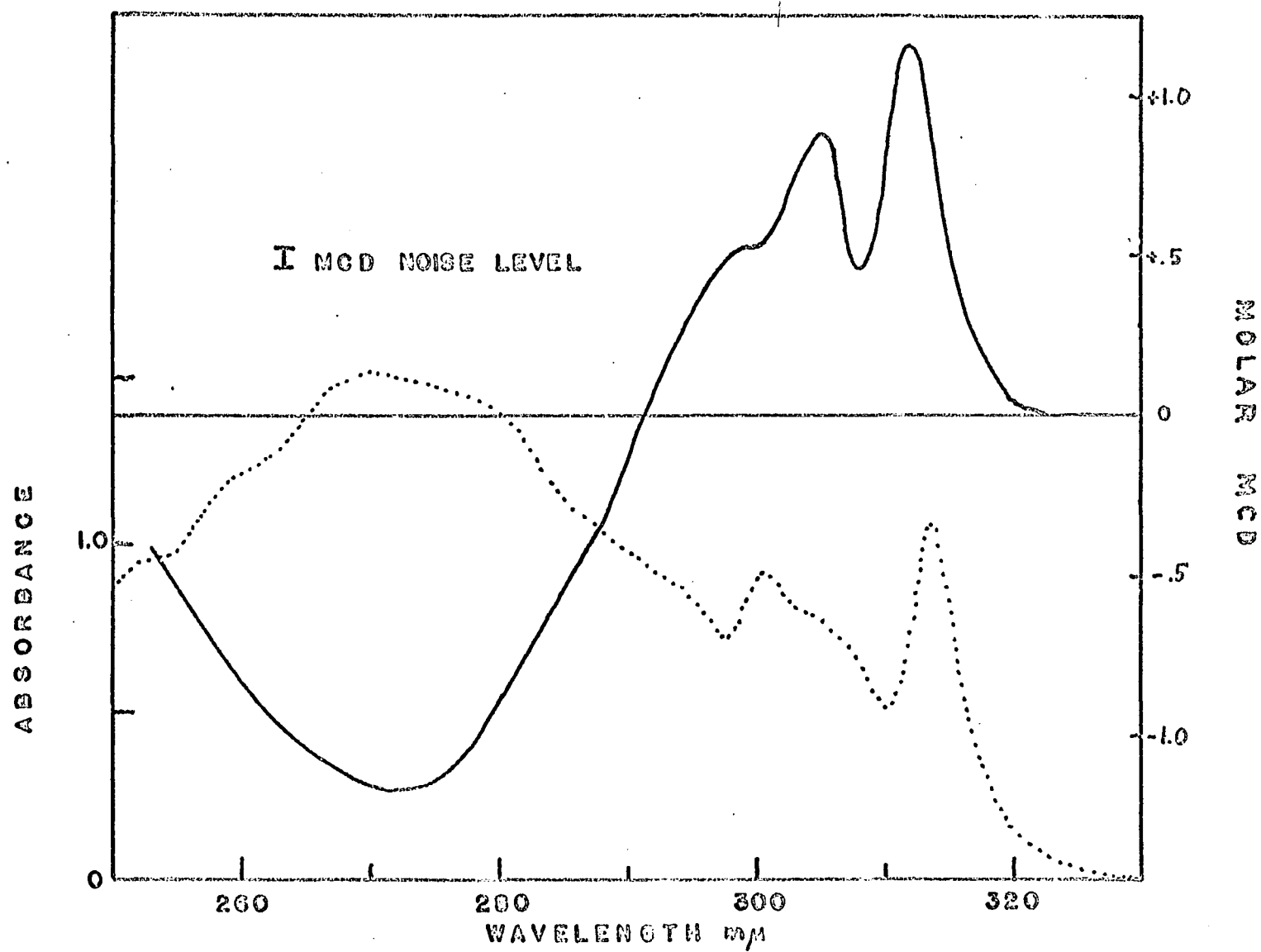
Fig. 61. Absorption (- - - -) and MCD (———) of quinoline

quinolinium ion is shown in Fig. 62.

## The MCD spectra

The MCD spectrum of quinoline is shown in Fig. 61. The $L_a$ and $L_b$ bands appear to be mixing magnetically, giving opposite and almost equal MCD. The positive sign for the long wavelength transition is in agreement with the fact that the ring nitrogen causes this to be a $\pi$-electron-deficient system. Therefore the charges involved in the transitions can be considered to be holes rather than electrons. From the results of Fig. 61 one would assign those bands above 290 m$\mu$ as $L_b$ and those from 250-290 m$\mu$ as $L_a$.

The MCD of quinolinium ion (Fig. 62) retains the same sign as that for quinoline, but the crossover point has moved to the red approximately 20 m$\mu$. This indicates that the interacting bands have moved much closer together as suspected from the absorption spectrum. One might also expect the MCD to increase considerably with the bands more nearly equal in energy, but some cancellation of the positive and negative MCD contributions from the overlapping absorptions will reduce this.

A number of substituted quinolines were studied in an attempt to correlate the sign of the MCD with the type and position of the substituent. The position of the substituted group was found to be of little effect, what was much more important was the relative electron-donating or -withdrawing power. MCD spectra very similar to that obtained for quinoline were recorded for the following substitutions: 5-$NO_2$, 8-$SO_3H$, 2-$CH_3$, 5-$NH_3^+$, 8-$CH_3$, 4-$COO^-$, 8-$NO_2$. An attempt was made to find a substituent with strong enough electron-donating ability to overcome the
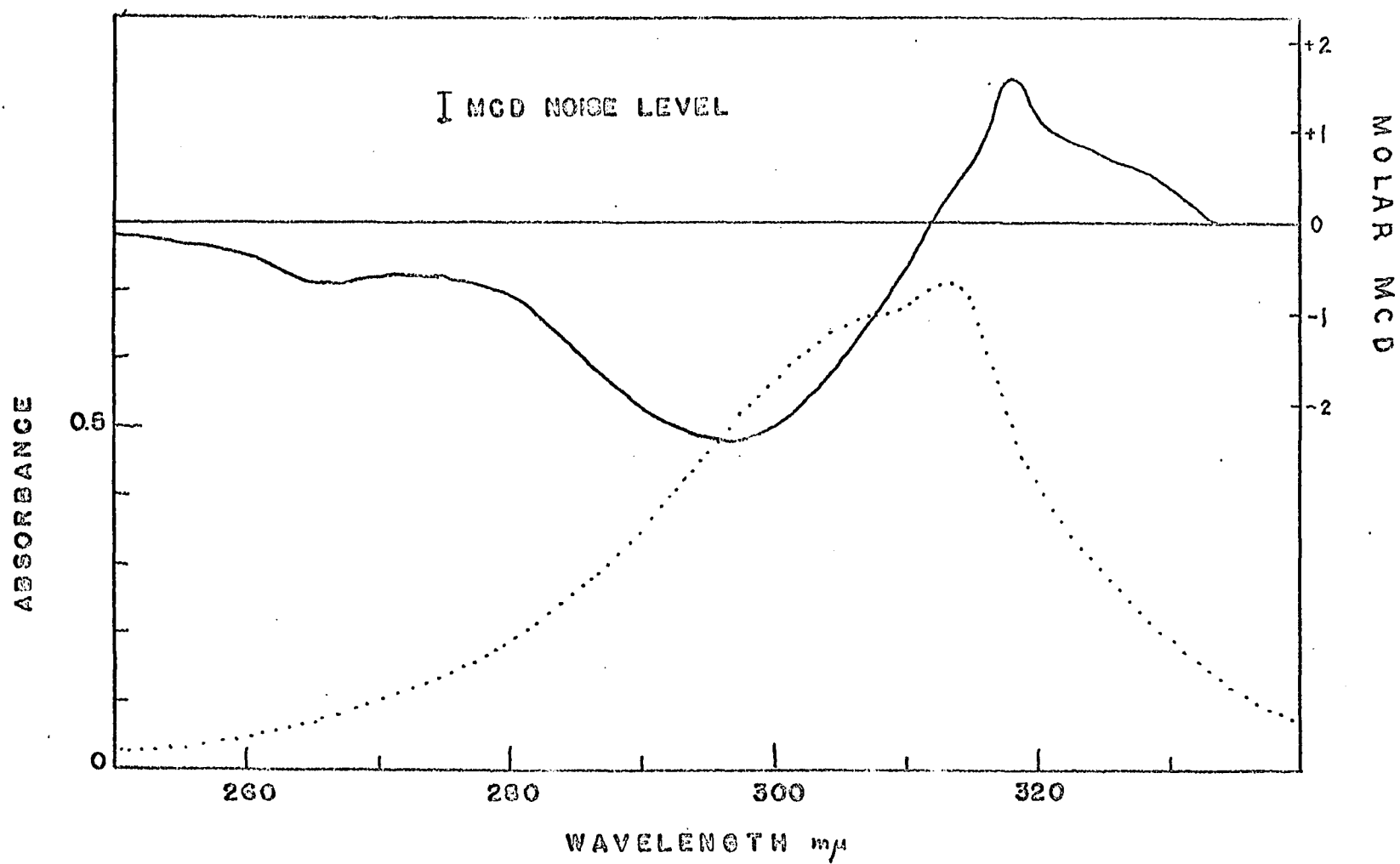
Fig. 62. Absorption (- - - -) and MCD (———) of quinolinium ion

effect of the ring nitrogen and therefore change the sign of the MCD.

Only two such compounds were found among those available, the 4-OH and

5-OH quinolines in strongly basic solution. The spectra for the 4-OH case

are shown in Fig. 63. The hydroxy group does not donate $\pi$ electrons so

readily as -O$^-$ and in acid solution even more electrons must be withdrawn

to bind a proton to the ring nitrogen. It is only in basic solution where

the substitutent is in anionic form that an excess of $\pi$ electrons is found

in the ring.

Fig. 64 represents another case where a narrow band appears to be

interacting with, and overlapped by, a broader band. The 5-OH and 8-OH

quinolines in acidic solutions also are of this type. An understanding

of these results may have to await the development of a theory for

accidentally degenerate systems for the results do not agree with the

assumption that the B term equations we have been using are valid for

overlapping bands. This situation occurred above in the discussion of

anthracene.
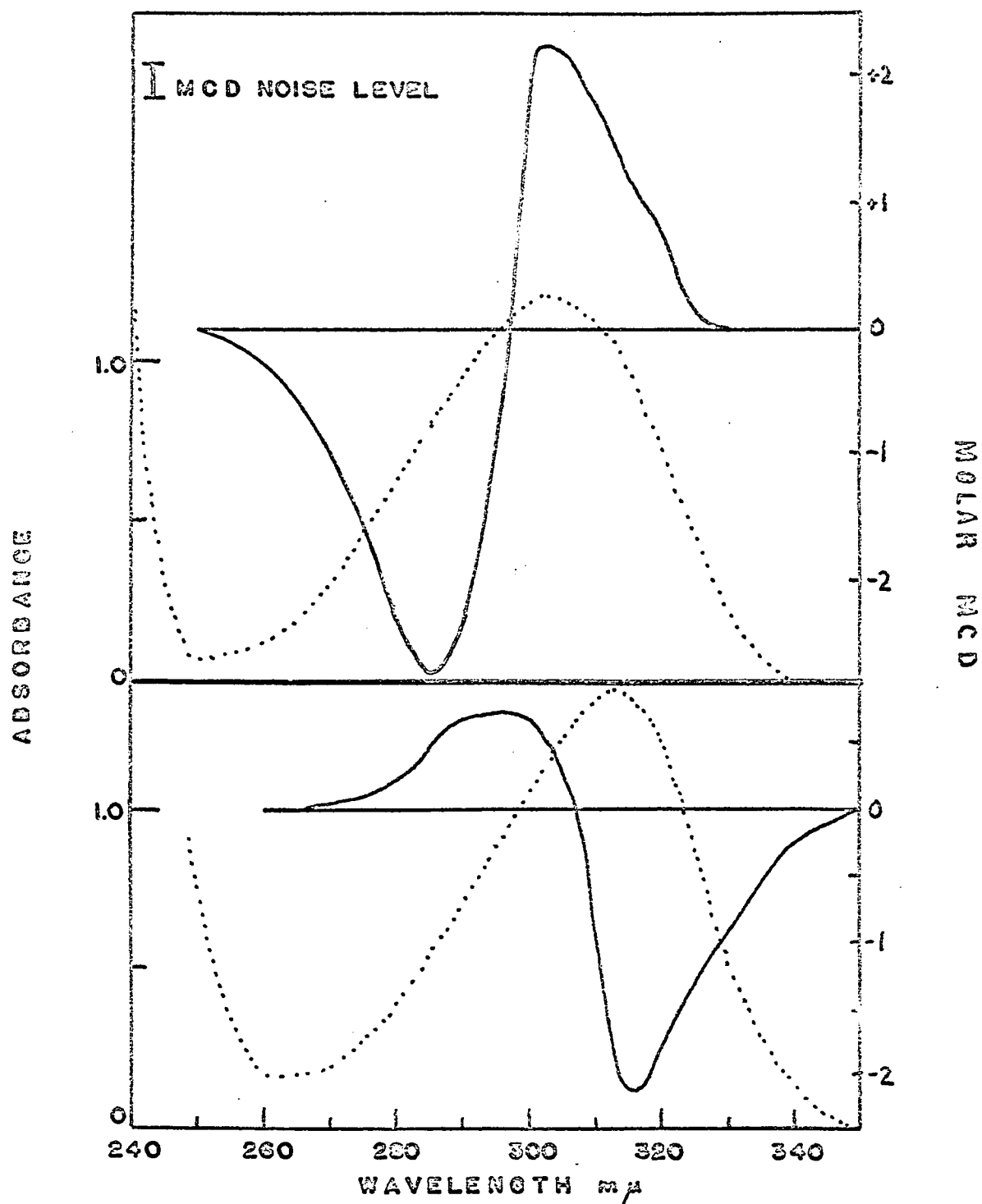
Fig. 63. Absorption (·-·-·) and MCD (———) of 4-OH quinoline in (top) acidic and (bottom) basic solution
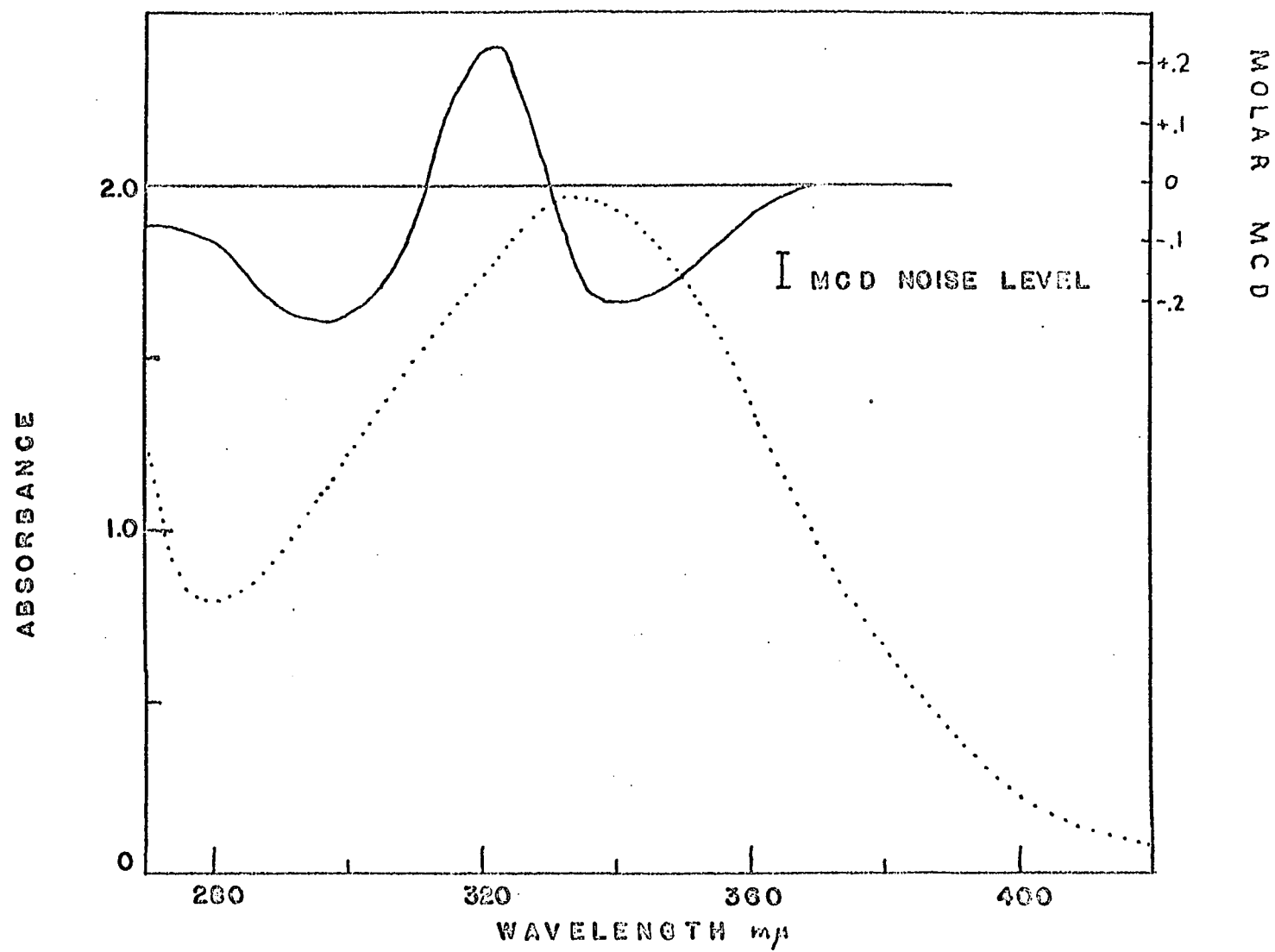
Fig. 64. Absorption (----) and MCD (———) of 5-NH$_2$ quinoline

## The Purines and Pyrimidines

The purines and pyrimidines are often involved in important biological systems. Knowledge of their optical properties is particularly necessary in view of the fact that optical spectroscopy is one of the most promising means of studying the structure and function of these biological systems. In particular, the incorporation of purines and pyrimidines into RNA and DNA leads to interactions between the bases which can be understood satisfactorily only if the spectroscopy of the independent bases has been mastered. An example of these interactions is found in the hypochromism of polynucleotides as they make the transition from a random to a helical structure. Information is needed on the types of electronic transitions, their energies and directions, factors which MCD studies may help determine.

### The purines

<u>The UV spectra</u>    A considerable amount of work has been done on the electronic spectroscopy of the purines. Mason (60) collected absorption data on the purines, Stewart and Davidson (61) examined the polarized absorption spectra of crystals of 9-Me adenine, Callis, Rosa and Simpson (62), Clark and Tinoco (63) and Cohen and Goodman (64) attempted to demonstrate by solvent effects and polarization of emission that an accidental degeneracy occurs in certain purine derivaties. Studies by Drobnik, Kleinwachter and Augenstein (65,66,67,68) have been reported most recently, also using various solvents and polarized emission.

In the solvents used, ring nitrogens of both types, $(=N-)$ and $(-\overset{\frown}{N}-R)$, are found. Transitions of the $n \longrightarrow \pi^*$ type are not always visible, but one is seen as a long wavelength tail in the purine spectrum in Fig. 65. The
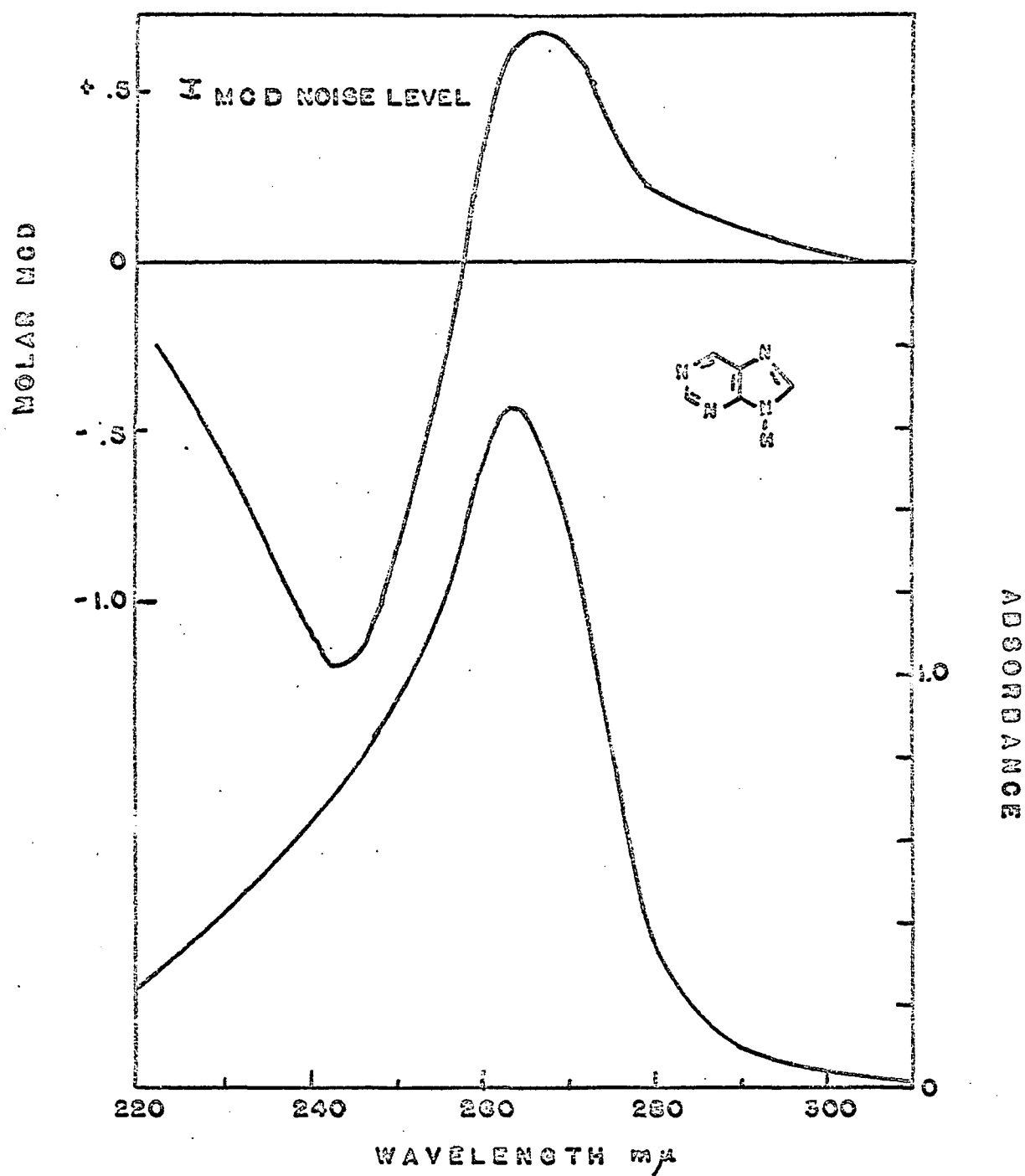
Fig. 65. Absorption and MCD of purine

two $\pi \rightarrow \pi^*$ transitions of lowest energy are generally considered to be related with the $L_a$ and $L_b$ bands of benzene. Experimental determinations of the polarizations of these transitions are still quite uncertain. There is some theoretical speculation that the $L_a$ and $L_b$ bands are parallel in purine (68). Clark and Tinoco observed a series of substituted purines which seem to show the gradual merging of the $L_a$ and $L_b$ bands as the substituent perturbation is increased (63). Considerable effort has been expended in an attempt to show that the 260 m$\mu$ band of adenine actually consists of two unresolved transitions (63-68).

The MCD spectra    The technique of MCD is, at least in theory, well suited to the determination of accidental degeneracy. If two overlapping bands interact magnetically the result will in general be an MCD which changes sign at some energy within the absorption curve. This is a clear indication of an accidental- or near-degeneracy.

While the method of MCD can be a powerful one for the situation of interest here, several limitations must be kept in mind to avoid making unwarranted conclusions. These precautions are listed below.

1. There is the possibility that the different vibrational components of a single absorption band might interact, giving the appearance of an accidental degeneracy. This could occur if the different vibrational peaks were polarized with some perpendicular component relative to one another. This situation probably occurs very rarely, but is not unknown (44, p. 133). For this reason, supplementary evidence for accidental degeneracy is still essential. Such evidence is difficult to find since the

techniques of polarization studies are all affected by this
problem.

2. Although this technique can reveal an accidental degeneracy, it
   can offer no information concerning the relative energies of the
   interacting bands. The sign of the MCD will not depend on which
   band is at the longest wavelength.

3. Due to overlapping of the two opposite MCD contributions, the
   MCD maxima will usually not coincide with the maxima of the
   individual absorption. Information on the values for the
   absorption peak energies is available only after resolution of
   the bands into their separate components, a technique involving
   considerable uncertainty.

Clark and Tinoco studied the absorption of the series; purine,
6-chloro purine, 6-methoxy purine, adenine for evidence of a gradual
merging of the $L_a$ and $L_b$ bands (63). The MCD for three of these are
shown in Figs. 65, 66, 67. For purine the MCD peaks almost coincide with
the absorption bands at 240 mμ ($L_a$) and 263 mμ ($L_b$), indicating that
these are the interacting bands. The situation is almost the same for
6-chloro purine although the $L_a$ band is now somewhat closer to the $L_b$ band.
In adenine there is no evidence from the absorption spectrum for the
presence of two bands, but the MCD changes sign at approximately the wave-
length of the absorption peak. This crossover is at a wavelength between
the $L_a$ and $L_b$ peaks. The different sign for the MCD of the long-wave-
length band of adenine can be attributed to the increased electron-
donating ability of the amino group at the 6 position as compared to
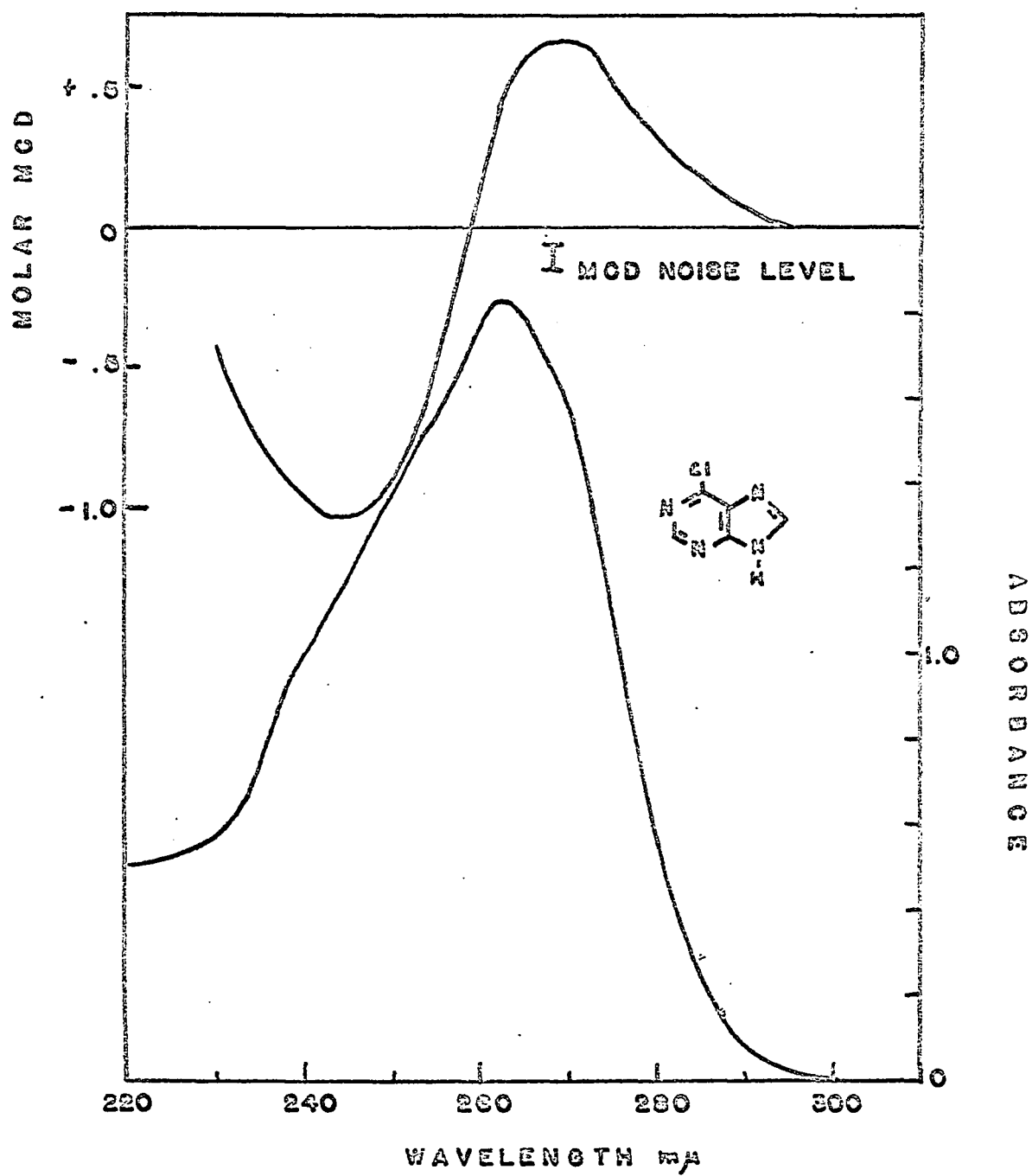
F.g 66. Absorption and MCD of 6-Cl purine
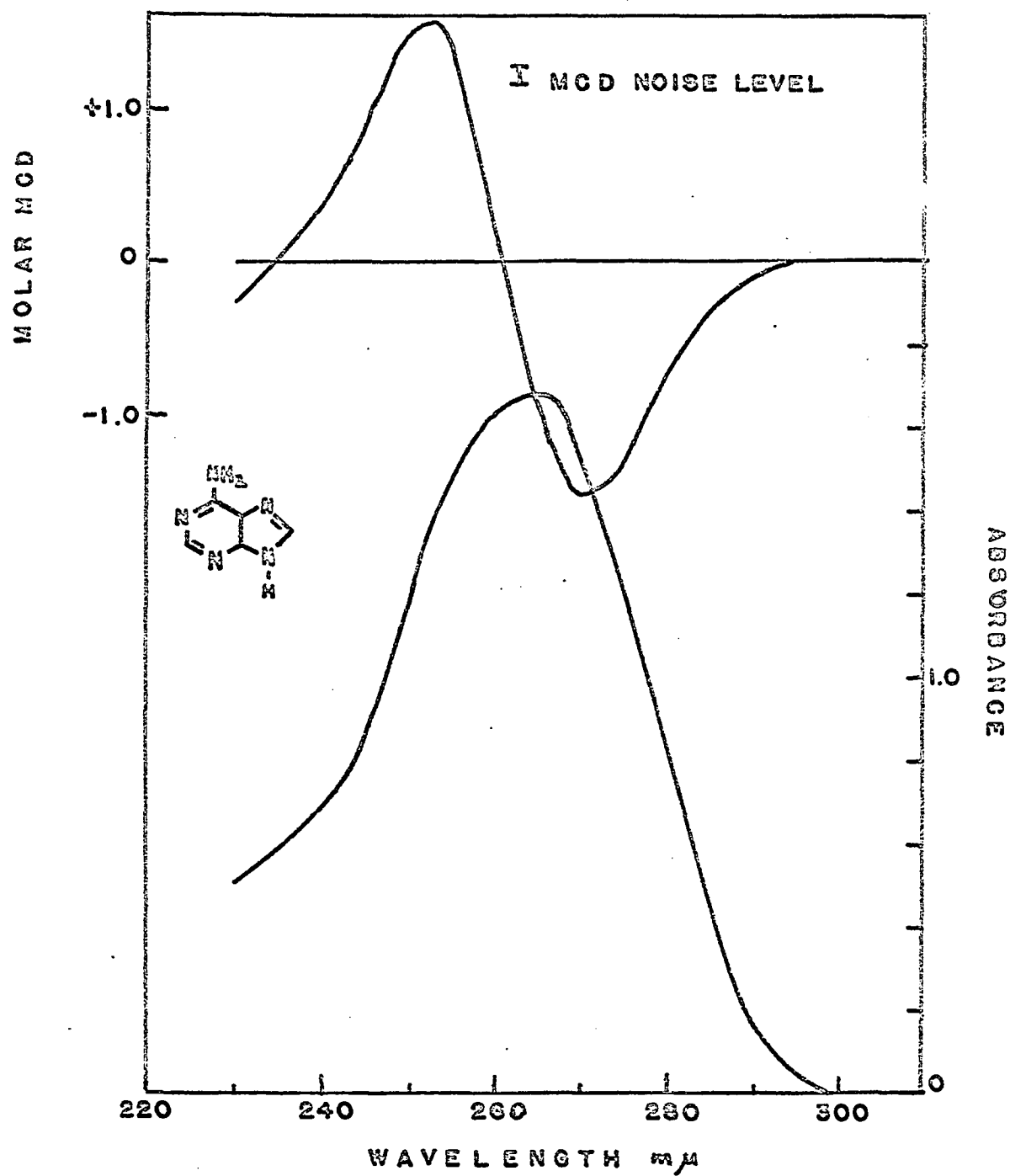
Fig. 67. Absorption and MCD of adenine

chlorine.

The MCD of 6-methoxy purine is in Fig. 68. This result is somewhat puzzling since it indicates that the interaction involves the very small tail at 270 mμ. Comparison of this result with the other three members of the series suggests that the peak at 251 mμ is $L_a$ and that at 270 mμ is $L_b$. The molar MCD may be small compared to the other compounds because the methoxy group donates just enough electrons so that only a small excess of holes is involved in the electronic transitions.

The MCD of guanine in Fig. 69 suggests that the band at 247 mμ belongs to the $L_a$ transition, that at 274 mμ is the $L_b$ band. When guanine is bonded at the 9 position, which is the case for purines in nucleotides, the relative intensities for the $L_a$ and $L_b$ transitions are changed. As seen from Fig. 70, these two bands are well separated and from the MCD may be assigned as the 248 mμ and 275 mμ peaks respectively.

The accidental degeneracy of the absorption bands for two other purines was also detected. They were the 255 mμ band of 9-methyl hypoxanthine (MCD peaks at 247 mμ and 264 mμ), and the 260 mμ band of 9-methyl adenine (MCD peaks at 252 mμ and 270 mμ).

The sign of the low energy MCD band was positive for only three of the purines studied, purine, 6-chloro purine and 6-methoxy purine. This may be interpreted as meaning that the substituents on the other purines were capable of donating enough electrons to produce a π-electron excess in the ring.

The MCD found for the purines reveals some information concerning the relative directions for the $L_a$ and $L_b$ bands. The most obvious
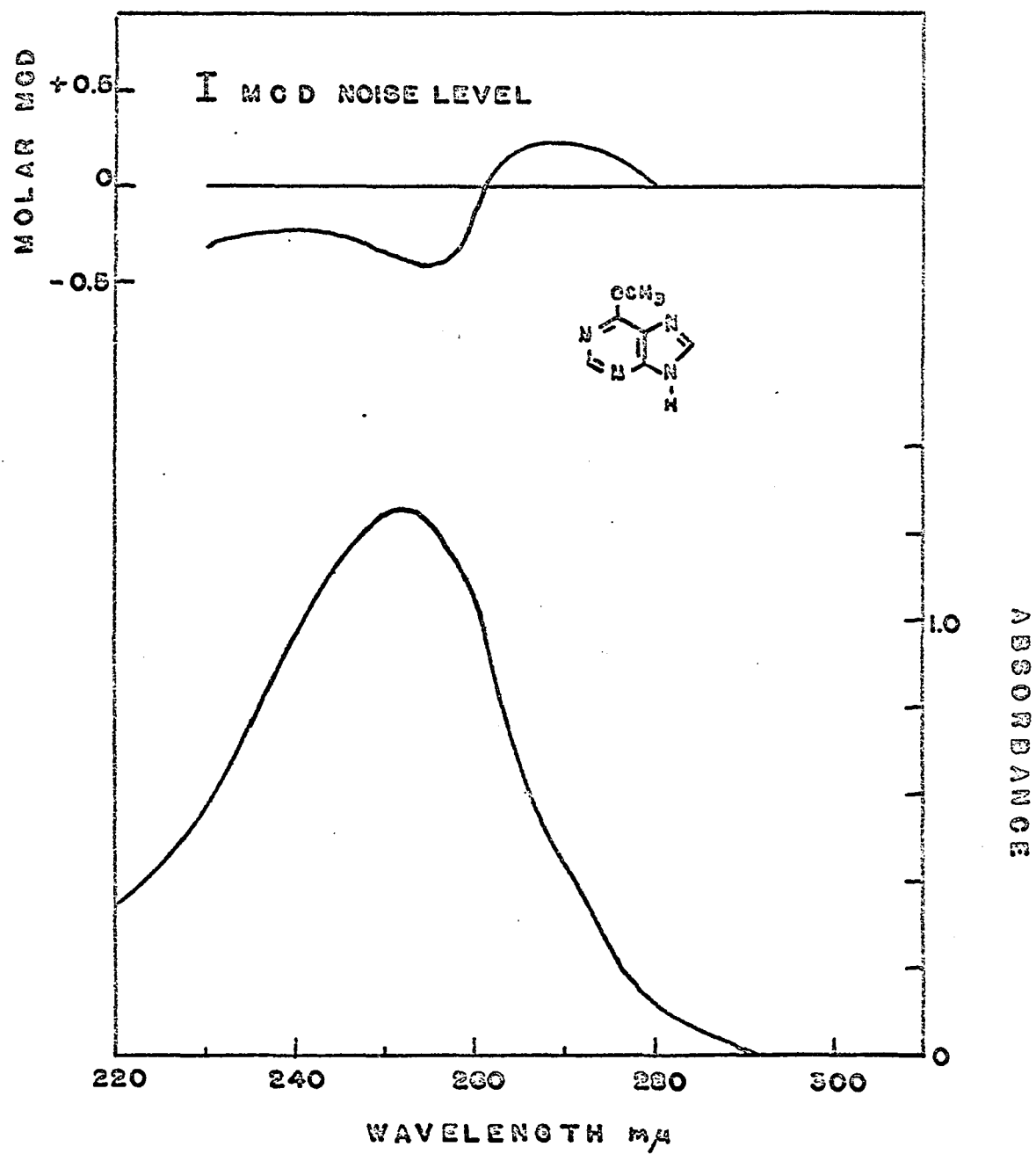
Fig. 68. Absorption and MCD of 6-methoxy purine
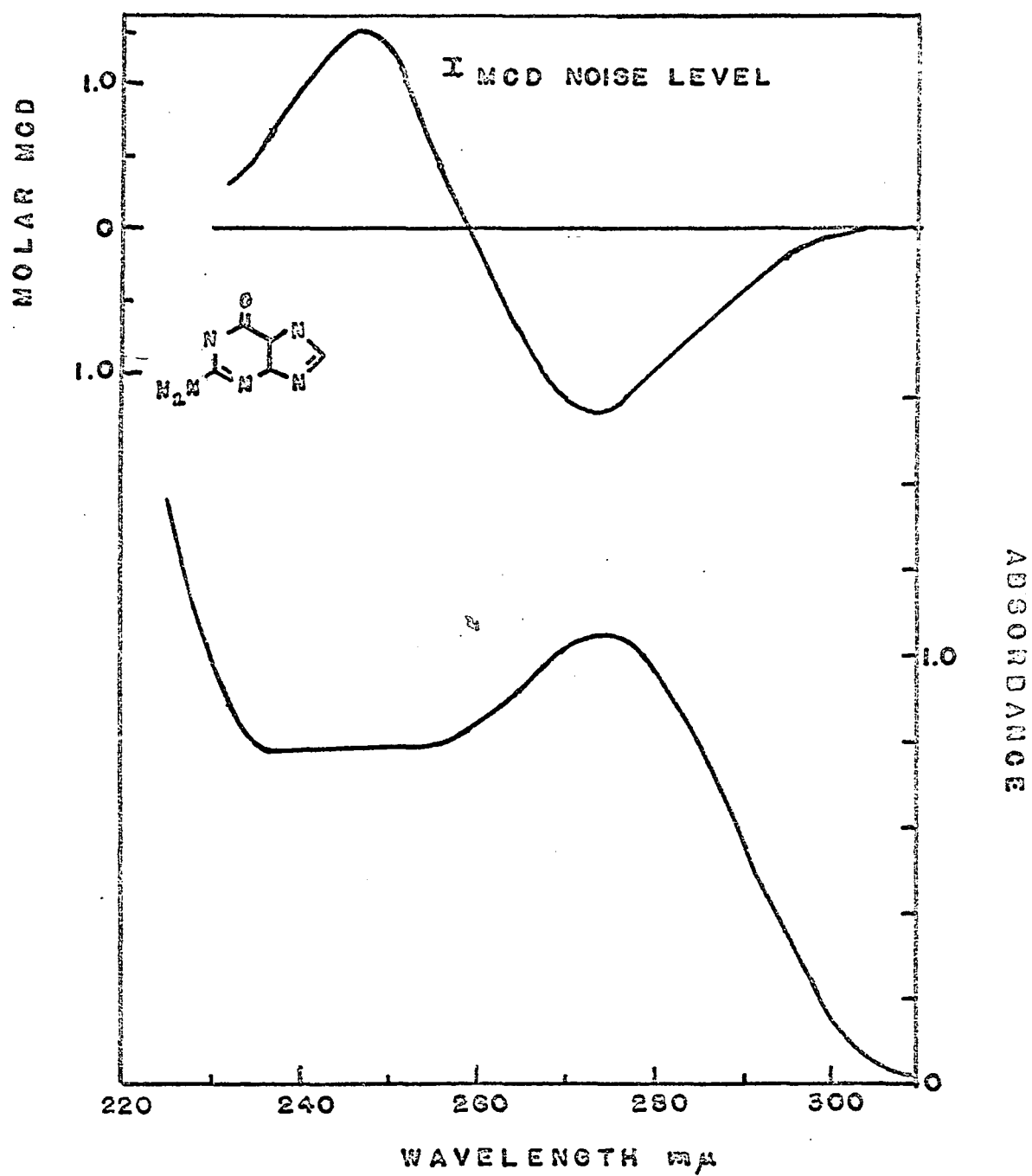
Fig. 69. Absorption and MCD of guanine
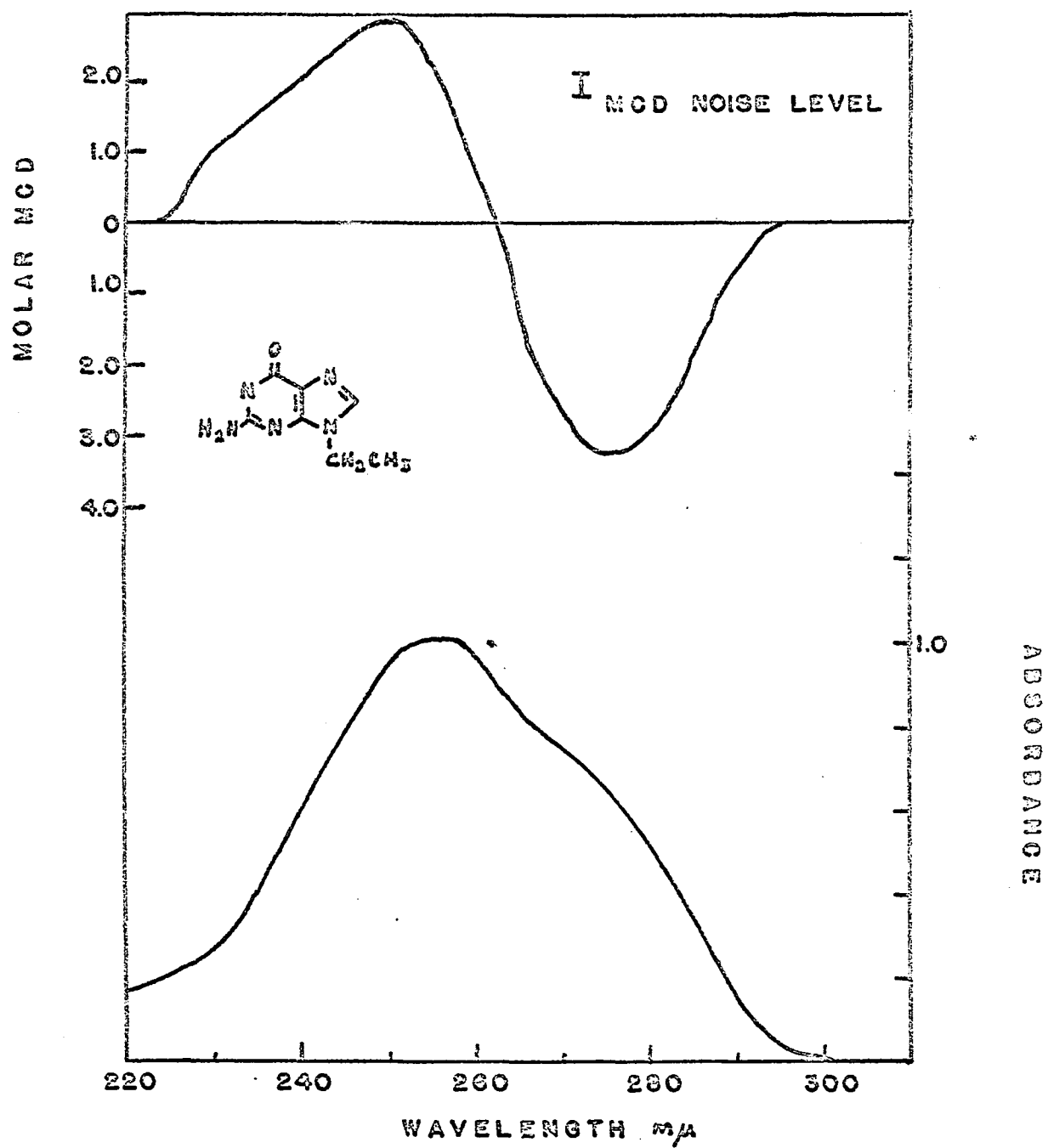
Fig. 70. Absorption and MCD of 9-ethyl guanine

conclusion is that since MCD is observed the two transition moments cannot be parallel. Secondly, the magnitude of the MCD gives a rough idea of the size of the angle between the transition moments. The molar MCD for purine is approximately +0.68 at 267 mμ, of the same order of magnitude as the MCD for naphthalene and anthracene where the angle is known to be nearly 90° (44,p.305). Although other variables are involved (e.g., the size and direction of the magnetic transition moment) which cannot be specified with the information available, this comparison suggest that the angle is a large one.

The MCD of a relative of purine, benzimidazole, is shown in Fig. 71. The bands related to benzene may again be picked out and on the basis of the MCD are assigned as $L_a$ from 240-260 mμ and $L_b$ above 260 mμ. The sign of the MCD indicates that the imidazole ring is causing a depletion of π electrons from the benzene ring. Indole, which has only one hetero-nitrogen but is otherwise identical with benzimidazole, has an MCD much like Fig. 71 in appearance.

## The pyrimidines

The UV spectra    Many of the properties of electronic absorption for the purines are also present for the pyrimidines. Bands related to the $L_a$ and $L_b$ transition of benzene are observed, and with some pyrimidines $n \rightarrow \pi^*$ bands may be seen. Pyrimidine itself, Fig. 72, has an $n \rightarrow \pi^*$ band beginning at 320 mμ and peaking at 293 mμ. The $L_a$ transition is uncertain, but may be the shoulder at 210 mμ (50). The substituted pyrimidines often retain the $L_b$ band at approximately 260-280 mμ.
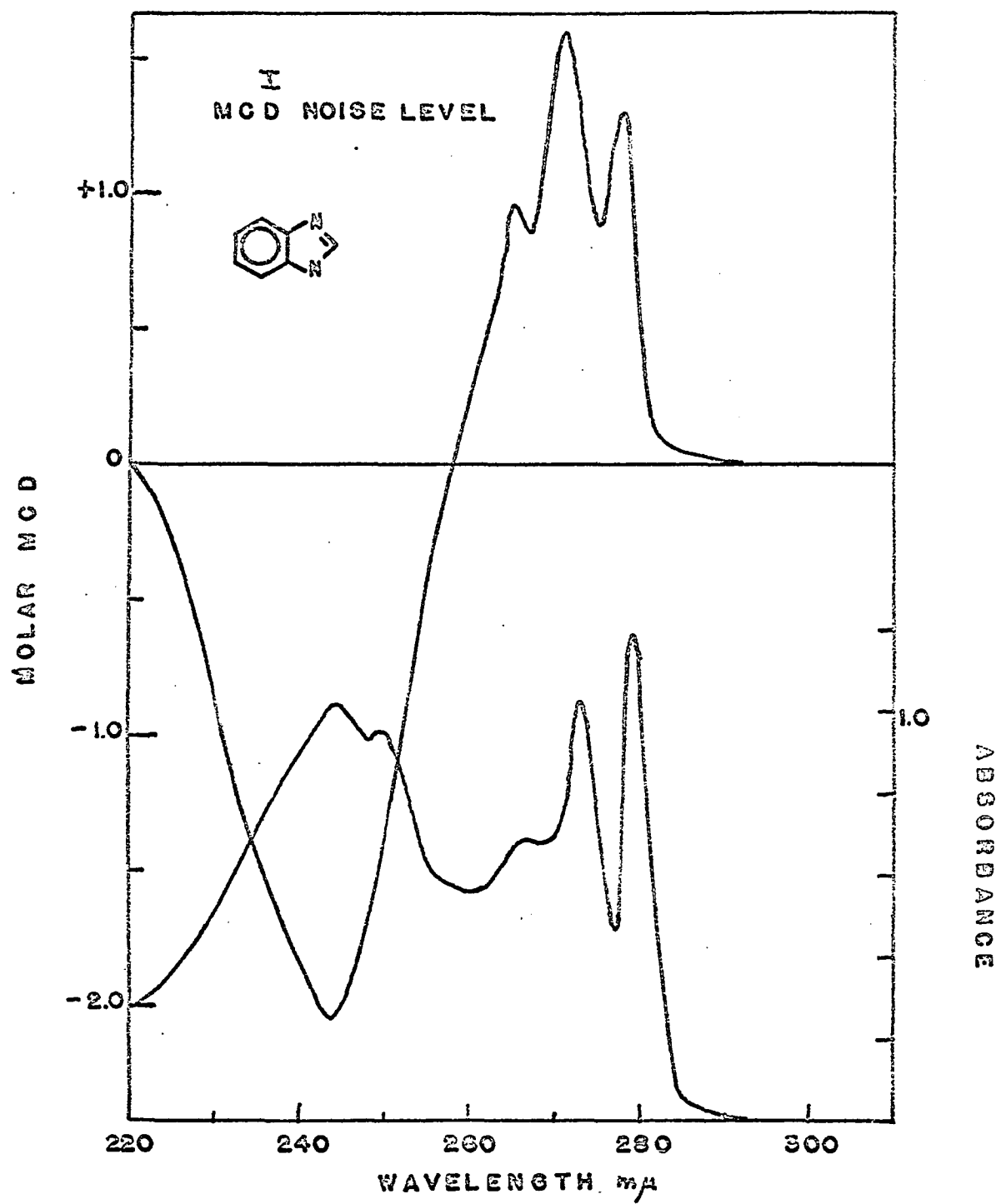
Fig. 71. Absorption and MCD of benzimid azole
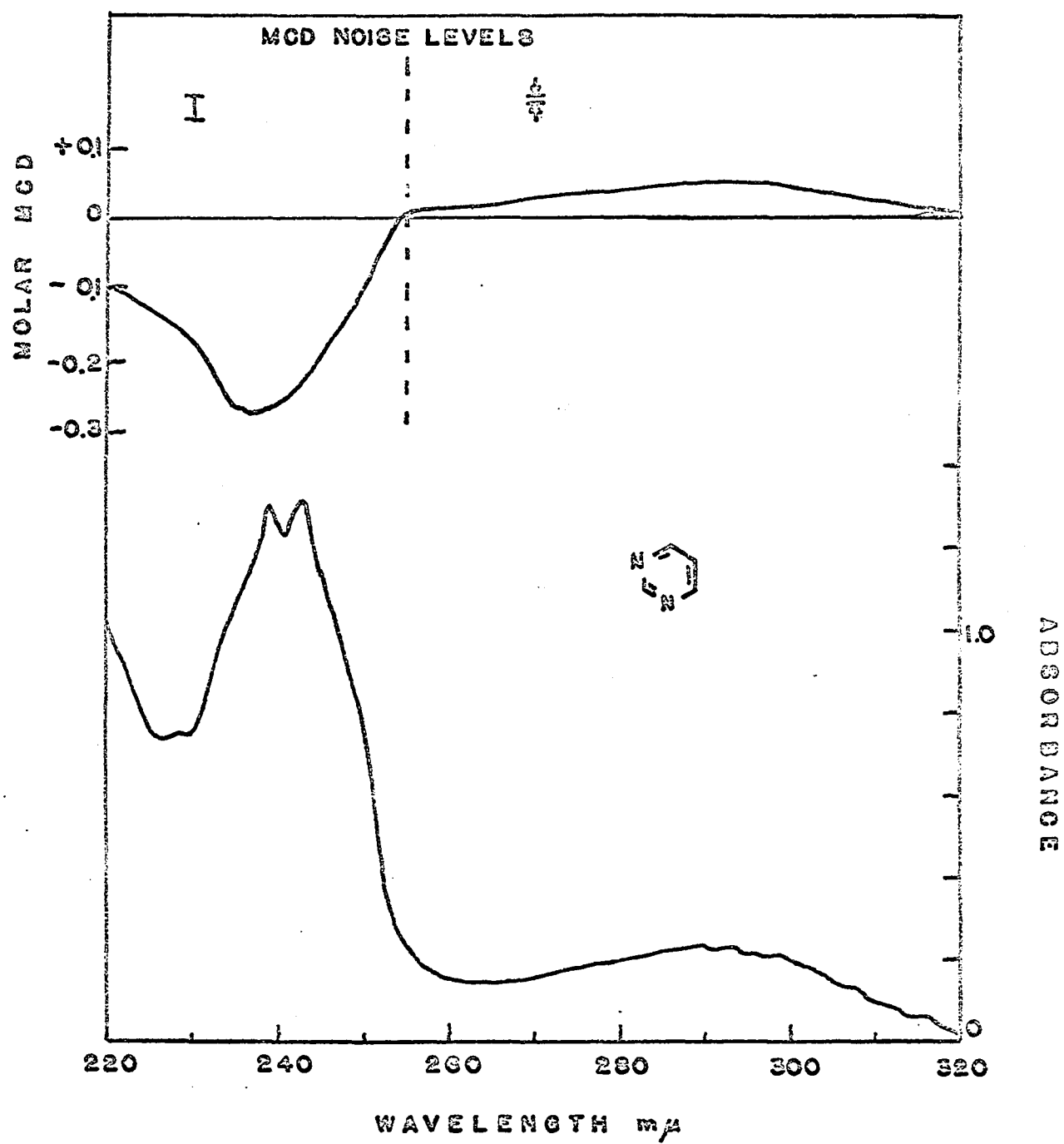
Fig. 72. Absorption and MCD of pyrimidine

The MCD spectra      The MCD for pyrimidine is shown in Fig. 72.  The
$n \rightarrow \pi^*$ band is probably interacting with the $L_b$ band.  Most $n \rightarrow \pi^*$
transitions are polarized perpendicular to the plane of the ring while
the $L_b$ transition moment is expected to lie in the plane.  The sign of
the long wavelength MCD indicates a $\pi$-deficient ring system due to the
electron attraction of the two ring nitrogens.  Unfortunately the $L_a$ band
for the pyrimidines seems to lie out of range of the instrument, therefore
no help for assigning that band is forthcoming from these results.  A
compound related to the pyrimidines, 6-aza uracil, also has a long-wave-
length $n \rightarrow \pi^*$ absorption and an MCD similar to that in Fig. 72.

The MCD of uracil is pictured in Fig. 73.  The negative sign of the
lowest energy band now indicates that the substituents have donated
enough electrons to make this a $\pi$-excess ring system.  Similar MCD results
were obtained for uracil at pH 13, cytosine in TMP, 5-fluoro uracil,
dimethyl uracil and 6-methyl uracil.
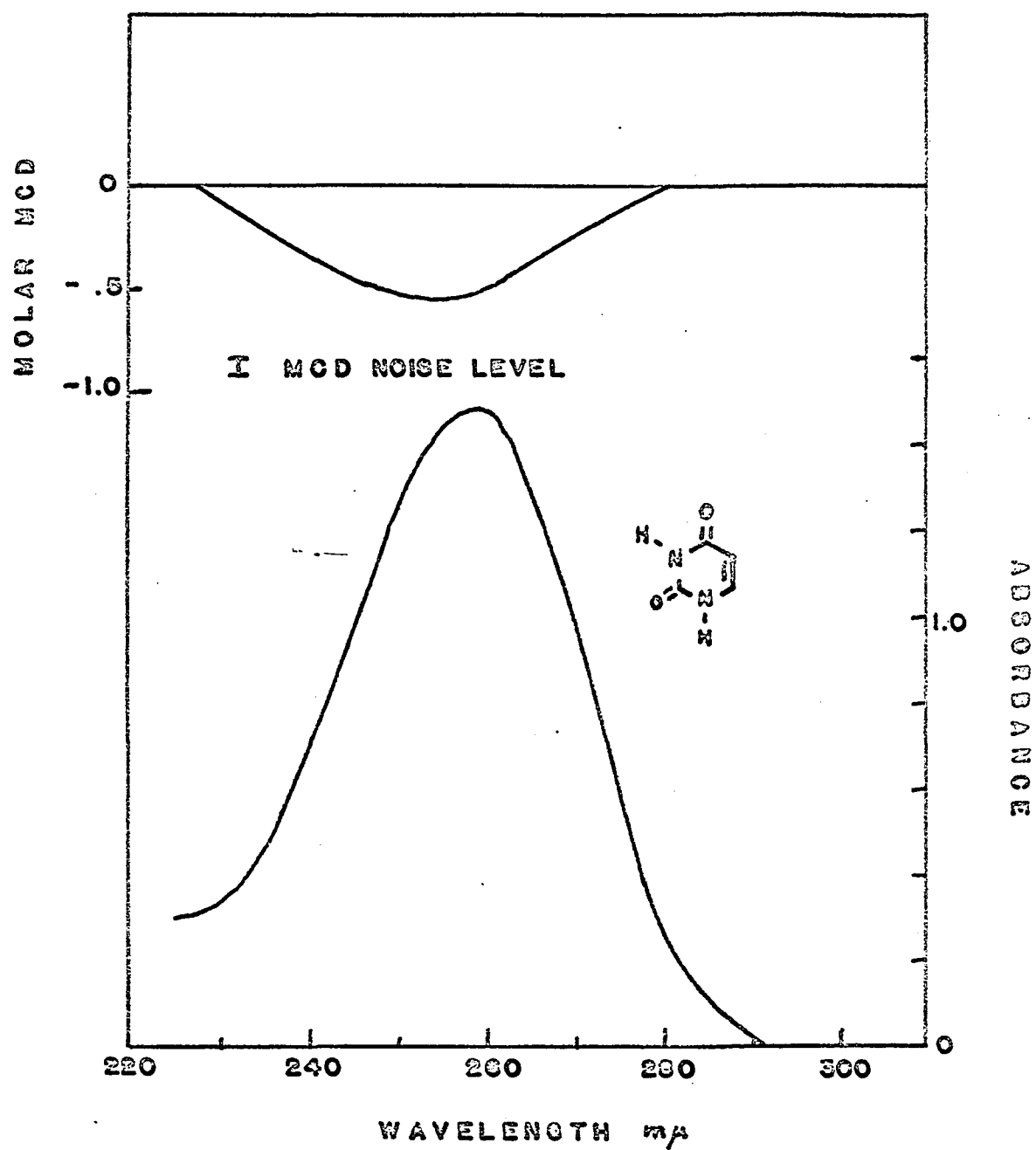
Fig. 73. Absorption and MCD of uracil

Miscellaneous Results

A number of results which did not fit into the categories already discussed should be reported, for they illustrate what may be expected in specific cases.

A free radical – 2,2-diphenyl-1-picrylhydrazyl

This molecule contains a stable unpaired electron at room temperature and therefore is paramagnetic and is sometimes used as a standard for electron spin resonance. There are two easily accessible electronic absorption bands at 327 mμ and 516 mμ. One might at first expect large MCD effects due to the unpaired electron, however, presumably because of the reasons discussed in the theoretical section, only a small MCD is observed. This is shown in Fig. 74.

The pyridine, quinoline, acridine series

The spectra of these three compounds are compared in Fig. 75. The $L_a$ and $L_b$ transitions of acridine seem to be combined under the band system peaking at 356 mμ. There is disagreement on the question of whether it is the $L_a$ or $L_b$ band which lies at the longest wavelength (69, p. 178). However, the two bands are considerably closer together in energy for acridine than for quinoline, which is probably at least part of the reason for the molar MCD of acridine to be the larger. Both quinoline and acridine have a sign of MCD which corresponds to a π-deficient ring system, which is expected on account of the electron-withdrawing character of the ring nitrogens.

The $L_a$ band of pyridine is probably at 205 mμ, about 9900 $cm^{-1}$ from the $L_b$ band, compared to 3900 $cm^{-1}$ for quinoline. This difference alone
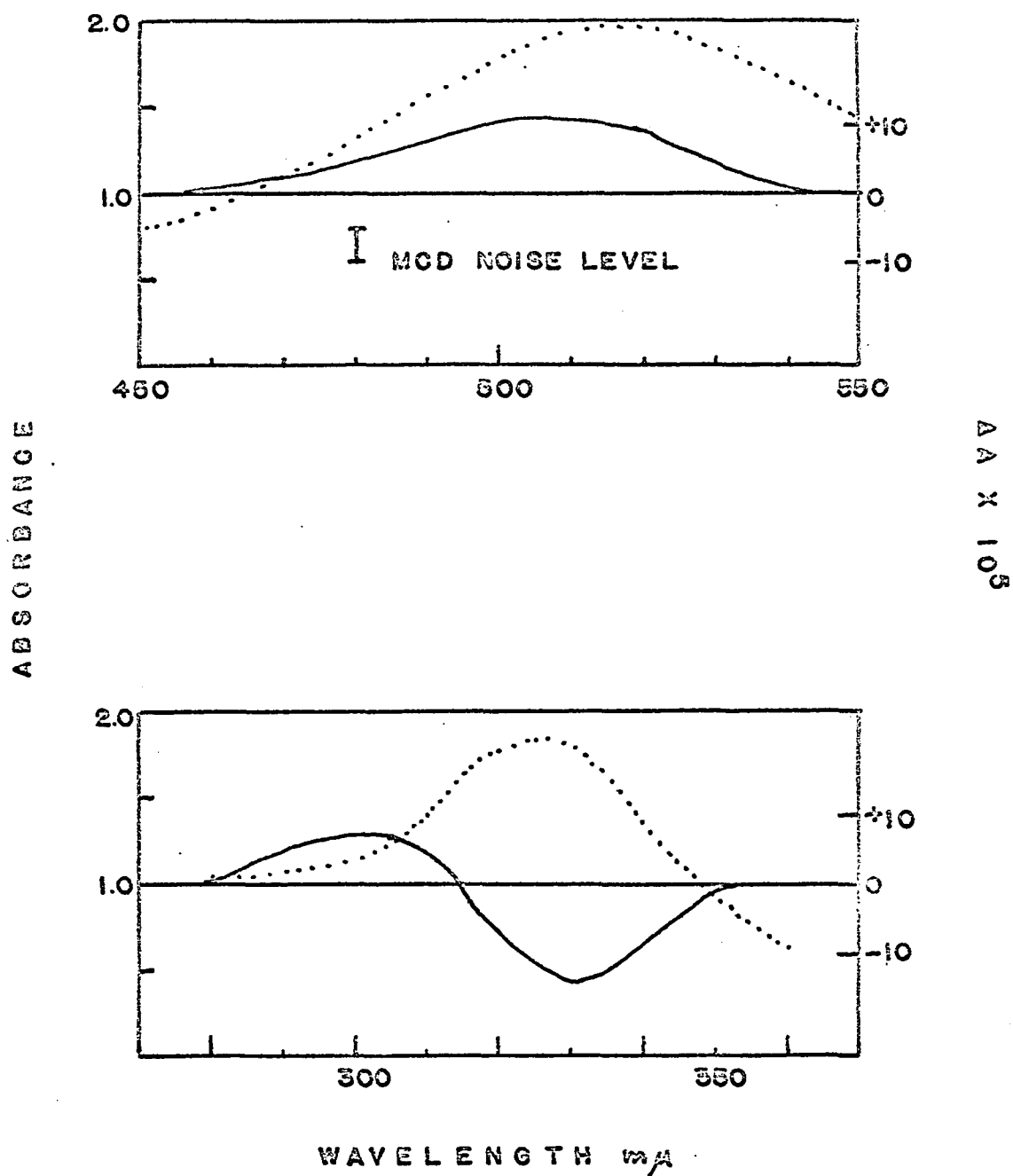
Fig. 74. Absorption (- - -) and MCD (———) of 2,2-diphenyl-1-
picrylhydrazyl
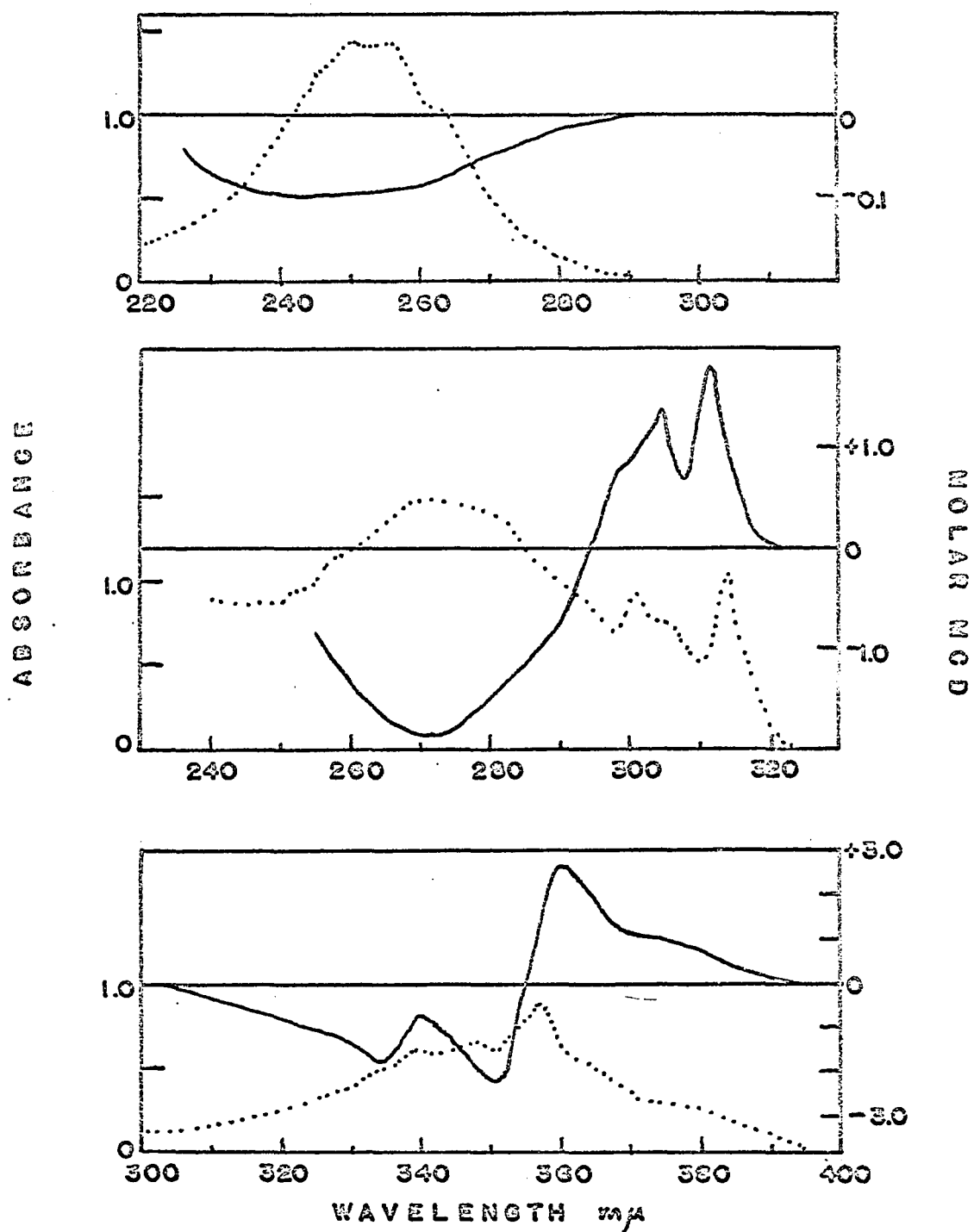
Fig. 75. Absorption (- - -) and MCD (———) of (top) pyridine, (middle) quinoline and (bottom) acridine

will therefore not account for the order of magnitude decrease in molar

MCD in going from quinoline to pyridine. Here again, as with the substi-

tuted benzenes, the comparatively high symmetry of pyridine ($C_{2v}$) may be

a major influence.

The sign for the MCD of pyridine is anomalous compared to quinoline

and acridine. This situation has occurred before, for the case of

N,N dimethyl aniline. In that case also, there was an $n \rightarrow \pi^*$ band

apparent. The MCD of pyridine appears only in nonpolar solvents, in

aqueous solution neither the MCD nor the tail of the $n \rightarrow \pi^*$ band from

275-290 mμ could be measured. Therefore it seems that the presence of

an $n \rightarrow \pi^*$ transition may be involved in the anomalous sign, and that the

MCD of pyridine results from the interaction of the $n \rightarrow \pi^*$ transition

with one of higher energy. This suggests that the MCD reveals the true

position of the $n \rightarrow \pi^*$ absorption band.

## The aromatic amino acids, proteins

Tyrosine, tryptophan and phenylalanine were examined for MCD with

results very similar to the corresponding simple aromatic systems.

Tyrosine, in acidic or basic solution, has an MCD like that of phenol

in the same solutions. Tryptophan's MCD is similar to that of indole.

No MCD was detected for phenylalanine, a situation corresponding to the

very small MCD found for toluene or ethyl benzene. The MCD of proteins

containing tyrosine and tryptophan is just what would be expected if their

individual spectra were multiplied by the number of respective amino acid

residues in the protein and the results added. Due to limitation of the

apparatus measurements were not made in the region of 225 mμ, where the

protein bands related to helical structure occur.

## V.   REFERENCES

1.  Faraday, M.  Diary.  London, England, G. Bell and Sons, Ltd.  1932.

2.  Zeeman, P.  On the influence of magnetism on the nature of light
    emitted by a substance.  Phil. Mag. 43: 226.  1897.

3.  Buckingham, A. D. and Stephens, P. J.  Magnetic optical activity.
    Ann. Rev. Phys. Chem. 17: 399.  1966.

4.  Scherer, M.  Dichroism circulaire magnetique et abnormal des
    solutions de chlorure de cobalt.  Compt. rend. 195: 950.  1932.

5.  Palik, E. D. and Henvis, B. W.  A bibliography of magnetooptics
    of solids.  Applied Optics 6: 603.  1967.

6.  Grosjean, M. and Legrand, M.  Appareil de mesure du dichroisme
    circulaire dans le visible et l'ultraviolet.  Compt. rend. 251: 2150.
    1960.

7.  Stephens, P. J.  Theoretical studies of magneto-optical phenomena.
    Unpublished Ph.D. thesis.  Library, Oxford, England, Oxford Univ.
    1964.

8.  Schatz, P. N., McCaffery, A. J., Suetaka, W., Henning, G. N.,
    Ritchie, A. B. and Stephens, P. J.  Faraday effect of charge-
    transfer transitions in $Fe(CN)_6{}^{---}$, $MnO_4{}^-$, and $CrO_4{}^{--}$.  J. Chem. Phys.
    45: 722.  1966.

9.  Schooley, D. A., Bunnenberg, E. and Djerassi, C.  Magnetic circular
    dichroism studies.  II.  Preliminary results with some aromatic
    compounds.  Proc. Nat. Acad. Sci. 56: 1377.  1967.

10. Dratz, E. A.  The geometry and electronic structure of biologically
    significant molecules as observed by natural and magnetic optical
    activity.  Unpublished Ph.D. thesis.  Berkeley, California, Library,
    Univ. of California.  1966.

11. Foss, J. G. and McCarville, M. E.  Magnetic circular dichroism and
    magnetic optical rotatory dispersion.  J. Am. Chem. Soc. 87: 228.
    1965.

12. Martin, D. S., Foss, J. G., McCarville, M. E., Tucker, M. A. and
    Kassman, A. J.  Magnetic circular dichroism for tetrachloroplatinate
    (II) ion.  Inorganic Chemistry 5: 491.  1966.

13. Foss, J. G. and McCarville, M. E.  MCD of simple and catacondensed
    aromatics.  J. Chem. Phys. 44: 4350.  1966.

14. Foss, J. G. and McCarville, M. E.  Some generalizations concerning the magnetic circular dichroism of substituted benzenes.  J. Am. Chem. Soc. 89: 30.  1967.

15. Foss, J. G.  Improved Rudolph spectropolarimeter.  Anal. Chem. 35: 1329.  1963.

16. Schurcliff, W. A.  Polarized light.  Cambridge, Mass., Harvard University Press.  1962.

17. Jerrard, H. G.  Transmission of ligh through birefringent and optically active media:  the Poincaré Sphere.  J. Opt. Soc. Am. 44: 634.  1954.

18. Velluz, L., Legrand, M. and Grosjean, M.  Optical circular dichroism. New York, N.Y., Academic Press Inc.  1965.

19. Jones, R. C.  A new calculus for the treatment of optical systems. J. Opt. Soc. Am. 32: 486.  1942.

20. Jenkins, F. A. and White, H. E.  Fundamentals of optics.  3rd ed. New York, N.Y., McGraw-Hill Book Co., Inc.  1957.

21. Rossi, B.  Optics.  Reading, Mass., Addison-Wesley Publ. Co., Inc. c1957.

22. Gottfried, K.  Quantum Mechanics.  Vol. 1.  New York, N.Y., W. A. Benjamin, Inc.  1966.

23. Beth, R. A.  Mechanical detection and measurement of the angular momentum of light.  Phys. Rev. 50: 115.  1936.

24. Condon, E. U. and Shortley, G. H.  The theory of atomic spectra. Cambridge, England, Cambridge University Press.  1963.

25. Eyring, H., Walter, J. and Kimball, G. E.  Quantum chemistry.  New York, N.Y., John Wiley and Sons, Inc.  c1944.

26. Corson, D. R. and Lorrain, P.  Introduction to electromagnetic fields and waves.  San Francisco, Calif., W. H. Freeman and Co. c1962.

27. Phillips, L. F.  Basic quantum chemistry.  New York, N.Y., John Wiley and Sons, Inc.  c1965.

28. Kauzmann, W.  Quantum chemistry.  New York, N.Y., Academic Press Inc.  1957.

29. Condon, E. U., Altar, W. and Eyring, H.  One-electron rotatory power. J. Chem. Phys. 5: 753.  1937.

30. Barrow, G. M.  Molecular spectroscopy.  New York, N.Y., McGraw-Hill Book Co., Inc.  1962.

31. Anderson, J. M.  Mathematics for quantum chemistry.  New York, N.Y., W. A. Benjamin, Inc.  1966.

32. Bohm, D.  Quantum theory.  New York, N.Y., Prentice-Hall, Inc. c1951.

33. Merzbacher, E.  Quantum mechanics.  New York, N.Y., John Wiley and Sons, Inc.  c1961.

34. Hanna, M. W.  Quantum mechanics in chemistry.  New York, N.Y., W. A. Benjamin, Inc.  1965.

35. Slichter, C. P.  Principles of magnetic resonance.  New York, N.Y., Harper and Row.  c1963.

36. Herzberg, G.  Atomic spectra and atomic structure.  2nd ed.  New York, N.Y., Dover Publications.  1944.

37. Tinoco, I. and Bush, C. A.  The influence of static electric and magnetic fields on the optical properties of polymers.  Biopolymers Symposia No. 1: 235.  1964.

38. Falk, J. E.  Porphyrins and metalloporphyrins.  Vol. 2.  New York, N.Y., Elsevier Publ. Co.  1964.

39. Ballhausen, C. J.  Introduction to ligand field theory.  New York, N.Y., McGraw-Hill Book Co., Inc.  c1962.

40. Tobias, I. and Kauzmann, W.  Faraday effect in molecules.  J. Chem. Phys. 35: 538.  1961.

41. McCaffery, A. J., Stephens, P. J. and Schatz, P. N.  The magnetic optical activity of d   d transitions.  [To be published in Inorganic Chemistry, ca. Fall, 1967.]

42. Platt, J. R.  Classification of spectra of catacondensed hydrocarbons.  J. Chem. Phys. 17: 484.  1949.

43. Ferguson, L. N.  The modern structural theory of organic chemistry.  Englewoods Cliffs, N.J., Prentice-Hall, Inc.  c1963.

44. Jaffe, H. H. and Orchin, M.  Theory and applications of ultraviolet spectroscopy.  New York, N.Y., John Wiley and Sons, Inc.  c1962.

45. Lang, L., ed.  Absorption spectra in the ultraviolet and visible region.  New York, N.Y., Academic Press Inc.  c1961-1965.

46. Forbes, W. F.  Light absorption studies.  Part XVIII.  The ultra-
violet absorption spectra of bromobenzenes.  Canadian J. Chem.
39: 1131.  1961.

47. Wilson, E. B., Decius, J. C. and Cross, P. C.  Molecular vibrations.
New York, N.Y., McGraw-Hill Book Co., Inc.  1955.

48. Jaffe, H. H. and Orchin, M.  Symmetry in chemistry.  New York, N.Y.,
John Wiley and Sons, Inc.  c1965.

49. Schepp, O. and Kopelman, R.  Near ultraviolet spectrum of crystalline
hexachlorobenzene.  J. Chem. Phys. 30: 868.  1959.

50. Innes, K. K., Byrne, J. P. and Ross, I. G.  Electronic states of
azabenzenes:  a critical review.  J. Mol. Spectr. 22: 125.  1967.

51. Ginsberg, D., ed.  Non-benzenoid aromatic compounds.  New York, N.Y.,
Interscience Publishers.  1959.

52. Murrell, J. N. and Longuet-Higgins, H. C.  Electronic spectrum of
the cycloheptatrienyl (tropylium) ion.  J. Chem. Phys. 23: 2347.
1955.

53. Doering, W. von E. and Knox, L. H.  The cycloheptatrienyl (tropylium)
ion.  J. Am. Chem. Soc. 76: 3203.  1954.

54. Rumpf, P. and Seguin, M.  Magnetochemical investigations on some
compounds chelated or associated by the hydrogen bond.  Bull. soc.
Chim. France D1949: 366.  1949.

55. Broersma, S.  The magnetic susceptibility of organic compounds.
J. Chem. Phys. 17: 873.  1949.

56. Khatavkar, S. B. and Khanolkar, D. D.  Magnetism and molecular
structure:  proximity effect in ortho-substituted benzoic acids.
J. Sci. Ind. Res. B18: 259.  1959.

57. Klevens, H. B. and Platt, J. R.  Spectral resemblances of cata-
condensed hydrocarbons.  J. Chem. Phys. 17: 470.  1949.

58. Albert, A.  Heterocyclic chemistry.  London, England, The Athlone
Press.  1959.

59. Jaffe, H. H.  Theoretical considerations concerning Hammett's
equation.  III.  $\sigma$-values for pyridine and other aza-substituted
hydrocarbons.  J. Chem. Phys. 20: 1554.  1952.

60. Mason, S. F.  Purine studies.  Part II.  The ultraviolet absorption
spectra of some mono- and poly-substituted purines.  J. Chem. Soc.
1954: 2071.  1954.

61. Stewart, R. F. and Davidson, N. Polarized absorption spectra of purines and pyrimidines. J. Chem. Phys. 39: 255. 1963.

62. Callis, P. R., Rosa, E. J. and Simpson, W. T. Search for accidental degeneracy in purines. J. Am. Chem. Soc. 86: 2292. 1964.

63. Clark, L. B. and Tinoco, I. Correlations in the ultraviolet spectra of the purine and pyrimidine bases. J. Am. Chem. Soc. 87: 11. 1965.

64. Cohen, B. J. and Goodman, L. Luminescence of purines. J. Am. Chem. Soc. 87: 5487. 1965.

65. Drobnik, J. and Augenstein, L. Spectroscopic studies of purines. I. Factors affecting the first excited levels of purines. Photochem. Photobiol. 5: 13. 1966.

66. Drobnik, J. and Augenstein, L. Spectroscopic studies of purines. II. Properties of purine substituted at the second and sixth carbons. Photochem. Photobiol. 5: 83. 1966.

67. Kleinwachter, V., Drobnik, J. and Augenstein, L. Spectroscopic studies of purines. III. Properties of purines substituted at the sixth and ninth positions. Photochem. Photobiol. 6: 133. 1967.

68. Drobnik, J., Kleinwachter, V. and Augenstein, L. Spectroscopic studies of purines. IV. Polarization of emission from purine and some of its derivatives. Photochem. Photobiol. 6: 147. 1967.

69. Albert, A. The Acridines. 2nd ed. New York, N.Y., St. Martin's Press. 1966.

70. I'Haya, Y. Magneto-optical rotation in molecules. Theoret. Chim. Acta 6: 1. 1966.

71. Stone, J. M. Radiation and optics. New York, N.Y., McGraw-Hill Book Co., Inc. c1963.

72. Brown, L. S. Spin absorption spectra. IBM J. Res. Dev. 6: 338. 1962.

# VI.  ACKNOWLEDGMENTS

The author would like to thank his major professor, Dr. John Foss, for his help with this research and in general for four very interesting and stimulating years of acquaintance.

Thanks are also due to a number of persons who contributed their ideas for this work, in particular Dr. Donald Martin and Dr. William Simpson.

VII.   APPENDIX I

Derivation of an Expression for MCD using Perturbation Theory

In this section we will derive an expression for the MCD using

perturbation theory.  This derivation and a number of others similar

to it have appeared in the literature, however, they are almost always

in very compact form and therefore difficult to follow.  In particular,

the manipulation of frequency terms needs clarification.  The following

is an expansion of one of the clearest derivations in the literature and

has been included for the benefit of those who might find it useful.

The procedure will follow that of I'Haya (70) for the development of the

Vevdet constant of molecules with narrow absorption bands and then

continue using Stephen's method (3) to find the MCD of molecules with

broad bands.

The calculations using time-dependent perturbation theory will follow

the usual steps:

1.   Write the Hamiltonian operator of the system.

2.   Write the time dependent Schroedinger equation for the perturbed

     system.

3.   Expand the perturbed wave functions in terms of unperturbed wave

     functions.

4.   Substitute the expansions from step 3 into the Schroedinger

     equations.

5.   Reduce the expression in step 4 by deleting the equal terms

     from each side of the equation.

6.   Multiply both sides of the equation by the complex conjugate

wave functions and integrate over all space.

7.  The integration in step 6 gives the transition rates, these may be integrated with respect to time to give the coefficients for the expansions in step 3.

With the completion of the perturbation calculation, the following steps can be taken.

8.  Using the perturbed wave functions from step 3 with their coefficients from step 7, the desired expectation values may be calculated.

9.  Calculate the expectation value at a given temperature.

10.  Average the expectation value over all molecule orientations.

11.  With the expectation values and using Maxwell's equations, the magnetic optical rotation may be calculated.

12.  Expression for MCD developed according to Stephens.

## 1. The Hamiltonian operator of the system

Assuming that there is no spin-orbital coupling, the total Hamiltonian for the case of a molecule subjected to perturbations from both light and a static magnetic field is (25, p. 109)

$$\mathcal{H} = \sum_j [\frac{1}{2m} (\overline{p}_j - \frac{e}{c} \overline{A}_j)^2 + e \phi_j] + U \qquad \text{Eq. 1}$$

where:

$j$ is the $j^{th}$ electron

$m$ is the electronic mass

$\overline{p}$ is the linear momentum

$e$ is the electronic charge

c is the speed of light

$\overline{A}_j$ is the vector potential

$\phi$ is the scalar potential

U is the interval potential

The vector potential $\overline{A}_j$ is the sum of two parts, that due to the light wave $\overline{a}_j$ and that due to the magnetic field $\overline{a}_j^{\ f}$

$$\overline{A}_j = \overline{a}_j + \overline{a}_j^{\ f} \qquad\qquad \text{Eq. 2}$$

The time dependence of $\overline{a}_j$ is (71, p. 35) (70, p. 3),

$$\overline{a}_j = \frac{1}{2}\{a_o^o \ i \ x \ p \ [\nu(t - \frac{n}{c}(\overline{r}\cdot\overline{k}))] + \text{complex conjugate}\} \qquad \text{Eq. 3}$$

where:

$a_o^o$ is the complex amplitude, $a \ e^{i\theta}$

ixpf is $e^{2\pi i f}$

$\nu$ is the frequency of the light wave

t is time

n is the refractive index of the medium

$\overline{r}$ is the position vector

$\overline{k}$ is the unit vector in the z direction

The expression for $a_j^{\ f}$ is:

$$a_j^{\ f} = \frac{1}{2}[H^f\cdot\overline{r}_j] \qquad\qquad \text{Eq. 4}$$

where

$H^f$ is the intensity of the magnetic field

The square in Eq. 1 may be expanded to give;

$$\left( p - \frac{e}{c} a - \frac{e}{c} a^f \right)^2 = p^2 - 2 p \frac{e}{c} a^f + 2 \frac{e^2}{c^2} a \, a^f$$

Eq. 5

$$+ \frac{e^2}{c^2} a^{f\,2} + \frac{e^2}{c^2} a^2 - 2 p \frac{e}{c} a$$

The fourth and fifth terms are dropped because we will neglect all non-linear terms. This leaves:

$$p_j^2 \qquad\qquad\text{zeroth order perturbation term}$$

$$-2 \frac{e}{c} o_j \, (a_j + a_j^f) \qquad\qquad\text{first order perturbation term}$$

$$2 \frac{e^2}{c^2} a_j \, a_j^f \qquad\qquad\text{second order perturbation term}$$

It is because of the cross term $a_j \, a_j^f$ in the Hamiltonian as we apply simultaneously fields from the light wave and the static magnetic field that we call this derivation a second order perturbation. The first and second order Hamiltonians will now be:

$$\mathcal{H}^{(1)} = - \frac{e}{mc} \sum_j \left( p_j \cdot (a_j + a_j^f) \right) \qquad\qquad\text{Eq. 6}$$

$$\mathcal{H}^{(2)} = \frac{e^2}{mc^2} \sum_j \left( a_j \cdot a_j^f \right) \qquad\qquad\text{Eq. 7}$$

The vector potential $a_j$ can be expanded in a Taylor's series:

$$a_j = \bar{a}_0 + \bar{r}_j \, [\nabla \cdot a]_0 + \quad \text{neglected terms} \qquad \text{Eq. 8}$$

where
$$\bar{a}_0 = \frac{1}{2} \left\{ a_0^0 \, \exp(\nu t) + a_0^{0*} \, \exp(-\nu t) \right\}$$

$$[\nabla \cdot a]_0 = \frac{1}{2} \left\{ [\nabla \cdot a]_0^0 \, \exp(\nu t) + [\nabla \cdot a]_0^{0*} \, \exp(-\nu t) \right\}$$

$$\nabla = \frac{d}{dx} + \frac{d}{dy} + \frac{d}{dz}$$

The first order perturbation will now be

$$H^{(1)} = - \frac{e}{mc} \sum_j \bar{P}_j \left( \bar{a}_0 + \bar{r}_j \cdot [\nabla \cdot a]_0 + a_j^f \right)$$

$$= - \frac{e}{mc} \sum_j \bar{P}_j \cdot \bar{a}_0 - \frac{e}{mc} \sum_j (\bar{P}_j \times \bar{r}_j)[\nabla \cdot a]_0$$

$$- \frac{e}{mc} \sum_j (\bar{P}_j \times \bar{r}_j) \frac{H^f}{2} \qquad \text{Eq. 9}$$

now since the magnetic dipole moment is $\quad M = \frac{e}{mc} \sum_j (\bar{r}_j \times \bar{P}_j)$ ,

$$H^{(1)} = - \frac{e}{mc} \sum_j \bar{P}_j \cdot \bar{a}_0 - 2 \sum_j M \, [\nabla \cdot a]_0 - \sum_j M \, H^f \qquad \text{Eq. 10}$$

The second order perturbation will be:

$$H^{(2)} = \frac{e^2}{mc^2} \sum_j \left[ a_j^f \cdot \bar{a}_0 + a_j^f \cdot [\nabla \cdot a]_0 \cdot \bar{r}_j \right]$$

$$= \frac{e^2}{mc^2} \sum_j \left[ \frac{H^f}{2} \bar{r}_j \cdot \bar{a}_o + \frac{H^f}{2} \bar{r}_j \cdot \bar{r}_j [\nabla \cdot a]_o \right] \qquad \text{Eq. 11}$$

The second term in Eq. 11 represents a quadrupole moment and will be neglected. Since the electric dipole moment is $R = e\Sigma_j r_j$, Eq. 11 can be written as:

$$\mathcal{H}^{(2)} = \frac{e}{mc^2} R \frac{H^f}{2} \bar{a}_o \qquad \text{Eq. 12}$$

Now we will rewrite the Hamiltonian operators in a form useful for making the actual calculations.

$$\mathcal{H}^{(1)a} = -\frac{e}{mc} \sum_j \bar{P}_j \cdot \bar{a}_o = -\frac{e}{2mc} \sum_j \frac{\partial}{\partial \bar{r}_j} \left\{ a_o^o \ i \varkappa_p (\nu t) + \right.$$

$$\left. a_o^{o*} \ i \varkappa_p (-\nu t) \right\} \qquad \text{Eq. 13}$$

Eq. 13 is written in a form using the linear momentum operator. However it may be shown that this is equivalent to the following since $p_j = m \frac{d r_j}{dt}$,

$$\mathcal{H}^{(1)a} = -\frac{2\pi i \nu(n'n)}{c} a_o R = -\frac{\pi i \nu(n'n) R}{c} \left\{ a_o^o \ i \varkappa_p (\nu t) + \right.$$

$$\left. a_o^{o*} \ i \varkappa_p (-\nu t) \right\} \qquad \text{Eq. 14}$$

where $\quad \nu(n'n) = \dfrac{E^o_{n'} - E^o_n}{\hbar}$

$$\mathcal{H}^{(1)b} = -2 \sum_j M [\nabla \cdot a]_o = -M \left\{ [\nabla \cdot a]_o^o \ i \varkappa_p (\nu t) + \right.$$

$$+ [\nabla \cdot a]_0^{\circ *} \; \exp(-\nu t) \hspace{3cm} \text{Eq. 15}$$

$$\mathcal{H}^{(1)c} = - M H^f \hspace{3cm} \text{Eq. 16}$$

$$\mathcal{H}^{(2)} = \frac{e}{2mc^2} R H^f \, \bar{a}_0 = \frac{e}{4mc^2} R H^f \{ a_0^0 \exp(\nu t) +$$

$$a_0^{0 *} \exp(-\nu t) \} \hspace{3cm} \text{Eq. 17}$$

## 2. The time dependent Schroedinger equation

We can now write the time-dependent Schroedinger equation,

$$i \hbar \dot{\Psi}_n = (\mathcal{H}_0 + \mathcal{H}^{(1)} + \mathcal{H}^{(2)}) \Psi_n \hspace{2cm} \text{Eq. 18}$$

where the dot denotes the time derivative.

## 3. Expanding the perturbed wave functions

The $\Psi_n$ may be expanded in terms of the unperturbed wave functions $\Psi_n^{\circ}$ as follows:

$$\Psi_n = \Psi_n^{\circ} + \sum_{n' \neq n} c_n'(t) \Psi_n^{\circ} \hspace{2cm} \text{Eq. 19}$$

The unperturbed wave functions satisfy

$$i \hbar \dot{\Psi}_n^{\circ} = \mathcal{H}_0 \Psi_n^{\circ} \hspace{3cm} \text{Eq. 20}$$

and have the form

$$\Psi_n^{\circ} = \psi_n^{\circ} \exp\left(-i \frac{E_n^{\circ} t}{\hbar}\right) = \psi_n^{\circ} \exp(-\nu(n) t) \hspace{1.5cm} \text{Eq. 21}$$

where $\psi_n^{\circ}$ is a time independent wave function and $E_n^{\circ}$ is its energy.

## 4. Substitution of the wave functions into Schroedinger's equation

Substituting Eq. 21 into Eq. 19, and then Eq. 19 into Eq. 18 we obtain:

$$i\hbar \left[ \psi_n^0 \frac{d \exp\left(-i \frac{E_n t}{\hbar}\right)}{dt} + \sum_{n'\neq n} c_n'(t) \psi_{n'}^0 \frac{d \exp\left(-i \frac{E_{n'}^0 t}{\hbar}\right)}{dt} \right. $$

$$+ \sum_{n'\neq n} \psi_{n'}^0 \exp\left(-\frac{i E_{n'}^0 t}{\hbar}\right) \frac{dc_{n'}(t)}{dt} = \left[ \mathcal{H}_0 + \mathcal{H}^{(1)} + \mathcal{H}^{(2)} \right]$$

$$\left[ \psi_n^0 \exp\left(-i \frac{E_n^0 t}{\hbar}\right) + \sum_{n'\neq n} c_n'(t) \psi_n^0 \exp\left(-i \frac{E_{n'}^0 t}{\hbar}\right) \right] \qquad \text{Eq. 22}$$

## 5. Reducing Eq. 22

Since we know by definition Eq. 20, these terms in Eq. 22 are equal and can be canceled out. Multiplying out what remains we find:

$$i\hbar \sum_{n'\neq n} \psi_{n'}^0 \exp\left(-i \frac{E_{n'}^0 t}{\hbar}\right) \frac{dc_{n'}(t)}{dt} = \mathcal{H}^{(1)} \psi_n^0 \exp\left(-i \frac{E_n^0 t}{\hbar}\right)$$

$$+ \mathcal{H}^{(1)} \sum_{n'\neq n} c_{n'}(t) \psi_{n'}^0 \exp\left(-i \frac{E_{n'}^0 t}{\hbar}\right) + \mathcal{H}^{(2)} \psi_n^0 \exp\left(-i \frac{E_n^0 t}{\hbar}\right)$$

$$+ \mathcal{H}^{(2)} \sum_{n'\neq n} c_{n'}(t) \psi_{n'}^0 \exp\left(-i \frac{E_{n'}^0 t}{\hbar}\right) \qquad \text{Eq. 23}$$

## 6. Multiplying by the complex conjugate wave functions and integrating

We will now multiply term by term Eq. 23 times the complex conjugate wave function $\psi_{n'}^{0*}$, and integrate over all space.

$$i\hbar \int \sum_{n'\neq n} \psi_{n'}^{0*} \psi_{n'}^0 \, d\tau \frac{dc_{n'}(t)}{dt} = i\hbar \, \dot{c}_{n'} \qquad \text{Eq. 24}$$

$$\int \Psi_{n'}^{0*} \mathcal{H}^{(1)} \Psi_n^0 \, d\tau = \int \psi_{n'}^{0*} \mathcal{H}^{(1)} \psi_n^0 \, d\tau \; e^{2\pi i \left( \frac{E_{n'}^0 - E_n^0}{h} \right) t}$$

where n' and n stand for stationary states

$$= \langle n' | \mathcal{H}^{[1]} | n \rangle \; i \chi_p \{ \nu(n'n) t \} \qquad \text{Eq. 25}$$

Note the use of brackets to simplify notation for integration.

$$\int \Psi_{n'}^{0*} \mathcal{H}^{(1)} \sum_{n' \neq n} c_{n'}(t) \Psi_n^0 \, d\tau = \sum_{n'' \neq n} c_{n''} \langle n' | \mathcal{H} |^{(1)} n'' \rangle$$

$$i \chi_p \{ \nu(n'n'') t \} \qquad \text{Eq. 26}$$

where we allow one of the states n' to called n".

$$\int \Psi_{n'}^{0*} \mathcal{H}^{(2)} \Psi_n^0 \, d\tau = \langle n' | \mathcal{H}^{(2)} | n \rangle \; i \chi_p \{ \nu(n'n) t \} \qquad \text{Eq. 27}$$

Other higher order terms could be developed but these will be neglected.

Writing Eqs. 24-27 together again:

$$i \hbar \dot{c}_{n'} = \langle n' | \mathcal{H}^{(1)} | n \rangle \; i \chi_p \{ \nu(n'n) t \} + \langle n' | \mathcal{H}^{(2)} | n \rangle$$

$$i \chi_p \{ \nu(n'n) t \} + \sum_{n'' \neq n} c_{n''} \langle n' | \mathcal{H}^{(1)} | n'' \rangle \; i \chi_p \{ \nu(n'n'') t \}$$

$$\text{Eq. 28}$$

This equation is I'Haya's Eq. 18 and is the time derivative of the coefficient appearing in our Eq. 19. Eq. 25 may be considered a first order perturbation correction to the wave functions and Eqs. 26 and 27 are second order corrections.

## 7. Calculation of the correction coefficients

We will now substitute the Hamiltonian (Eqs. 14-17) into Eq. 28 and integrate with respect to time to obtain the correction coefficients. The constant of integration is chosen so that $c_{n'} = 0$ when $t = 0$.

First, substituting Eq. 14 into Eq. 25:

$$i\hbar \int \dot{c}_{n'} \, dt = \langle n'|R|n \rangle \left[ -\frac{i\pi \nu(n'n)}{c} \right] \int \left\{ a_o^o \, i\times_p (\nu t) + a_o^{o*} \, i\times_p (-\nu t) \right\} \, i\times_p \left\{ \nu(n'n) \, t \right\} \, dt$$

$$c_{n'} = \langle n'|R|n \rangle \left[ -\frac{i\pi \nu(n'n)}{c} \right] \left[ \frac{1}{2\pi i \cdot i\hbar} \right] \left[ a_o^o \, F_+(n'n) + a_o^{o*} \, F_-(n'n) \right]$$

where

$$F_+(n'n) \sim \frac{i\times_p \left\{ \nu(n'n) + \nu \right\} t}{\nu(n'n) + \nu} \qquad F_-(n'n) = \frac{i\times_p \left\{ \nu(n'n) - \nu \right\} t}{\nu(n'n) - \nu}$$

Eq. 29

$$c_{n'} = \frac{i \nu(n'n)}{2 \hbar c} \langle n'|R|n \rangle \left[ a_o^o \, F_+(n'n) + a_o^{o*} \, F_-(n'n) \right] \qquad \text{Eq. 30}$$

This is the first term in I'Haya's Eq. 21 and corresponds to a correction in the unperturbed wave function caused by the electric vector of the incident light.

Next we substitute Eq. 17 into Eq. 27: $i\hbar \int \dot{c}_n \, dt =$

$$\langle n'|R|n\rangle \left[\frac{e H^f}{4 m c^2}\right] \int \left\{ a_o^o \, i x_p (\nu t) + a_o^{o*} \, i x_p (-\nu t) \, i x_p \left\{ \nu(n'n) t \right\} \right\} dt$$

$$c_{n'} = -\frac{e H^f}{8\pi m c^2 \hbar} \langle n'|R|n\rangle \left[ a_o^o \, F_+ (n'n) + a_o^{o*} \, F_- (n'n) \right] \qquad \text{Eq. 31}$$

This is the fourth term in I'Haya's Eq. 21, a second order correction caused by both the electric vector of the light and the static magnetic field. We have neglected the second and third terms of I'Haya's Eq. 21 as they contain only the small magnetic dipole corrections. We will calculate only one more term from I'Haya's Eq. 21. It is by far the most important term and is the only one we will need to account for the MCD of all but a few molecules. This expression is I'Haya's fifth term and results when we substitute Eq. 16 into Eq. 26. However, since the coefficient $c_{n''}$ is present in Eq. 26, we must find it first. The term $c_{n''}$ may be found by substituting Eq. 14 into Eq. 25 as this is the only part of $c_{n''}$ which will not give non-linear terms at the end of the calculation for $c_{n'}$.

So finding $c_{n''}$:

$$i\hbar \int \dot{c}_{n''} \, dt = \langle n''|R|n\rangle \left[-\frac{\pi \, i \, \nu(n''n)}{c}\right] \int \left\{ a_o^o \, i x_p (\nu t) + \right.$$

$$a_o^{o*} \, i x_p (-\nu t) \left\} \, i x_p \left\{ \nu(n''n) t \right\} dt$$

$$c_{n''} = \frac{i \pi \nu(n''n)}{c h} \langle n'' | R | n \rangle \left[ a_0^0 F_+ (n''n) + a_0^{0*} F_- (n''n) \right]$$

Now putting this value for $c_{n''}$ into Eq. 26 and finding $c_{n'}$:

$$i \hbar \int \dot{c}_{n'} \, dt = \sum_{n'' \neq n} \sum_{n' \neq n} \frac{i \pi \nu(n''n)}{c h} \langle n'' | R | n \rangle \langle n' | M | n'' \rangle \left[ -H^f \right]$$

$$\int \left[ a_0^0 F_+ (n''n) + a_0^0 F_- (n''n) \, i x_p \left\{ \nu(n'n'') \, t \right\} \right] dt$$

$$c_{n'} = \sum_{n'' \neq n} \sum_{n' \neq n} \langle n'' | R | n \rangle \langle n' | M | n'' \rangle \left[ \frac{i \nu(n''n) H^f}{4 \pi c \hbar^2} \right] \left[ \frac{a_0^0 F_+ (n'n)}{\nu(n''n) + \nu} + \frac{a_0^{0*} F_- (n'n)}{\nu(n''n) - \nu} \right]$$

<div align="right">Eq. 32</div>

Now we have found the important terms needed to write the perturbed wave functions. This is done by substituting Eqs. 30, 31 and 32 into Eq. 19.

8. Expectation value for the induced electric moment

The expectation value of the induced electric moment in the perturbed state n is

$$\int \Psi_n^* \, R \, \Psi_n \, d\tau = \langle R \rangle_n$$

Using our values for the perturbed wave functions:

$$\langle R \rangle_n = \int \left[ \Psi_n^{0*} + \sum_{n' \neq n} c_n \Psi_{n'}^0 \right] R \left[ \Psi_n^0 + \sum_{n' \neq n} c_n \Psi_{n'}^0 \right] d\tau$$

Expanding this

$$= \int \Psi_n^{o*} R \, \Psi_n^o \, d\tau + \int \Psi_n^{o*} R \sum_{n' \neq n} c_{n'} \Psi_{n'}^o \, d\tau$$

$$+ \int \sum_{n' \neq n} c_{n'} \Psi_{n'}^{o*} R \, \Psi_n^o \, d\tau + \int \left( \sum_{n' \neq n} c_{n'}^2 \right) \Psi_{n'}^{o*} R \, \Psi_{n'}^o \, d\tau$$

<div align="right">Eq. 33</div>

In Eq. 33 the first term is the permanent electric dipole moment of the

ground state $\quad \int \Psi_{n^o}^{*} R \, \Psi_n^o \, d\tau = \langle n | R | n \rangle \quad .$

The second and third terms of Eq. 33 are equal giving

$$2 \sum_{n' \neq n} c_{n'} \langle n' | R | n \rangle$$

The fourth term contains squares and is neglected.

The resulting expression is:

$$\langle R \rangle_n = \langle n | R | n \rangle + 2 \sum_{n' \neq n} c_{n'} \langle n' | R | n' \rangle \, i \times p \left( \nu_{(n'n)} t \right) \qquad \text{Eq. 34}$$

Substituting our expression for $c_{n'}$ into Eq. 34, and using only the parts of $c_{n'}$ which give linear terms for MCD, that is Eqs. 30 and 32, we find:

$$\langle R \rangle_n = \langle n | R | n \rangle + 2 \sum_{n'' \neq n} \sum_{n' \neq n} \left[ \frac{i \, \nu_{(n'n)}}{2 \, \hbar_c} \langle n | R | n' \rangle \langle n' | R | n \rangle \right]$$

$$\left[ a_o^o F_+ (n'n) + a_o^{o*} F_- (n'n) \right] i \times p \left[ - \nu_{(n'n)} t \right] \quad +$$

$$+2 \sum_{n''\neq n} \sum_{n'\neq n} \frac{i\nu(n''n)}{4\pi c \hbar^2} H^f \langle n'|R|n\rangle \langle n''|R|n\rangle \langle n'|M|n''\rangle$$

$$\left\{ \frac{a_o^o \, F_+(n'n)}{\nu(n''n)+\nu} + \frac{a_o^{o*} \, F_-(n'n)}{\nu(n''n)-\nu} \right\} \, ixp\left[-\nu(n'n)\, t\right] \qquad \text{Eq. 35}$$

We will find it convenient to express the vector potential in terms of the field strength, E. The time derivative of $a_o$ is:

$$\dot{a}_o = i\pi\nu\left\{ a_o^o \, ixp\,(\nu t) - a_o^{o*} \, ixp\,(-\nu t)\right\} = -cE$$

Also:

$$a_o = \tfrac{1}{2}\left\{ a_o^o ixp\,(\nu t) + a_o^{o*} ixp\,(-\nu t)\right\} = \frac{c\dot{E}}{4\pi^2\nu^2} \qquad (25,\ \text{sec. 17.2})$$

Rewriting the frequency terms in brackets from the second term of Eq. 35 we get:

$$\frac{a_o^o \, ixp\left\{\nu(n'n)+\nu\right\}t}{\nu(n'n)+\nu} + \frac{a_o^{o*} \, ixp\left\{\nu(n'n)-\nu\right\}t}{\nu(n'n)-\nu}$$

$$= \frac{a_o^o ixp\left\{\nu(n'n)+\nu\right\}t\,[\nu(n'n)-\nu] + a_o^{o*} ixp\left\{\nu(n'n)-\nu\right\}t\,[\nu(n'n)+\nu]}{\nu^2(n'n)-\nu^2}$$

$$= r(n'n)\left[\nu(n'n)\left[a_o^o ixp\{\nu t\}+a_o^{o*} ixp\{-\nu t\} - \nu\left[a_o^o ixp(\nu t)-a_o^{o*}ixp(-\nu t)\right]\right]ixp\,\nu(n'n)t$$

$$= T(n'n) \left[ \frac{\nu(n'n)\, c\, \dot{E}}{2\pi^2 \nu^2} + \frac{c\, E}{i\pi} \right] i x_p \; \nu(n'n) t$$

Inserting this back into Eq. 35:

$$2 \sum_{n' \neq n} \left[ \frac{i\nu(n'n)}{2\hbar c} \langle n|R|n' \rangle \langle n'|R|n \rangle \right] T(n'n) \left[ \frac{\nu(n'n)\, c\, \dot{E}}{2\pi^2 \nu^2} + \frac{cE}{i\pi} \right] \frac{2\, i\, 2\pi\, c\, \pi^2 \nu^2}{2\hbar c}$$

$$= Re \sum_{n' \neq n} \langle n|R|n' \rangle \langle n'|R|n \rangle \frac{T(n'n)}{\hbar \pi \nu^2} \left[ 2\nu(n'n)\pi \nu^2 E + i\nu^2(n'n)\dot{E} \right]$$

If we now modity only the frequency terms in curly brackets of Eq. 35, we will have

$$\frac{a_o^0 \; ix_p \left[ (\nu(n'n)+\nu)t \right]}{\left[ \nu(n'n)+\nu \right]\left[ \nu(n''n)+\nu \right]} + \frac{a_o^{0*} \; ix_p \left[ (\nu(n''n)-\nu)t \right]}{\left[ \nu(n''n)-\nu \right]\left[ \nu(n'n)-\nu \right]}$$

$$= \frac{a_o^0 \; ix_p \left[ (\nu(n'n)+\nu)t \right] \left[ \nu(n''n)\nu(n'n) - \nu\nu(n''n) - \nu\nu(n'n) + \nu^2 \right]}{\left[ \nu^2(n''n) - \nu^2 \right]\left[ \nu^2(n'n) - \nu^2 \right]}$$

$$+ \frac{a_o^{0*} \; ix_p \left[ (\nu(n'n)-\nu)t \right] \left[ \nu(n'n)\nu(n''n) + \nu\nu(n'n) + \nu\nu(n''n) + \nu^2 \right]}{\left[ \nu^2(n''n) - \nu^2 \right]\left[ \nu^2(n'n) - \nu^2 \right]}$$

$$= T(n''n)\, T(n'n)\, ix_p \left( \nu(n'n)t \right) \left[ \left[ a_o^0 ix_p(\nu t) + a_o^{0*} ix_p(-\nu t) \right]\left[ \nu(n'n)\nu(n''n) + \right.\right.$$

$$\left.\left. \nu^2 \right] - \left[ a_o^0 ix_p(\nu t) - a_o^{0*} ix_p(-\nu t) \right]\left[ \nu\nu(n'n) + \nu\nu(n''n) \right] \right]$$

where
$$T(n''n) = \frac{1}{\nu^2(n''n) - \nu^2}$$

$$= c\, T(n''n)\, T(n'n)\, \exp\left[\nu(n'n)t\right]\left[\frac{\left[\nu(n'n)\nu(n''n)+\nu^2\right]}{2\pi^2\nu^2}\,\dot{E}\right.$$

$$+ \left.\frac{\left[\nu(n'n)+\nu(n''n)\right]}{i\pi}\,E\right]$$

$$= \frac{c\, T(n'n)\, T(n''n)}{i\, 2\pi^2\nu^2}\left[\,i\,\nu(n''n)\left[\nu(n'n)\nu(n''n)+\nu^2\right]\dot{E}\right.$$

$$+ \left.2\pi\,\nu^2\nu(n''n)\left[\nu(n'n)+\nu(n''n)\right]E\right]\exp\left[\nu(n'n)t\right]$$

Now when we insert these back into Eq. 35,

$$\langle R\rangle_n = \langle n|R|n\rangle + \mathrm{Re}\sum_{n'\neq n}\langle n|R|n'\rangle\langle n'|R|n\rangle\frac{T(n'n)}{h\pi\nu^2}\left[\right.$$

$$2\,\nu(n'n)\,\pi\,\nu^2\,E + i\,\nu^2(n'n)\,\dot{E}\left.\right]$$

$$+\sum_{n''\neq n}\sum_{n'\neq n}\frac{H^F}{\pi h^2}\,\mathrm{Re}\,\langle n'|R|n\rangle\langle n''|R|n\rangle\langle n'|M|n''\rangle$$

$$\frac{T(n'n)\,T(n''n)}{\nu^2}\left[\,i\nu(n''n)\left[\nu(n'n)\nu(n''n)+\nu^2\right]\dot{E} +\right.$$

$$2\pi\nu^2\,\nu(n''n)\left[\nu(n'n)+\nu(n''n)\right]E \qquad\qquad \text{Eq. 36}$$

where the ixp $[\nu(n'n)t]$ disappears since it is multiplied by the ixp $[-\nu(n'n)t]$ term from the time dependent wave function, and the real part (Re) is taken since only real results are observable. Eq. 36 is the desired part of I'Haya's Eq. 27.

## 9. The average moment at a given temperature

Since the energy states of the molecule will be populated according to the Boltzmann factor, it is necessary to find the average moment per molecule at a given temperature. We multiply by Bn where Bn is the probability that the molecule will be found in state n with energy En at this temperature, and sum over all possible n (n also includes both vibrational and rotational quantum numbers). The Boltzmann factor Bn under the influence of a magnetic field is:

$$B_n = \frac{\exp\left(-\frac{E_n}{kT}\right)}{\sum_{n'} \exp\left(-\frac{E_{n'}}{kT}\right)}$$

$$= \frac{\exp\left[-\frac{E_n^o + \langle n|M|n\rangle H^f}{kT}\right]}{\sum_{n'} \exp\left(-\frac{E_{n'}}{kT}\right)}$$

Expanding the numerator and taking only the term linear in $H^f$, we have:

$$B_n = B_n^o \left\{1 + \frac{\langle n|M|n\rangle H^f}{kT}\right\}$$

where
$$B_n^o = \frac{\exp\left(-\frac{E_n^o}{kT}\right)}{\sum_{n'} \exp\left(-\frac{E_{n'}}{kT}\right)}$$

Eq. 37

Applying this now to our expectation value, Eq. 36,

$$\langle R \rangle_{nT} = \sum_{n} B_{n}^{o} \left[ \langle R \rangle_{n} + \frac{\langle n|M|n\rangle H^{f}}{kT} \langle n|R|n\rangle + \frac{\langle n|M|n\rangle}{kT} \right.$$

$$Re \sum_{n' \neq n} \langle n|R|n'\rangle \langle n'|R|n\rangle \frac{T(n'n)}{h \pi \nu^{2}} \left[ 2 \nu(n'n) \pi \nu^{2} E + i \nu^{2}(n'n) \overset{o}{E} \right] \left. \right]$$

<div align="right">Eq. 38</div>

Eq. 38 introduces the temperature-dependent paramagnetic terms. Only the first and third terms on the right-hand side of Eq. 38 contribute to the MCD.

## 10. The average moment over all orientations

Up to this point we have considered the molecules to be held rigidly in one position. Actually, in solution they are tumbling and so their properties must be averaged over all positions. The process of taking this average is rather involved and is discussed by a number of authors (25, p. 121)(28, p.707)(72). However, the result for this case is simple, multiplication by the factor 1/3.

## 11. Calculation of the magnetic optical rotation

Only the terms of Eq. 38 containing E are of interest for MCD. These are after averaging over all orientations

$$\langle R \rangle_{nT} = \frac{H^{f}}{6\pi h^{2}} \sum_{n} B_{n}^{o} \ I_{m} \sum_{n' \neq n} \sum_{n'' \neq n} \left[ \frac{T(n'n) T(n''n)}{\nu^{2}} \right.$$

$$\left[ i\nu(n''n) \left(\nu(n'n)\nu(n''n) + \nu^2\right) \dot{E} \right] \langle n'|R|n\rangle \langle n''|R|n\rangle \langle n'|M|n''\rangle$$

$$- \frac{1}{kT} \frac{i\nu^2(n'n)}{\pi\, h\, \nu^2} \langle n|M|n\rangle \langle n'|R|n\rangle \langle n|R|n'\rangle$$

Since only complex wave functions contain angular or linear momentum they must be used here. Therefore we can replace Re[i(f)] with -Im[f].

Since
$$\frac{\tau(n'n)\,\nu^2(n'n)}{\nu^2} = \frac{1}{\nu^2} + \tau(n'n)$$
(25 p. 336)

the frequency part of the first term in Eq. 39 becomes

$$\frac{\tau(n'n)\tau(n''n)\,\nu(n''n)\left[\nu(n'n)\nu(n''n) + \nu^2\right]}{\nu^2} = \frac{\tau(n'n)\nu(n'n)}{\nu^2} + \frac{\tau(n'n) - \tau(n''n)}{\nu(n''n')}$$

Only the last term still contains all three states n, n' and n" and only it will be used in the final evaluation. However, two cases must be distinguished. If $\nu(n'n)$ and $\nu(n''n)$ are far from being the same then $\frac{\tau(n'n) - \tau(n''n)}{\nu(n''n')}$ will be used. If $\nu(n'n)$ and $\nu(n''n)$ are almost degenerate as in the case of Zeeman splitting, then the term can be expanded in powers of $\nu(n''n')\ \tau(n'n)$ because this quantity is small.

$$\frac{T(n'n) - T(n''n)}{\nu(n''n')} = 2\nu(n'n) T^2(n'n) \left[ 1 - 2\nu(n'n)\nu(n''n') T(n'n) + \ldots \right]$$

Neglecting the terms after the first, Eq. 39 becomes,

$$\overline{\langle R \rangle_{nT}} = \frac{H^f}{6\pi h^2} \sum B_n{}^o I_m \sum_{n' \neq n} \sum_{n'' \neq n} \left[ -\frac{T(n'n) - T(n''n)}{\nu(n''n')} \right.$$

$$\dot{E}\langle n'|R|n\rangle\langle n''|R|n\rangle \langle n'|M|n''\rangle - 2\nu(n'n) T^2(n'n) \dot{E}$$

$$\langle n'|R|n\rangle\langle n|R|n'\rangle\langle n'|M|n'\rangle \qquad \qquad \text{Eq. 40}$$

$$- \frac{\nu^2(n'n) T(n'n)}{kT \pi h \nu^2} \langle n|M|n\rangle\langle n'|R|n\rangle\langle n|R|n'\rangle$$

From Maxwell's equations it may be shown that the indices of refraction for right and left handed light are:

$$n_r = \varepsilon^{1/2} + 2\pi\nu g \qquad \qquad g = 4\pi N \frac{-R_c}{c} \qquad N = \text{no. molecules per unit volume}$$

$$n_\ell = \varepsilon^{1/2} - 2\pi\nu g$$

where $\varepsilon$ is the dielectric  onstant of the medium (we will use $\varepsilon=1$).  The rotation per unit length is then $\frac{\pi\nu}{c}(n_\ell - n_r) = \phi$ .

$$\phi = \left(\frac{4\pi^2 \nu^2}{c}\right)\left(4\pi N - \frac{Rc}{c}\right) = \frac{16\pi^3 \nu^2 N}{c}\overline{\langle R \rangle}_{uT} \qquad \text{Eq. 41}$$

Substituting Eq. 40 into Eq. 41 gives the value for the Verdet constant.

This may be compared to I'Haya's Eq. 67 and Stephen's Eq. 27 except that

Stephens has not yet averaged over all orientations.

## 12. Development of the expression for MCD according to Stephens

Beginning with Stephens Eq. 27 which we see is identical with our

Eq. 41 before averaging, we use his results of treating for wide absorp-

tion bands.

We are interested in the case where electronic transitions occur in

a molecule in a liquid or solution and the absorption band consists of

many unresolved vibrational bands. If the vibrational bands act similarly,

(they will for an electronically allowed transition or one which is

electronically forbidden but vibrationally allowed by a single vibration

and where the absorption band consists of a totally symmetric vibrational

progression super-imposed on a single quantum in this vibration) then

the various vibronic transitions may be added. These may be treated

as sharp, well-resolved lines but with $\nu(n''n') \ll \Gamma(n'n)$, that is, the

Zeeman splitting is much smaller than the bandwidth. In this event

the shape of the rotation (or circular dichroism) band remains essentially

the same although its magnitude changes as the Zeeman splitting changes.

The rotation in this case will be

$$\phi_{(n'n)} = -\frac{4\pi}{\hbar c} N \left\{ \frac{4\pi \, \nu(n'n) \, \nu^2 \left[ 4\pi^2(\nu^2(n'n)-\nu^2)^2 - \nu^2 T^2(n'n) \right] A_{(n'n)}}{\hbar \left[ 4\pi^2(\nu^2(n'n)-\nu^2)^2 + \nu^2 T^2(n'n) \right]^2} \right.$$

$$\left. + \frac{4\pi^2 \nu^2 (\nu^2(n'n)-\nu^2)}{4\pi^2(\nu^2(n'n)-\nu^2)^2 + \nu^2 T^2(n'n)} \left[ B_{(n'n)} + \frac{C_{(n'n)}}{kT} \right] \right\} H_z$$
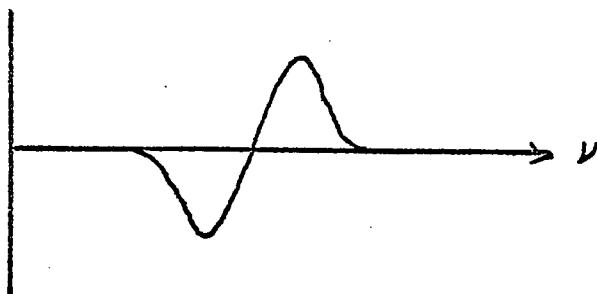
Now since the MORD and MCD are related by the Kramers-Kronig relation

$$\theta_{(n'n)}(\nu) = -\frac{1}{\pi^2} \, P.V. \int_0^\infty \frac{\phi_{(n'n)}(\nu')}{(\nu')^2 \left[ (\nu')^2 - \nu^2 \right]} \, d\nu'$$
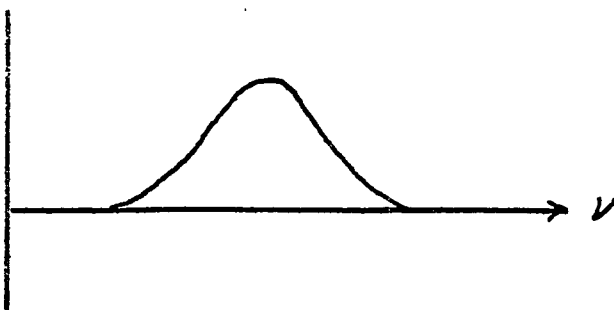
where P.V. is the Cauchy principal value we find the MCD has the form:

$$\theta_{(n'n)} = -\frac{4\pi}{\hbar c} \cdot N \left\{ \frac{16\pi^2 \, \nu(n'n) \, \nu^3 (\nu^2(n'n)-\nu^2) \, T(n'n) \, A_{(n'n)}}{\hbar \left[ 4\pi^2(\nu^2(n'n)-\nu^2) + \nu^2 T^2(n'n) \right]^2} \right.$$

$$\left. + \frac{2\pi \, T^2(n'n)}{4\pi^2(\nu^2(n'n)-\nu^2) + \nu^2 T^2(n'n)} \left[ B_{(n'n)} + \frac{C_{(n'n)}}{kT} \right] \right\} H_z$$

where the freq. term for the A term looks like



and the freq. term for the B and C terms looks like

## APPENDIX II

There has been some confusion concerning the sign convention for magnetic circular dichroism. In the past the convention used in this laboratory has been the conventional one for Faraday rotation. This leads to a positive sign for the 520 mµ band of cobaltous salts as obtained by Scherer (4). However, the other workers have chosen the opposite convention (8,9,10).

Since the sign of MCD is of particular importance in this research, and since the other workers will eventually be providing the majority of the research papers, it was decided to adopt their convention throughout this thesis. In addition, it is seen (see the Simplified Theory) when using the circular dichroism convention of Condon, Altar and Eyring (29), the orbital angular momentum convention of Condon and Shortley (24, p. 146) and the photon angular momentum convention of Beth (23), that the sign for the cobalt band should be negative. These are the most commonly used conventions but caution should be used since the opposite conventions are often found in the literature, particularly in the field of high energy physics.